Optimized Neural Stem Cell Delivery of the TRAIL Protein for Targeted Glioblastoma Therapy

Shu Song

A thesis submitted to the University of Ottawa
in partial fulfillment of the requirements for the
Master's degree in Microbiology and Immunology

Department of Biochemistry, Immunology and Microbiology
Faculty of Medicine, University of Ottawa

Abstract

Effective delivery of therapeutics to the brain remains elusive, contributing to poor outcomes in diseases like glioblastoma, where median survival is under 15 months. Here, we explore a novel therapeutic strategy using human neural stem cells derived by direct reprogramming of peripheral blood erythroblasts (PBiNSCs). Pilot studies show that PBiNSCs have an intrinsic ability to home to glioblastoma cells in vivo and in vitro, supporting their use as delivery vehicles for targeted treatment of aggressive brain tumors. We genetically engineered PBiNSCs to express the membrane-bound variant of TNF-related apoptosis-inducing ligand (TRAIL), a potent pro-apoptotic protein with stronger cytotoxicity than its soluble form. Lentiviral transduction resulted in successful exogenous expression of TRAIL but showed some toxicity to the PBiNSCs themselves. To overcome this, we used CRISPR-Cas9 to knock out the endogenous DR5 receptor, generating a TRAIL-resistant PBiNSC population (DR5KO-PBiNSC). Following ectopic expression of TRAIL in this new population (TRAIL-DR5KO-PBiNSCs), we detect TRAIL predominantly in the media in exosomes. TRAIL-DR5KO-PBiNSCs exhibited improved viability and enhanced cytotoxicity against a primary glioblastoma cell line when tested either in co-culture or using conditioned media from these modified cells. We further tested several sensitizing agents to enhance TRAIL-mediated apoptosis. AZD5582, a small-molecule Smac mimetic and inhibitor of IAPs, demonstrated sensitizing effects at low concentrations and killing of $>90\%$ in one primary glioblastoma cell line. Our findings establish a genetic engineering strategy for TRAIL delivery in neural stem cells for targeted glioblastoma therapy.

Acknowledgments

I would like to first and foremost thank my thesis supervisor, Dr. Ian Lorimer, for his unwavering support throughout my Master's degree. It is only through his encouragement and guidance that I am able to present a body of work I am proud of. Over the past two years, his mentorship and expertise have given me a deep appreciation for research and science.

I would also like to thank Margarita Lui for all her help in the lab. She has taught me numerous laboratory techniques and offered invaluable advice on troubleshooting experiments. She was always there to lean on. I am equally grateful to all my lab mates, who have made each day in the lab more enjoyable and rewarding.

Contents

List of Figures

Chapter 3: Results

Appendix

List of Abbreviations

7-AAD	7-aminoactinomycin D
AAVS1	Adeno-associated virus integration site 1
AKT	Protein kinase B
BSA	Bovine serum albumin
CAR	Chimeric antigen receptor
CAR-T	Chimeric antigen receptor T-cell
CC3	Cleaved caspase-3
CM	Conditioned media
CMV	Cytomegalovirus
CNS	Central nervous system
CRISPR	Clustered Regularly Interspaced Short Palindromic Repeats
cFLIP	Cellular FLICE-inhibitory protein
CLYBL	Citrate Lyase Beta-Like
DNA	Deoxyribonucleic acid
DR4	Death receptor 4
DR5	Death receptor 5
DSB	Double-stranded break
EF1-alpha	Elongation factor 1-alpha
EV	Extracellular vesicle
FACS	Fluorescence-activated cell sorting
FDA	Food and Drug Administration

GAPDH	Glyceraldehyde-3-phosphate dehydrogenase
GBM	Glioblastoma multiforme
GFP	Green fluorescent protein
gRNA	Guide RNA
HDR	Homology-directed repair
IDT	Integrated DNA Technologies
IAP	Inhibitor of apoptosis protein
NHEJ	Non-homologous end joining
NSC	Neural stem cell
OHRI	Ottawa Hospital Research Institute
PBiNSC	Peripheral blood-derived induced neural stem cell
PBS	Phosphate-buffered saline
PCR	Polymerase chain reaction
PFA	Paraformaldehyde
PriGO	Primary glioblastoma
PTEN	Phosphatase and tensin homolog
RFU	Relative fluorescence unit
RNP	Ribonucleoprotein
TBST	Tris-buffered saline with Tween 20
TIDE	Tracking of Indels by DEcomposition
TRAIL	TNF-related apoptosis-inducing ligand
tracrRNA	Trans-activating CRISPR RNA

Chapter 1

Introduction

1.1 Glioblastoma

Glioblastoma multiforme (GBM) is a primary malignant tumor of the brain and is classified by the 2021 World Health Organization (WHO) as a grade IV adult-type diffuse glioma, a tumor type thought to arise from glial cells or their precursors (1). The WHO grading system categorizes central nervous system (CNS) tumors into four levels based on histological features and molecular markers, with higher grades associated with more aggressive behavior and poorer outcomes. GBM, being of the highest grade, is the most aggressive and lethal CNS tumor, with an incredibly poor patient prognosis and limited treatment options. Median survival following standard-of-care treatment, which is currently maximal surgical resection followed by radiotherapy with temozolomide, is approximately 15 months (2, 3). Fewer than 5% of patients survive beyond 5 years (4). Despite treatment, recurrence is nearly universal and begins within 6–9 months of the initial intervention (5, 6, 7).

GBM is the most common primary brain malignancy, accounting for over half of all cancers originating from the CNS (4). The annual incidence of GBM in the United States is approximately 3.19 per 100,000 individuals (4). The median age of diagnosis is 64, at which point patients typically present to the clinic with nonspecific symptoms such as headaches, nausea, seizures,

or impairments to cognitive function (4, 7, 8). At diagnosis, GBM is often advanced, having arisen rapidly de novo and infiltrated surrounding brain tissue. Clinical imaging with computed tomography (CT) or magnetic resonance imaging (MRI) shows lesions in the white matter of the cerebral hemisphere, most frequently in the frontal and temporal lobes. GBM can also develop in the cerebellum, brain stem, and spinal cord (9, 10).

Macroscopic hallmarks of glioblastoma include extensive intratumoral necrosis, ill-defined tumor margins, multifocal hemorrhage, and aberrant neovascularization (11, 12). Necrosis and microvascular proliferation are defining features of high-grade gliomas. GBM specimens show neoplastic cells arranged into hypercellular multilayers surrounding necrotic regions, a morphology termed palisading necrosis (13). These structures arise as hypoxic stress induces tumor cells to migrate away from ischemic cores (13). The neovasculature structure within GBM is abnormal and disorganized, forming glomeruloid bodies, which are vascular channels lined by multilayered endothelial cells, pericytes, and smooth muscle cells (14, 15, 16). These vessels exhibit marked permeability and fenestration, contributing to peritumoral edema, regional hypoxia, and increased tumor aggressiveness (17).

GBM exhibits the classical hallmarks of malignancy and aggressiveness at the cellular level. Tumor tissue is pleomorphic and hypercellular, composed of poorly differentiated cells with irregular multinuclei (12, 18). Nuclear staining reveals a high frequency of mitotic figures, reflecting the tumor's high proliferative activity (19). The neoplastic cell population resembles immature glial cells, showing mixed oligodendroglial-astrocytic phenotypes (20). Although the exact cell of origin is unknown, GBM is thought to arise from neural stem cells or glial precursor cells (21). In GBM, there is a population of cells that resemble stem cells, possessing self-renewal capacity and the ability to recapitulate tumor heterogeneity upon transplantation (22). These cells, often referred to as cancer stem cells (CSCs), can be sorted based on markers such as CD133, SOX2, and Nestin, and are found to be enriched in recurrent GBM tissue following chemotherapy (23, 24, 25). However, the existence of true cancer stem cells in GBM, analogous to those in leukemia, remains uncertain due to experimental limitations and evidence suggesting that solid tumors often

lack a strict stem cell hierarchy.

Several defining genetic features characterize GBM according to the 2021 WHO classification. Gliomas must be wild-type for the isocitrate dehydrogenase (IDH) gene to be designated as glioblastoma, marking a shift from the previous classification that included IDH-mutant tumors. GBM may also harbor TERT promoter mutations, EGFR gene amplification, and the combined gain of chromosome 7 with loss of chromosome 10 (26). Comprehensive genomic analyses of GBM lesions identify the most frequently dysregulated signaling pathways as the receptor tyrosine kinase/RAS/PI3K pathway, the p53 pathway, and the RB pathway (27). Bulk transcriptomic profiling stratifies GBM into three main molecular subtypes: proneural, mesenchymal, and classical (28). These subtypes are categorized by genomic alterations in key driver genes including PDGFRA, EGFR, and NF1 and reflect responsiveness to treatment. Among the three, the mesenchymal subtype is associated with the worst prognosis and greatest resistance to therapy.

1.2 Challenges in developing glioblastoma therapy

Designing effective therapeutics for glioblastoma remains challenging. Patient outcomes have scarcely improved in the past 25 years, as standard intervention remains highly invasive and fails to meaningfully prolong life. Phase III clinical trials for GBM have been diverse in their approach, but most have failed to meet their primary endpoints or improve overall patient survival (29).

1.2.1 Inter- and Intratumoral Heterogeneity

A central challenge in GBM is the extensive heterogeneity present both within individual tumors (intra-tumoral) and between patients (inter-patient). Tumor heterogeneity refers to differences at the genetic, molecular, cellular, and phenotypic levels that contribute to variability in tumor behavior and, ultimately, therapeutic response. Although molecular classification of GBM into subtypes, as mentioned above, provides a useful framework, it has had limited practical application in the clinic. Tumor subtype varies spatially within a single tumor and temporally over disease

progression (30, 31). Multiple subtypes can coexist within the same tumor region. In response to drug treatment, glioma cells convert between molecular subtypes, demonstrating a high degree of transcriptional plasticity. Notably, the mesenchymal subtype tends to predominate in recurrent GBM, regardless of the primary tumor's original subtype (30).

At the genomic level, integrated genomic analysis reveals substantial heterogeneity in copy number alterations (CNAs) within tumors, indicating the coexistence of multiple subclones and distinct cell lineages. Major intratumoral differences in CNAs are frequently observed in putative driver genes, including the PDGFRA, MDM4, AKT3, and EGFR loci, as well as deletions of the PTEN locus (31, 32). For example, although PTEN loss of heterozygosity occurs in 70% of patients, it is spatially heterogeneous within tumors, as some subpopulations retain both functional copies (31). Consequently, subclones exhibit varying proliferative and differentiation capacities, as well as differential responses to drug treatment (33). Across patient populations, CNAs are commonly detected at the MTAP, EGFR, CDK6, and MDM4 loci, but are not present in every patient. The partial loss of chromosome 10 and gain of chromosome 7 are nearly universal in GBM (30, 31).

Given the extensive heterogeneity in GBM at both the genotypic and molecular levels, it is understandably difficult to design broadly effective therapies, whether targeting for specific tumor antigens or identifying relevant biomarkers. When therapies fail to address such heterogeneity, resistant clonal populations emerge and propagate. For this reason, the success of novel therapies like chimeric antigen receptor (CAR)-T cells in treating hematological malignancies has not been translated to GBM (34, 35). The effectiveness of CAR-T therapy relies, in part, on uniform expression of the tumor antigen, which is targeted by the engineered CAR. In GBM, CARs have been designed to recognize the IL-13Ralpha2 or EGFRvIII receptor. Although these tumor antigens were expressed in over half of GBM cells, the anti-tumor response from CAR-T therapy was transient, with recurrence occurring within months (36). Post-infusion sampling of tumor tissue revealed decreased expression of the target antigen; however, the lack of a durable clinical response indicates rapid antigen escape (37). More recently, the use of bivalent CAR T cells targeting both

EGFR and IL-13Ralpha2 showed tumor regression in a majority of patients. However, the median progression-free survival remained low, as relapse occurred within 1.9 months (38). The targeting of single or multiple tumor antigens, despite being successful in other cancers, remains challenging in glioblastoma due to such pronounced intratumoral heterogeneity.

1.2.2 Blood brain barrier

Classical drug delivery methods, such as oral or intravenous administration, rely on systemic circulation and subsequent diffusion of drugs to target tissues. Treatment of diseases in the CNS requires delivery strategies that circumvent the blood-brain barrier (BBB), a specialized structure that separates the CNS milieu from the systemic circulation. The BBB is composed of endothelial tight junctions, drug transporters, and efflux pumps, which collectively restrict the passage of most therapeutics. It is estimated that the BBB excludes 98% of small-molecule drugs, as well as virtually all large molecules like antibodies and recombinant proteins (39). This not only limits the types of therapeutics capable of reaching the CNS but also prevents drug accumulation to levels required for an effective dose. Although the BBB is partially compromised in GBM, regions near the tumor margins remain intact, providing a protective niche for residual tumor cells (40).

Aside from the BBB, diffusion within the brain is limited. The organ is densely organized, consisting of closely packed neurons and glial cells, leaving only 20% of total brain volume as extracellular space (41). Consequently, drugs delivered directly into the brain, via injection or otherwise, are poorly dispersed, with biologically active substances diffusing no more than 2mm away from the injection site.

A clinically relevant strategy for delivering therapeutics to the CNS is the use of an Ommaya reservoir, which positions a catheter directly into the lateral ventricles of the brain to allow long-term access to the cerebrospinal fluid (CSF). The catheter connects to a reservoir implanted beneath the scalp, through which antibiotics, chemotherapy, or other drugs can be administered. Ommaya reservoirs are still commonly used in pediatric CNS relapse, where cancer cells are detected in the CSF (42). While this approach provides direct CNS access, diffusion from the CSF into brain

tissue is severely limited. Drug concentrations can drop to as little as 2% of CSF levels just 1–2 mm from the ependymal surface (43, 44). These pharmacological limitations significantly constrain the effectiveness of glioblastoma treatments.

1.2.3 Immune microenvironment

The tumor microenvironment in GBM is considered immunologically cold, characterized by a limited anti-tumor immune response, which subsequently lends to ineffective immunotherapy efforts.

The largest non-neoplastic cell population in GBM is tumor-associated macrophages (TAM), accounting for approximately 30% of the tumor mass (45, 46). This population includes both infiltrating peripheral macrophages and microglia, immune cells native to the CNS. While these immune cells normally function to clear pathogens and abnormal cellular growth, in GBM, TAMs exhibit well-documented pro-tumorigenic functions. TAMs express factors like matrix metallopeptidase-14, hypoxia-inducible factor 1 alpha, and TGF-beta, which contribute to tumor aggressiveness, invasion, immunosuppression, and disease progression (45, 46, 47). Elevated TAM infiltration correlates with shorter survival in patients with high-grade gliomas (47).

Within the adaptive arm of the immune system, effector cell infiltration and activity are markedly limited. T cells constitute a rare population in the tumor bulk, comprising less than 5% of the cellular population. T cells that are present frequently display markers of T-cell exhaustion, including high expression of PD-1, LAG-3, TIGIT, and CD39 (48, 49, 50).

The GBM microenvironment is immunologically unresponsive, with immune cells that are functionally impaired, pro-tumogenic, and immunosuppressive. In this context, the efficacy of immunotherapeutics has been severely limited. Phase III clinical trials using immune checkpoint inhibitors, such as PD-1 and CTLA-4 blockade, have failed to extend overall survival beyond 15 months (51). The challenge extends to CAR-T therapy, where there is poor activity of effector T cells. Consequently, effective therapeutics must address not only the neoplastic cell population but also the surrounding stromal and immune components that actively contribute to disease progression.

1.2.4 Invasion

Nearly 90% of all GBM patients experience recurrence within the first year of treatment, one of the highest rates among cancers (52). The majority of tumor recurrences occur locally near the primary tumor site, while a smaller fraction arises in more distant locations, including the contralateral hemisphere (6). GBM recurrence is driven by the cells that migrate away from the primary lesion, allowing them to repopulate after surgical removal and focal therapies (53). Recurrent lesions share similarities in early driver mutations with the initial tumor and are thus thought to be derived from clones that escaped the initial intervention (53).

1.3 Cell-based therapies for cancer

Cell-based therapies represent a unique category of therapeutic agents that utilizes living cells to treat disease. Unlike conventional drugs, such as small molecules and biologics that target specific pathways, cell-based approaches can engage multiple pathways. As such, these "living drugs" can respond and adapt dynamically to disease progression. Cell therapy has been applied in different contexts, including its use for tissue regeneration (e.g., stem cells), immune modulation (e.g., regulatory T cells or MSCs for autoimmune disorders), and cancer treatment (e.g., CAR-T cells, TILs).

Adoptive cell transfer utilizes immune cells to treat cancer. Most notably, CAR-T cells and tumor-infiltrating lymphocytes (TILs) have demonstrated promising clinical results. These approaches take immune cells from patients, genetically modify or expand the cell population ex vivo, and re-introduce them into the body. CAR-T cell therapy, in particular, has shown long-term remission in a subset of patients with refractory hematological malignancies (54, 55). Several CAR-T therapies are currently FDA-approved. Currently, tisagenlecleucel and axicabtagene ciloleucel are used for the treatment of B-cell precursor acute lymphoblastic leukemia and large B-cell lymphoma, respectively (56, 57). The use of cell-based therapies is not only safe and feasible for cancer but offers the potential for durable clinical outcomes.

Beyond immune effector cells, mesenchymal stem/stromal cells (MSCs) and other adult stem cells have been explored for their therapeutic potential for cancer treatment. Adult stem cells are multipotent, undifferentiated cells with self-renewal capacity. These cells selectively migrate to sites of tissue injury, possess intrinsic anti-tumor activity, and can serve as vehicles for drug delivery.

1.3.1 Neural stem cells as a therapeutic for GBM

Neural stem cells (NSCs) are currently being explored as a potential drug delivery vehicle for glioblastoma. Studies have identified NSCs as possessing inherent tumor-homing properties and demonstrating the ability to provide sustained delivery of cytotoxic payloads in the brain.

Tumor-tropism

NSCs are capable of migrating to sites of tissue injury as part of intrinsic mechanisms for maintaining homeostasis. In cases of stroke, injured brain tissue releases chemokines and cytokines that induce neural stem cells from the sub ventricular zone (SVZ) to naturally migrate towards ischemic lesions for tissue regeneration (58, 59). Similarly, NSCs have been observed to preferentially migrate to tumor lesions using similar chemotactic gradients (60, 61, 62, 63).

Endogenous neural stem cells from the SVZ have been found to migrate toward tumor foci in mouse models, even surrounding malignant cells that are distant from the central mass (63). Exogenous neural stem cells transplanted into the brain also demonstrate preferential migration toward areas of malignant growth (64, 65, 66). This migratory phenotype has been shown to be selective toward neoplastic cells rather than toward non-neoplastic cell populations, both in vivo and in vitro (64, 66, 67). The mechanisms underlying tumor-homing are not completely understood; however, several chemokine and growth factor axes thought to be involved in recruitment and attraction include SDF1 and CXCR4, SCF-c-Kit, HGF-c-Met, VEGF-VEGFR, PDGF-PDGFR, MCP-1-CCR2, and HMGB1-RAGE (60).

Delivery of cytotoxic payloads

Efforts have been made to genetically modify neural stem cells to deliver cytotoxic payloads, antitumor factors, and oncolytic viruses. For example, two independent groups engineered murine NSCs to secrete interleukins, which were subsequently transplanted into glioma-bearing mice, prolonging survival in the treated population (79, 80). Other cytotoxic payloads that have been engineered into NSCs include carboxylesterase, TRAIL, and IFN-beta (73, 74, 75, 76).

The therapeutic potential of engineered NSCs was evaluated in a phase I dose-escalation study involving 15 patients with recurrent glioblastoma (77, 81). Patients received intracerebral injections of immortalized human fetal NSCs (HB1.F3) retrovirally transduced to express cytosine deaminase, followed by systemic 5-fluorocytosine administration. The enzyme-prodrug system enabled localized conversion to 5-fluorouracil within the tumor environment. Despite acceptable safety profiles and a median progression-free survival of approximately 2 months, allogeneic immune responses resulted in anti-NSC antibody formation in 3 patients, emphasizing the clinical necessity for patient-specific, autologous cell sources.

1.3.2 Generating human neural stem cells by epigentic reprogramming

Differentiated adult cells can be reprogrammed to a pluripotent state through the forced expression of transcription factors (88). As discovered by Yamanaka et al., the ectopic expression of four factors Oct3/4, Sox2, c-Myc, and Klf4, removes epigenetic markers that determine cellular identity, thereby reverting them into a stem cell-like state. These reprogrammed cells, which now possess self-renewal capacity and pluripotency, are referred to as induced pluripotent stem cells (iPSCs). More recently, the same strategy has been applied to directly convert somatic cells into other committed cell types through a process known as transdifferentiation or direct reprogramming. Transdifferentiation bypasses the pluripotent state, and the derivatives of this process are thought to be much safer for therapeutic application.

Research has explored generating NSCs through various epigenetic reprogramming strategies, as harvesting endogenous NSCs is impractical due to their rarity and restricted localization in the

brain. Additionally, the use of human fetal NSCs raises both ethical concerns and the risk of allogeneic immune reactions. Neural stem cells transdifferentiated from adult fibroblasts have been tested to treat glioma-bearing mice. Induced murine NSCs lines selectively migrated to GBM both in vitro and in vivo and were also effective at delivering the cytotoxic protein TRAIL, reducing tumor burden by more than 90% (82). Bago et al. explored transdifferentiating human fibroblasts into NSCs. Following exogenous expression of TRAIL, these human induced-NSCs reduced glioma tumor growth and prolonged survival in mice (83). Although induced-NSCs have not yet been tested in a clinical setting for GBM, their efficacy and feasibility have been established in animal models (94).

Sheng et al. demonstrate that human neural stem cells can be directly reprogrammed from peripheral blood cells (89). Erythroblasts were first isolated from the peripheral blood of patients. The transient expression of SOX2 and c-MYC through non-integrating Sendai viruses was sufficient to directly convert erythroblasts into neural stem cells (PBiNSCs). These cells exhibited the ability to differentiate into three functional neuronal lineages: neurons, astrocytes, and oligodendrocytes. The same group found that these induced neural stem cells stably engrafted into mouse brains and persisted for the entire 24-week study period (90).

1.4 Genetic engineering in neural stem cells

Genetic modification of neural stem cells can be approached in several ways with different techniques. Genetic engineering enables the manipulation of both the cellular proteome and transcriptome. Achieving long-term and permanent changes requires direct alterations to the genome. These modifications can be achieved through three main approaches: (1) viral-mediated gene delivery, (2) the use of nucleic acid–binding proteins, and (3) transposon-based systems.

1.4.1 Viral vectors

Viral-based gene therapy involves delivering genetic material into target cells using modified viral vectors. Viral vectors are generated by removing genes in the viral genome required for viral replication, rendering them replication-deficient. Common viral vector systems include adenoviruses, adeno-associated viruses, and lentiviruses. For example, the third-generation lentiviral vector system uses separate plasmids, each encoding different viral components needed to assemble viral particles. The intended genetic material to be introduced is carried by the transfer plasmid and flanked by long terminal repeats, which are used for integration into the host genome.

Lentiviral vectors, as opposed to other viral system, provide highly efficient transduction and stable, long-term expression of the transgene. Lentiviral particles can infect non-dividing cells and exhibit low immunogenicity, making them widely used for clinical purposes (137). Concerns with viral transduction arise from the semi-random integration of the transgene into the genome, which carries a low but non-negligible risk of insertional mutagenesis.

1.4.2 Nucleic acid binding protein based systems

Currently, there are three generations of nucleic acid-binding protein systems for genome editing: zinc-finger nucleases (ZFNs), transcription activator-like effector nucleases (TALENs), and clustered regularly interspaced short palindromic repeats (CRISPR). The former two systems have protein-based recognition domains fused to an endonuclease, such as FokI. When FokI dimerizes on opposite strands, the endonuclease generates a double-stranded break at the targeted sites. DNA sequence specificity is directed by zinc finger domains or TALEs, a bacterial protein, which when multiple are linked together, recognize continuous DNA sequences and confer specificity in cleavage (138, 139).

CRISPR-CAS9 is a modern genetic engineering technique that repurposes the bacterial adaptive immune system (140). Unlike ZFNs or TALENs, which use proteins to recognize specific DNA sequences, the CRISPR system relies on a 20-nucleotide RNA sequence known as the CRISPR RNA (crRNA). The crRNA is base paired with the trans-activaiting crRNA (tracrRNA) to

form a single guide RNA (gRNA), which forms a complex with the CAS9 enzyme. This ribonucleoprotein complex (RNP) is directed to a complementary sequence in the host genome, determined by the crRNA sequence, where CAS9 induces cleavage of the DNA.

Genome repair mechanisms

Cleavage of the DNA by endonucleases results in a double-stranded break that is repaired by the mammalian host machinery in one of two ways: non-homologous end joining (NHEJ) or homologous directed repair (HDR). NHEJ is the most frequent repair pathway, occurring rapidly on the scale of minutes (141). NHEJ occurs when a double-stranded break is directly ligated together, but this process generates random insertions and deletions known as an indel pattern. NHEJ is often used to mediate protein knockout when targeted at a gene coding sequence as the gene is now mutated. The competing repair process, HDR is a less frequent event but allows for precise repair of the break through a homologous DNA template. The template, derived either from the sister chromatid or supplied exogenously, guides the synthesis of the template sequence at the break site. This allows for the permanent incorporation of the template sequence into a desired location in the genome. HDR is less efficient process and is primarily active during specific phases of the cell cycle (141).

1.5 Tumor necrosis factor (TNF)-related apoptosis inducing ligand (TRAIL) as cancer therapeutic

There has been considerable interest in optimizing the delivery of TRAIL for cancer treatment. TRAIL appears to selectively induce apoptosis in transformed cells both in vivo and in vitro (101, 104, 105, 106, 107). TRAIL rapidly induces of cell death in a range of cancer cell lines, including colon, lung, kidney, breast, melanoma, and brain cancers at low concentrations. At similar concentrations, normal human tissues are largely resistant to TRAIL-mediated apoptosis. The exact mechanisms underlying this selectivity are not fully understood and appear complex with many

exceptions. Notably, several studies have reported finding sensitivity in normal human cell lines such as astrocytes, hepatocytes, epithelial cells, and keratinocytes (101, 108, 109, 110, 111, 112).

TRAIL is a type II transmembrane protein encoded by the TNFSF10 gene on chromosome 3 (3q26). Its RNA transcript is detectable in multiple adult tissues, including the spleen, thymus, prostate, and lungs, while protein expression is found in the lung, spleen, cerebellum, and thyroid (91, 92). TRAIL is mainly expressed by immune cells, such as NK cells, B cells, monocytes, and dendritic cells following cytokine stimulation by IFN-y, but can also be expressed by other cell types including glial and follicular cells (92, 93, 94, 95, 96, 97). Belonging to the TNF superfamily, TRAIL contains a conserved TNF homology domain at its C-terminus and a single pass transmembrane domain. This membrane-bound form is approximately 35 kDa in size and 281 amino acids long (98, 99). TRAIL can be proteolytically cleaved from the cell surface into a soluble form (24 kDa). The most well-documented biological activity of TRAIL is its induction of apoptosis via the extrinsic pathway. While TRAIL has pro-apoptotic functions, its physiological role is less clear and may involve roles in anti-tumor immune surveillance and autoimmunity.

There are five human receptors for TRAIL: death receptors 4 (DR4), death receptor 5 (DR5), decoy receptor 1 (DcR1), decoy receptor 2 (DcR2), and osteoprotegerin. DR4 and DR5 are cell surface receptors with functional intracellular death domains. Upon binding to TRAIL, the receptors undergo trimerization and initiate the formation of the death-inducing signaling complex (DISC), which initiates apoptotic signaling (100, 101, 102). The intracellular death domains of DR4/5 recruit the adaptor protein Fas-associated protein with death domain (FADD), which activates caspases-8 and 10. This leads to the direct cleavage of caspase-3 and apoptotic cell death (103). In contrast, the latter three receptors can bind TRAIL, but lack a functional death domain and consequently do not induce apoptosis.

1.5.1 TRAIL-based therapies

Application of TRAIL-based therapeutics has yielded poor clinical results. First generation approaches focused on developing TRAIL receptor agonists and recombinant soluble human TRAIL.

Dulanermin (AMG-951) was a recombinant soluble human TRAIL protein developed by Amgen/Genentech (113). Although the drug was determined to be safe and well tolerated, phase III clinical trials showed no improvement in advanced non-small-cell lung cancer (114). DR4 and DR5 receptor agonists were also developed and tested, but showed only modest improvements following systemic delivery (115).

The development of second-generation approaches for TRAIL-based therapy aimed to improve the limited anti-tumor response in patients by addressing poor pharmacokinetics, limited receptor trimerization, and cancer resistance (115). Efforts have been made to improve TRAIL presentation in multimeric forms, as induction of strong downstream apoptotic signaling depends on effective clustering of TRAIL receptors (116). Accordingly, studies have found that transmembrane TRAIL, presentation on liposomes, fusion to Fc domains, incorporation into exosomes, and the addition of an isoleucine zipper hexamerization motif result in stronger cytotoxic activity compared to soluble derivatives (116, 117, 118, 119, 129).

1.5.2 TRAIL resistance

TRAIL-mediated apoptosis is regulated at multiple levels and sensitivity can be acquired through changes in a number of different pathways. Normal, non-transformed tissues are generally resistant to TRAIL-induced apoptosis. Studies have shown that non-transformed tissues express high levels of decoy receptors that sequester TRAIL binding and prevent binding to functional TRAIL receptors (100, 121, 122). It is speculated that expression of DcR1 and DcR2 confers some protection against TRAIL-mediated apoptosis (121, 123, 124). High and robust expression of anti-apoptotic proteins such as cFLIP, XIAP, and Bcl-2 family proteins in normal cells also contributes to resistance (125). The knockout of multiple anti-apoptotic proteins is often required to confer measurable changes in TRAIL sensitivity (125). During tumor progression, cancer cells acquire mutations in various oncogenic pathways, some of which result in acquired TRAIL sensitivity. Cancer cells exhibit elevated levels of pro-death receptors DR4 and DR5, which can be directly regulated by p53 (104, 126, 127, 128). However, sensitivity to TRAIL does not appear to

be directly correlated to receptor expression levels.

Resistance of cancer cells to TRAIL-mediated apoptosis is a common issue, with over half of all tested cancer cell lines exhibiting varying degrees of resistance (129). The mechanisms of resistance involve multiple signaling pathways and vary significantly across tumor types. Oncogenic pathways, such as c-Myc activation, have been shown to increase levels of pro-apoptotic proteins, including Bax and Bak, while reducing levels of anti-apoptotic proteins such as c-FLIP (130, 131, 132). Evasion of TRAIL-induced apoptosis due to upregulation of c-FLIP is found across various tumor types, where siRNA c-FLIP inhibition can restore partial sensitivity to TRAIL (133, 134). Loss of p53 function, the most commonly mutated tumor suppressor gene in cancer, is associated with reduced TRAIL sensitivity in lung and colon cancer cell lines (135). Attempts to reestore wildtype p53 activity has enhanced TRAIL killing in previously resistant lines. Another central pathway contributing to resistance is the loss of negative regulation of the PI3K/Akt pathway, commonly due to loss of the tumor suppressor PTEN. PTEN loss, fwhich requent in many cancers, results in constitutive Akt signaling, which promotes activation of anti-apoptotic pathways (136).

1.6 Study rationale and Objectives

The challenges in treating GBM necessitate novel and innovative delivery strategies that overcome poor brain penetration while simultaneously addressing tumor heterogeneity, aggressive invasion, and the immunosuppressive tumor microenvironment.

The use of neural stem cells as drug delivery vehicles offers a strategy to address several of the aforementioned challenges. NSCs can safely engraft into the brain for extended periods, enabling localized, concentrated, and sustained delivery of therapeutics. Moreover, NSCs possess intrinsic tumor-tropic properties, allowing them to home toward malignant cells that have infiltrated into surrounding tissue, thereby addressing potential recurrence resulting from residual microlesions. Previous work in our lab has shown that neural stem cells derived from the peripheral blood of patients (PBiNSCs) can stably and persistently engraft into the mouse brain for up to one month

(89). We have also established that this novel human induced NSC cell line displays the same tumor tropism. When glioma cells and induced NSCs are co-injected into the contralateral hemisphere of mice, the two cell populations exhibit selective migration toward each other.

Here, we demonstrate for the first time that peripheral blood-derived neural stem cells (PBiNSCs), developed by Sheng et al., can be engineered to express membrane-bound TRAIL as a therapeutic strategy for GBM (89). The use of PBiNSCs as the cellular delivery vehicle avoids the risk of allogeneic immunogenicity associated with HB1.F3, an FDA-approved NSC line for use in clinical trials. This novel autologous stem cell source is obtained through methods that are less invasive and less mutagenic than those required to derive induced NSCs from skin fibroblasts. The decision to use TRAIL as the cytotoxic payload is based on its non-toxic effects on normal tissue. In the brain, TRAIL expression is virtually absent under healthy conditions, with the exception of low levels produced by oligodendrocytes (142). Although TRAIL receptors DR4 and DR5 are expressed by glial cells and neurons in the CNS, these cells do not undergo apoptosis following TRAIL treatment (142, 143). While most studies examining TRAIL delivery from cellular vehicles have focused on its soluble form, we chose to engineer the expression of its membrane-bound form. Membrane-bound TRAIL on the cell surface exerts strong apoptotic activity as it induces supramolecular clustering of TRAIL receptors required for enhanced downstream signaling (116).

We also propose minimizing the use of viral transduction for gene modification, which is the current standard practice for introducing cytotoxic transgenes into cells. Viral transduction carries inherent risks, including increased potential for tumorigenesis from insertional mutagenesis. Furthermore, random insertion of the transgene produces a heterogeneous therapeutic product, as some cells integrate more copies of the transgene than others at different places in the genome. For clinical applications, however, a consistent and homogeneous therapeutic product should be the goal. To this end, we explore the potential and limitations of using CRISPR-CAS9 technology to genetically modify our PBiNSCs.

Thus, the following study explores the following two objectives:

(1) Optimize the genetic engineering of PBiNSCs to ectopically express and deliver membrane-bound TRAIL as an apoptotic factor

(2) Evaluate the impact of TRAIL delivery by our PBiNSCs on multiple primary glioblastoma cell lines, alone and in combination with potential sensitizing agents

Chapter 2

Methodology

2.0.1 Antibodies and Reagents

Anti-TRAIL (3219S) rabbit monoclonal antibody was purchased from Cell Signaling Technology. Anti-DR5 (69400) rabbit monoclonal antibody used for Western blot was also from Cell Signaling Technology. Markers of exosomes, including syntenin-1 (MA5-25984) and CD63 (MA5-43894), were detected using mouse monoclonal antibodies from Thermo Fisher Scientific. Probing for the housekeeping protein GAPDH was performed using an anti-mouse antibody from Abcam (ab8245).

For flow cytometry, human anti-DR5 PE-conjugated antibody (FAB6311P-025) was obtained from R&D Systems. For immunocytochemistry, anti-cleaved caspase-3 (9664S) rabbit antibody was purchased from Cell Signaling Technology.

Small molecule drugs used in this study included AZD7648, a DNA-PK inhibitor (TOCRIS), reconstituted in DMSO; AZD5582, an IAP antagonist (Sigma-Aldrich), reconstituted in DMSO; ARV-771 (Selleck Chemicals); SNS-032 (Selleck Chemicals); and APG-115 (Selleck Chemicals). Human recombinant IFN-gamma was purchased from R&D Systems.

2.0.2 Cell culture

PBiNSCs were provided by the Brüstle lab (89). Cells were cultured following their protocol (89). PBiNSCs were maintained on Matrigel-coated plates in DMEM/F12: Neurobasal (1:1) (Thermo Fisher) supplemented with N2, B27, Penstrep, L-gluamine, CHIR99021, A83-01, purmorphamine, hLIF, and LAAP. For routine maintenance, cultures were split twice weekly and passaged up to a maximum of 32 passages. Cells were passaged using pre-warmed accutase for 5 minutes at $37°$C. The single cell suspension was then diluted and centrifugaed at 1200 rpm for 4 minutes to obtain a cell pellet. The pellet was resuspended in fresh media and replated. Cultures were maintained at $37°$C under low oxygen conditions (5% O2 and 5% CO2).

Primary glioblastoma cells (PriGOs) were isolated from patients undergoing surgical resection for GBM at The Ottawa Hospital, as previously described (144). PriGOs were grown on laminin-coated flasks in Neurobasal-A medium (Thermo Fisher) supplemented with EGF, FGF, and heparin. Cell cultures were passaged and maintained using the same procedures as PBiNSCs.

2.0.3 CRISPR-CAS9 editing

All CRISPR-Cas9 reagents were purchased from Integrated DNA Technologies (IDT). The gRNA was formed by annealing the Alt-R™ CRISPR-Cas9 crRNA and tracrRNA at a 1:1 molar ratio by heating to $95°$C for 5 minutes. The RNP complex was then formed by incubating 1.4 ul of gRNA at 50uM and 1ul of Alt-R™ S.p. Cas9 Nuclease V3 at 62uM for 20 minutes. PBiNSCs were dissociated into single-cell suspension using pre-warmed Accutase. 500,000 PBiNSCs were pelleted and resuspended in 20ul of Lonza's P3 solution with the provided supplement. The RNP complex was added to the cell suspension. The final mixture was then nucleofected using the Lonza 4D-Nucleofector with pulse code DR114 in the cuvette format. Immediately after nucleofection, PBiNSCs were plated in 12-well plates using pre-warmed culture media supplemented with ROCK inhibitor. Media was changed every 24 hours until cells reached $>50\%$ confluence, after which media was changed every other day. CRISPR-edited PBiNSCs were maintained and passaged as described above until downstream applications.

All editing efficiencies reported were obtained using the Alt-R™ Cas9 Electroporation Enhancer, with 1ul of enhancer added to the final RNP mix. For HDR, the HDR template was synthesized from IDT as HDR Donor Blocks and resuspended at 500ng/ul. The appropriate amount (in ug) was then added to the RNP mixture for each reaction. All crRNA sequences are reported in Supplementary Figure 1. All HDR template sequences are presented in Supplementary Figures 2-5.

2.0.4 Editing efficiency using TIDE analysis

CRISPR-edited PBiNSCs were expanded for genomic DNA (gDNA) extraction using the Monarch Genomic DNA Purification Kit (New England Biolabs). A total of 3 million cells were collected and pelleted for gDNA extraction, following the manufacturer's protocol. The genomic region surrounding the predicted CRISPR cut site was amplified by PCR using primer sets purchased from IDT, with sequences provided in Supplementary Figure 1. PCR reactions were performed using Platinum™ SuperFi II PCR Master Mix, with 10ng of gDNA and primers at a final concentration of 2.5uM. Thermocycler conditions for all reactions were run at an annealing temperature of $56.2°$C for 35 cycles. The PCR product was resolved on a 1.5% agarose gel, and the correct band was extracted using the Monarch DNA Gel Extraction Kit (New England Biolabs). The purified PCR product was sent for Sanger sequencing at the Ottawa Hospital Research Institute (OHRI) core research facility, following their recommended template and primer concentrations. Sequencing results were analyzed using the Netherlands Cancer Institute TIDE software to obtain editing efficiency (https://tide.nki.nl/) (145).

2.0.5 Cell confluence following CRISPR-editing

Immediately after CRISPR editing, cells were treated with AZD7648 for 24 hours, after which the media was replaced with fresh growth media. Cellular confluence was assessed at 24, 48, and 72 hours post-nucleofection to evaluate cell viability. Images were acquired using a BioTek plate reader at 4× magnification with three independent fields of view per condition. Confluence was

quantified using ImageJ software and averaged across the three images.

2.0.6 Flow cytometry

PBiNSCs were prepared as single-cell suspensions. The desired number of cells for sorting was counted and pelleted out. Cells were resuspended in primary antibody diluted in PBiNSC media at the recommended concentration and incubated for 30 minutes at room temperature in the dark. Unbound antibody was removed by diluting the sample in 1mL of media and centrifuging cells down at 1200 rpm for 4 minutes. The final pellet was resuspended in 200 ul of PBiNSC media per 1 million cells. Viability dye 7-AAD was added at 4 ul per 1 million cells. Cells were filtered through a 40uM mesh prior to sorting.

All flow cytometry was performed at the OHRI Core Facilities (https://www.ohri.ca/FlowCytometry/) using the Beckman Coulter MoFlo XDP cell sorter.

For sorting GFP-positive cells, there was no primary antibody incubation step, and only viability dye needed to be added.

All flow data presented were generated using FlowJo™ v10.8 Software (BD Life Sciences).

2.0.7 TP53 gene sequencing

A total of 500,000 PriGOs were harvested, and RNA was extracted using the RNeasy Micro Kit (Qiagen) following the manufacture's protocol. RNA was reverse-transcribed into cDNA using primers (Supplementary Figure 1) and PCRs were performed following the OneStep RT-PCR Kit (Qiagen) recommendations. The resulting cDNA was resolved on a 1.5% agarose gel and gel-extracted for purification (Monarch DNA Gel Extraction Kit). The purified product was sent for Sanger sequencing at the OHRI sequencing facility, as mentioned above.

2.0.8 Lentiviral and plasmid constructs

Lentiviral and plasmid constructs were prepared from Addgene bacterial stabs. Stabs were streaked onto LB agar plates and incubated overnight at 37°C. Single colonies were picked and inoculated in 20mL of LB broth with ampicillin and cultured at 37°C with shaking at 220 rpm. This culture was used to make glycerol stocks by mixing with equal volumes of glycerol (100%). Large plasmid preparations were made from glycerol stocks using the Biobasic Maxiprep Plasmid DNA Extraction Kit, following manufacturer's instructions. Plasmid concentration and quality were determined by NanoDrop.

2.0.9 Lentiviral particle production and viral transduction

A four-plasmid system, pLP1, pLP2, pLP-VSVG, and the plasmid of interest, were transfected into HEK293T cells using Lipofectamine 2000 (Thermo Fisher) to create lentiviral particles. 48 hours after transfection, the virus-containing supernatant was collected and concentrated using Lenti-X Concentrator (Takara) at a 3: 1 volume ratio. The mixture was incubated overnight at 4°C with shaking. The following day, virus particles were pelleted by centrifugation at 1500 g for 40 minutes and resuspended in 1mL of Neurobasal-A medium.

HEK293T cells were cultured in DMEM supplemented with 10% heat-inactivated fetal bovine serum (FBS) and 0.1% penicillin–streptomycin.

PBiNSCs were cultured to 70–80% confluence. Viral particles (1 mL) were added to the culture media and removed the following day by replacing the culture media. Cells were then subjected to puromycin selection for 72 hours at a concentration of 0.6 µg/mL.

2.0.10 Immunocytochemistry

Cells were seeded onto 6-well plates containing Matrigel- or laminin-coated coverslips at a density of 400,000 cells per well and allowed to adhere for 24 hours prior to processing. Cells were washed with PBS and fixed in 4% paraformaldehyde (PFA) for 10 minutes. After fixation, cells

were washed with PBS (3 times for 5 minutes each) and then blocked in 3% BSA in PBS with 0.3% Tween-20 (PBS-T) for 1 hour at room temperature. Primary antibody was diluted according to the manufacture's recommendations in 3% BSA in 0.3% PBS-T to be incubated overnight at $4°$C. The primary antibody was removed and cells were washed with PBS (3 times for 5 minutes each). Appropriate secondary antibodies conjugated to Alexa Fluorophore (1:500) and Hoechst (1:1000) were diluted in 0.3% PBS-T were then applied to coverslips for 1 hour at room temperature. Coverslips were mounted onto glass slides with mounting medium and imaged using a Zeiss Axioplan fluorescent microscope.

Experiments without permeabilization were performed in PBS instead of 0.3% PBS-T.

2.0.11 Western blot

Western blots were performed to probe for total protein in cell lysates. Cells were lysed in 1X RBC Lysis Buffer (Invitrogen). Lysates were briefly sonicated at 30 kHz and centrifuged at maximum speed for 10 minutes. Protein concentration was determined using the Pierce BCA assay (Thermo Fisher), with samples incubated at $37°$C and absorbance measured at 562 nm using a spectrophotometer. Equal amounts of protein were combined with 6ul of Laemmli buffer containing beta-mercaptoethanol and topped up with lysis buffer. Samples were heated at $95°$C for 5 minutes. Proteins were loaded into precast NuPAGE Bis-Tris Mini Protein Gels and run at 150 V for 1 hour. Following electrophoresis, proteins were were transferred from the gel to an Immobilon PVDF membrane (Millipore Sigma) using wet transfer for 1 hour at 100V or overnight at $4°$C at 30V. Amido Black stain was performed to assess equal protein loading.

Membranes were blocked with 5% milk in TBST for 1 hour with shaking, followed by incubation with primary antibody diluted in 5% milk in TBST for 1 hour at room temperature with shaking. The membrane was washed 3 times in TBST for 5 minutes each. HRP-conjugated secondary antibody was applied at a 1:5,000 dilution for 1 hour with shaking. Membrane is washed with TBST (3 times, each for 5 minutes). HRP substrate (Millipore Sigma) was applied to the membrane, and the membrane was imaged using a ChemiDoc (Bio-rad). A colorimetric image of

the ladder was taken at 0.2 sec exposure, followed by a chemiluminescent image. Images were merged to obtain a full blot.

To confirm equal loading, membranes were stripped using stripping buffer for 15 minutes with shaking and re-probed for GAPDH following the same method.

2.0.12 Cytotoxity co-culture assays

PriGOs were plated on Matrigel-coated 96 well plates at a density of 5,000 cells per 50ul per well. PBiNSCs were subsequently added at the appropriate target-to-effector ratio in each well. Cells were allowed to adhere overnight. Fresh media (100ul) is changed after 24 hours, along with drug treatment if needed. 72 hours after the media change, each well was washed with PBS and the media replaced with 50ul of fresh media before measuring fluorescence intensity (Mean RFU) using the Biotek plate reader.

All experiments were performed using fully supplemented PBiNSC media.

2.0.13 Cytotoxicity with conditioned media

PriGOs were seeded on coverslips in 6-well plates at a density of 200,000 cells per well and allowed to adhere for 24 hours prior to processing. Conditioned media collected from PBiNSC cultures was centrifuged at 3,500 rpm for 20 minutes to remove cell debris and passed through a 0.22 uM filter. 2 mL of filtered conditioned media was added to each well. Following the treatment period, cells were processed according to the immunocytochemistry protocol.

2.0.14 Exosome purification

Exosomes were isolated from PBiNSC conditioned media using a differential centrifugation protocol (146). Approximately 7 million PBiNSCs were plated in T75 flasks with 15mL of fully supplemented PBiNSC media and cultured for 72 hours. The conditioned media was collected and centrifuged at 3,500 rpm for 20 minutes at 4°C to remove cell debris (Thermo Scientific Sorvall

ST 40 R Centrifuge). The supernatant was passed through a 0.22 uM filter and centrifuged at 20,000 g for 20 minutes at 4°C (Beckman Coulter Optima L-100 XP Ultracentrifuge). The final supernatant was further spun at 120,000 g for 1.5 hours at 4°C (Beckman Coulter Optima L-100 XP Ultracentrifuge). The resulting exosome pellet was resuspended in 150 ul of filtered 25 mM trehalose.

2.0.15 In vivo mouse injections and immunohistochemistry

PBiNSCs were labeled with GFP via lentiviral transduction, with expression driven by the CMV promoter alongside a hygromycin selection marker. Cells were maintained under hygromycin (200 ug/mL) selection for one week. PBiNSCs tested negative for mycoplasma prior to injections. On the day of injection, PBiNSCs were dissociated into single-cell suspensions. A total of 500,000 cells were pelleted by centrifugation, and resuspended in 50 uL of room-temperature DPBS.

Female Fox SCID beige mice underwent stereotaxic striatal injections with 100,000 PBiNSCs per mouse. Three mice received wildtype PBiNSCs labeled with GFP, while three mice received TRAIL-DR5KO-PBiNSCs labeled with GFP. Mice were monitored for one month, after which they were euthanized. Brains were extracted, perfused with 4% PFA, and embedded in OCT. Samples underwent coronal cryosectioning. Staining was performed with Hoechst and anti-TRAIL antibody (1:200) from Cell Signaling.

All injections and immunohistochemistry were performed by Margarita Lui.

2.0.16 Statistical analysis

All graphs were generated using GraphPad Prism version 10. Error bars represent standard error of the mean. All statistical analyses were performed as independent, non-parametric Mann–Whitney tests, with $P < 0.05$ considered statistically significant.

Chapter 3

Results

3.1 Genetic engineering of neural stem cells

3.1.1 Optimized protocol for CRISPR-Cas9 editing in PBiNSCs: delivery of ribonucleoproteins

Nucleofection efficiency is in part dependent on the pulse code parameters of the LONZA-4D system. The delivery of proteins and genetic material, such as RNPs, into cells is determined by the electrical parameters, including voltage and pulse duration, applied during electroporation, which alter cell membrane permeability. Pulse codes are selected on the basis of cell type and the nature of material being transfected. Publicly available data sourced from Lonza's database (knowledge.lonza.com) provide several pulse codes recommendations that have been successful for other users. Based on publications involving similar cell types, we selected four pulse codes for testing: CA137, CL133, DC104, and DR114.

As an initial readout, we transfected a small GFP-encoding plasmid, in the absence of RNPs, into PBiNSCs to determine optimal pulse code based on cell viability and GFP-positive population following nucleofection. Cellular viability was similar across all tested programs 48 hours post-nucleofection (Figure 3.1A). Percentage of positive GFP cells, however, varied between conditions: DR114 yielded the highest proportion of GFP expressing cells (Figure 3.1A). These results

suggest that pulse code DR114 most effectively allowed for the intracellular delivery of small plasmids considering viability and transgene expression. All subsequent nucleofection experiments with PBiNSCs were performed using pulse code DR114.

For RNP delivery, we used the gRNA:CAS9 ratios recommended in publicly available Integrated DNA Technologies (IDT) protocols (147). While further optimization is possible, the conditions used in initial experiments yielded satisfactory levels of CRISPR-editing for our purposes (Figure 3.1B). Following these optimized steps, PBiNSCs were targeted at two safe harbour sites. Genomic safe harbour sites are regions in the genome that allow for stable integration of exogenous genetic material without obvious adverse effects on the cell. The AAVS1 locus is one well-characterized safe harbor site, commonly used in gene engineering to achieve robust transgene expression. The guide RNA (gRNA) sequence used to target the AAVS1 locus was borrowed from Schubert et al., who evaluated multiple gRNA sequences for the AAVS1 locus and identified the gRNA with the highest on-target editing efficiency and lowest off-target score (148). We also investigated the CLYBL site, which was recently reported to enable 10-fold higher transgene expression than the AAVS1 site (149). We borrowed the gRNA sequence used in that study for targeting to the CLYBL locus.

Optimized cutting at the AAVS1 and CLYBL loci shows high editing efficiencies of 84% and 98% , respectively (Figure 3.1C), as determined by TIDE analysis following CRISPR-editing. Interestingly, the indel spectrum at both sites was similar with a single-base deletion being the predominant mutation generated at the cut site, followed by a single-base insertion as the second most frequent event (Figure 3.1C).

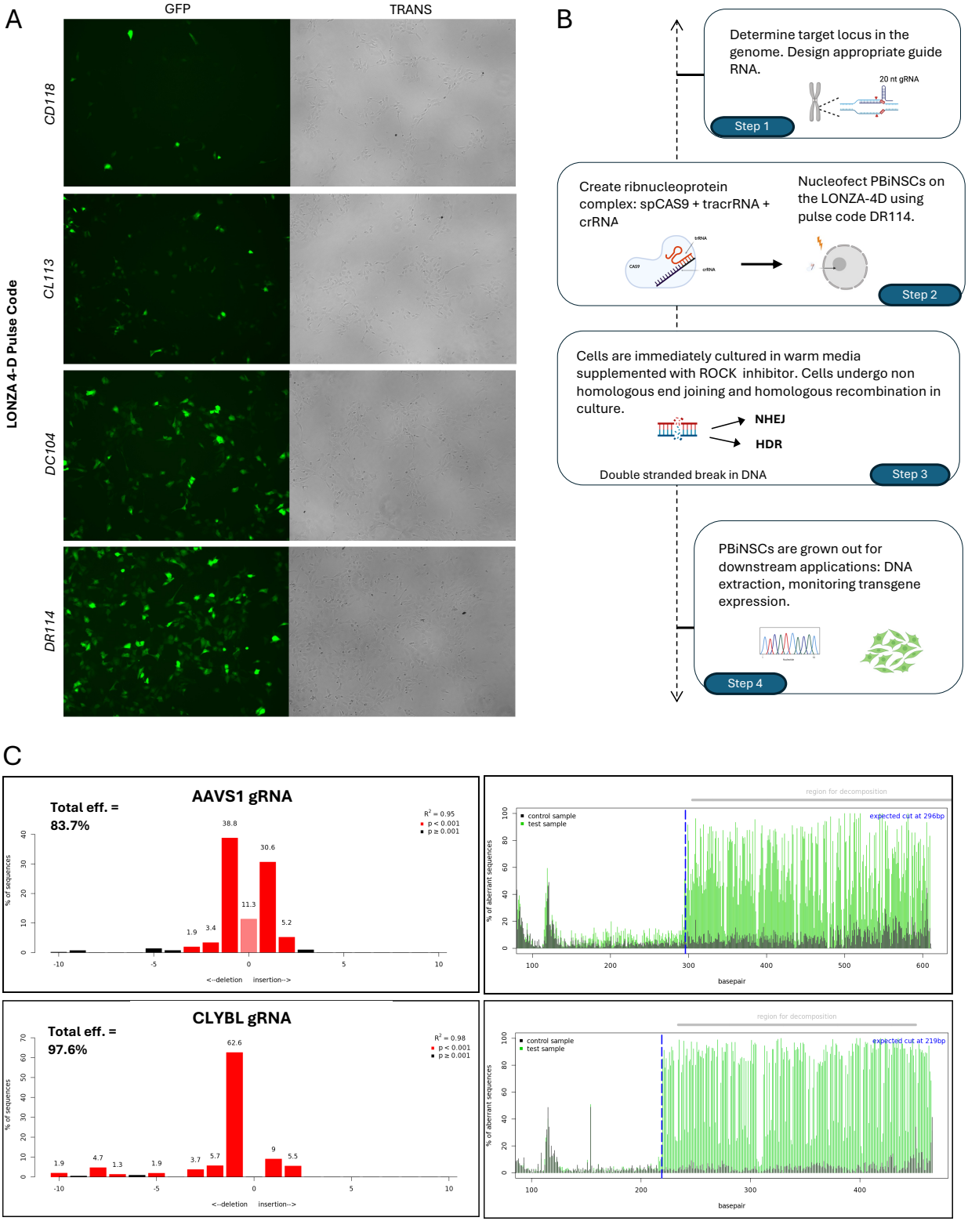
A
GFP
TRANS
LONZA 4-D Pulse Code
CD118
CL113
DC104
DR114
B
Determine target locus in the genome. Design appropriate guide RNA.
20 nt gRNA
Step 1
Create ribnucleoprotein complex: spCAS9 + tracrRNA + crRNA
Nucleofect PBiNSCs on the LONZA-4D using pulse code DR114.
Step 2
Cells are immediately cultured in warm media supplemented with ROCK inhibitor. Cells undergo non homologous end joining and homologous recombination in culture.
NHEJ
HDR
Double stranded break in DNA
Step 3
PBiNSCs are grown out for downstream applications: DNA extraction, monitoring transgene expression.
Step 4
C
AAVS1 gRNA
Total eff. = 83.7%
CLYBL gRNA
Total eff. = 97.6%
% of sequences
<--deletion insertion-->
% of aberrant sequences
basepair
control sample
test sample
expected cut at 296bp
expected cut at 219bp

Figure 3.1: **Optimized protocol for CRISPR-Cas9 editing in PBiNSCs (A)** Nucleofection of 400 ng pmaxGFP (from LONZA) into 400,000 PBiNSCs with pulse codes CA137, CL133, DC104, and DR114. Images were acquired 24 hours later under GFP and brightfield channels at 10x magnification using the EVOS microscope. **(B)** Schematic overview of the optimized CRISPR-Cas9 editing process in PBiNSCs. **(C)** Indel spectrum and aberrant sequence signal for two gRNAs targeting genomic safe harbor sites. Cells were nucleofected with CRISPR reagents using pulse code DR114, and genomic DNA was extracted one week later for Sanger sequencing. Editing efficiency is determined from TIDE analysis from sequencing files from the forward primer.

3.1.2 Successful targeting of genes for protein knockout in PBiNSCs: lethal giant larvae protein homolog 1 (LLGL1) and death receptor 5 (DR5)

We next tested the targeting of coding sequences for protein knockout in our PBiNSCs using our optimized CRISPR protocol.

Previous work in our lab was interested in the role of LLGL1 in glioblastoma, specifically related to its effect on cellular motility and maintenance of stem cell characteristics. We tested to see if knockout of LLGL1 protein function in PBiNSCs can improve tumor-homing abilities. To identify an appropriate gRNA sequence for LLGL1 targeting, we used IDT's predesigned Alt-R CRISPR-Cas9 guide RNA library (`https://www.idtdna.com/site/order/designtool/index/CRISPR_SEQUENCE`). IDT's predesigned gRNA library make recommendations based on on-target score and off-target score derived in part from the company's internal in vivo data set (148). The LLGL1 gRNA sequence was selected based on the best combination of predicted on-target and off-target scores, as well as its likelihood for full protein knockout by targeting an early exon. TIDE analysis revealed LLGL1 gRNA had an editing efficiency of 27.2% (Figure 3.2A). Validation of LLGL1 protein expression following CRISPR-editing is still needed.

We also tested the endogenous DR5 receptor for knockout in PBiNSCs using two different gRNAs. Reasons for DR5 knockout are highlighted later on in this chapter. The first gRNA (DR5 gRNA-1) was developed using IDT's tool, as described above. The second gRNA (DR5 gRNA-2) was based on UCSC Genome Browser's CRISPR/CAS9 Target track, which lists targetable sites in the genome based on the SpCas9 enzyme and its PAM sequence -NGG. The DR5 gRNA-2 was chosen for its high Doench/Fusi score of 97%, which predicts strong cleavage efficiency based on a machine learning model.

Both guide sequences target exon 1 of the gene for complete protein knockout. The predicted cut site of both gRNA is illustrated in Figure 3.2B, where DR5 gRNA-1 disrupts codon 59 and DR5 gRNA-2 interrupts the AUG start codon.

A

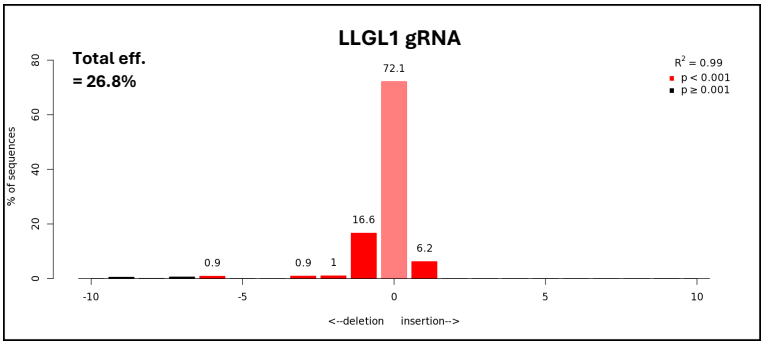

B

DR5 gRNA-1 (5'- 3'): GACAACGAGCACAAGGGTCT

DR5 gRNA-2 (5'- 3'): CTGTCCCCGTTGTTCCATGG

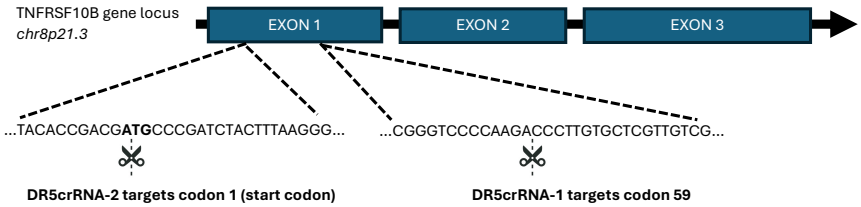

C

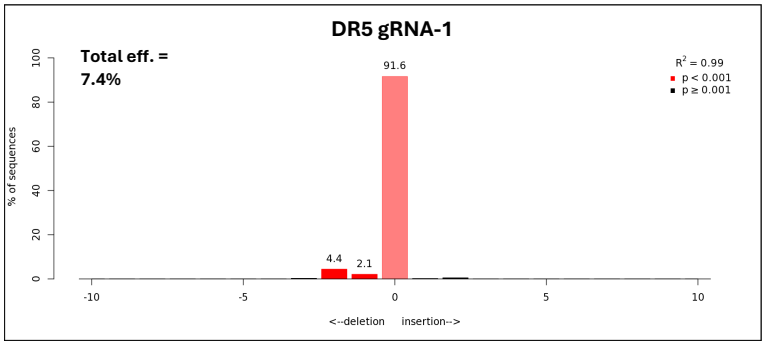

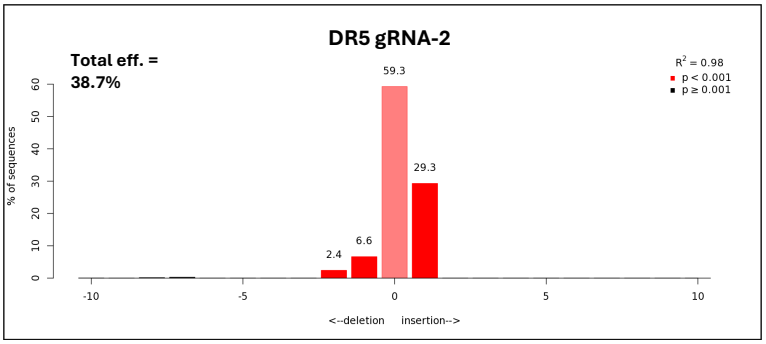

Figure 3.2: **Targeting of gene coding regions in PBiNSCs using CRISPR-Cas9 (A)** Indel spectrum generated from guide RNA targeting the LLGL1 locus in PBiNSCs. PBiNSCs are edited using the protocol developed above and cultured for a week prior to genomic DNA extraction. PCR product is sent for sequencing using the forward primer. Editing efficiency is determined using TIDE analysis. **(B)** Schematic representation of two guide RNAs targeting exon 1 of the endogenous DR5 locus for protein knockout. **(C)** Indel spectrum of the two DR5 gRNAs with associated editing efficiencies. PBiNSCs are edited following the same protocol as mentioned above. TIDE analysis presented here is using the forward primer.

TIDE analysis shows different efficiencies of the predesigned gRNAs. Editing efficiency for DR5 gRNA-1 is 7.4%, while that of DR5 gRNA-2 is 38.7% (Figure 3.2C). Given its higher efficiency and the lack of observed differences in cell viability post-nucleofection, DR5 gRNA-2 was used for all subsequent DR5 knockout experiments

Flow cytometry reveals that targeting with DR5 gRNA-2 resulted in complete protein loss in approximately 34% of the cell population (Figure 3.3A). This suggests a substantial proportion of cells underwent biallelic knockout. These DR5-negative cells were isolated through flow sorting (DR5KO-PBiNSCs) and expanded prior to Western blot analysis, which confirmed near complete DR5 loss in total cell lysates as well (Figure 3.3.B). Importantly, DR5KO-PBiNSCs continued to propagate normally in culture, demonstrating that DR5 protein knockout is possible without adversely affecting cellular viability or proliferation.

A

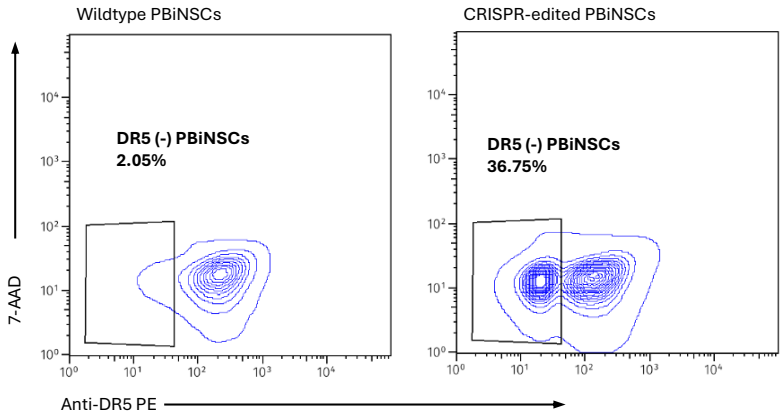
Wildtype PBiNSCs
CRISPR-edited PBiNSCs
DR5 (-) PBiNSCs
2.05%
DR5 (-) PBiNSCs
36.75%
7-AAD
Anti-DR5 PE

B

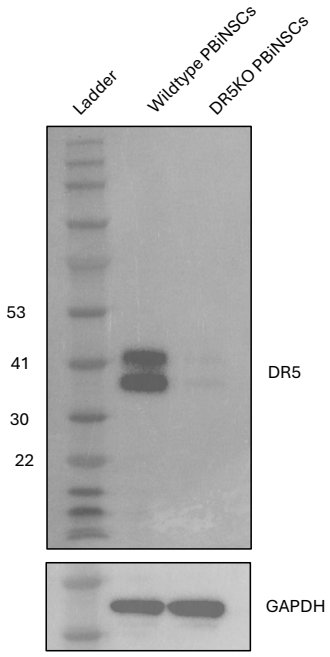
Ladder
Wildtype PBiNSCs
DR5KO PBiNSCs
53
41
30
22
DR5
GAPDH

Figure 3.3: **DR5 protein expression following CRISPR-mediated knockout using DR5 gRNA-2 (A)** Flow cytometry of surface expression of DR5 in PBiNSCs following CRISPR knockout of the DR5 receptor. **(B)** Western blot analysis of total endogenous DR5 protein levels in PBiNSCs. Cell lysates were collected from DR5 knockout cells, which were previously sorted to enrich for negative DR5 cells.

3.1.3 Effective targeted integration of expression cassettes can be achieved using synthetic DNA templates; however, sustained high level transgene expression was not achieved.

After ensuring high cutting efficiency with the optimized protocol and designed gRNAs described in section 2.1.1, attempts were made for targeted transgene knock-in through homology directed repair (HDR) in PBiNSCs. Multiple expression cassettes were designed using different combinations of promoters, regulatory elements, and integration sites (Figure 3.4A). Careful considerations were made during the design of these cassettes given that large templates pose potential toxicity problems while also negatively impacting knock-in efficiency. The cytomegalovirus (CMV) promoter is a strong and ubiquitous driver of transgene expression in mammalian systems. The human elongation factor 1 alpha (EF1-alpha) promoter was found to protect against silencing and allow for long-term expression in stem cells. Here, we used the core sequence to minimize toxicity from large sequence knock-ins. The SV40 polyadenylation sequence ensures proper cleavage of the transcript and addition of a poly-A-tail. The Woodchuck Hepatitis Virus Posttranscriptional Regulatory Element (WPRE) is widely used to stabilize mRNA and enhance transgene expression.

Nucleofection of synthetic double-stranded DNA donor templates (IDT donor blocks) alongside the RNP complex resulted in substantial cell death. For large templates (˜2000 bp), it was necessary to titrate the donor template concentration in the final solution. We found that 0.5 µg of template in the final CRISPR mixture was optimal as 1 µg caused excessive cell death post-nucleofection and 0.25 µg resulted in low HDR efficiency (Figure 3.4C). HDR efficiency was assessed as the percentage of the cell population expressing the target transgene; in this case, GFP was used as an easy readout of overall efficiency.

HDR efficiency, as determined by transgene expression, at the AAVS1 locus with template 1 was approximately 4.3% (Figure 3.4C). Successful knock-in of the template 1 at the AAVS1 locus was further confirmed by PCR at the predicted integration site (Figure 3.4B). Red arrowheads in Figure 3.4.B indicate the DNA bands corresponding to the size of the genomic sequence with

integrated exogenous template. The lower bands, indicated by the blue arrow head, reveal cells without integration at the targeted site. Successful knock-in of exogenous DNA was also achieved using template 4 at the CLYBL site (Figure 3.4C).

Attempts to enrich for a fully GFP-positive population were ineffective using fluorescence-activated cell sorting (FACS). Successive FACS sorts increased the GFP-positive PBiNSC fraction to 77%; however, after multiple passages and continued culture, this population declined rapidly to 42% with subsequent sorts (Figure 3.4D). Fluorescence microscopy also revealed that, despite three prior rounds of enrichment through FACS, there remained a substantial population of GFP-negative cells. PCR analysis in Figure 3.4B of genomic DNA at the AAVS1 site confirmed that, despite three prior sorts, a subset of cells still lacked the integrated template (as indicated by the blue arrowhead).

Due to reports of epigenetic silencing of the CMV promoter, we tested the EF1-alpha core promoter (template 2) and the endogenous DR5 promoter (template 3) to drive transgene expression. HDR efficiency was approximately 3.69% with template 2 and 0.63% with template 3. Subsequent attempts to enrich for a fully GFP-positive population encountered the same issue as before, with GFP expression at the population level never exceeding 50%. Template 3 exhibited similar instability as template 1 and 2, despite using the endogenous DR5 promoter, indicating that the unstable GFP expression is not due to episomal expression from the donor template as template 3 lacks an exogenous promoter.

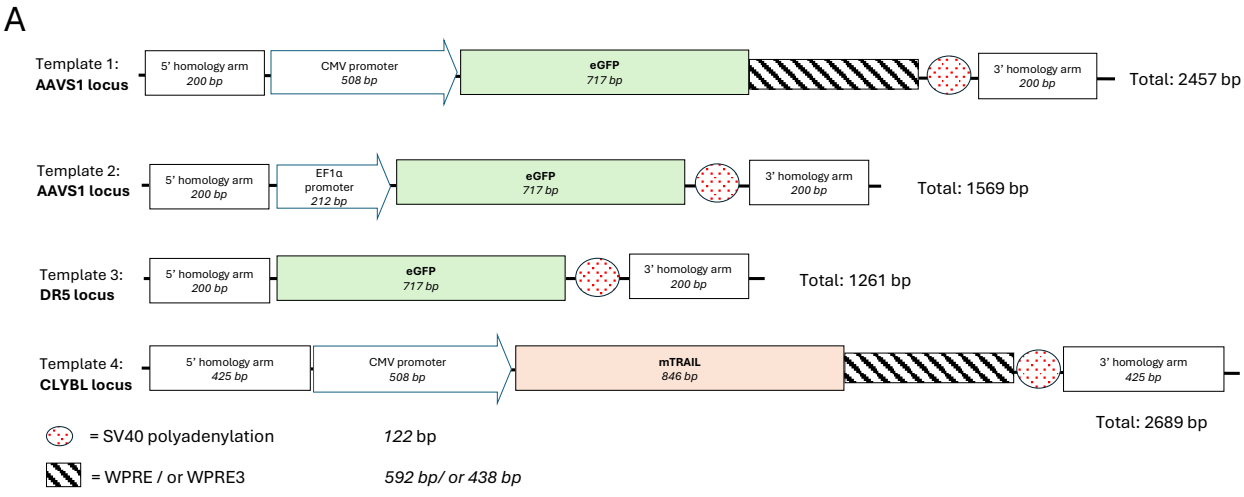

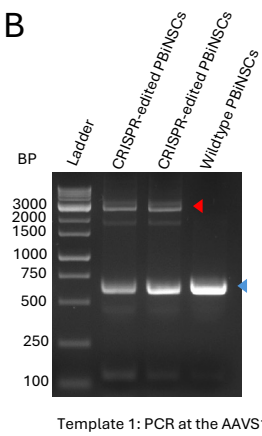

Template 1: PCR at the AAVS1 site

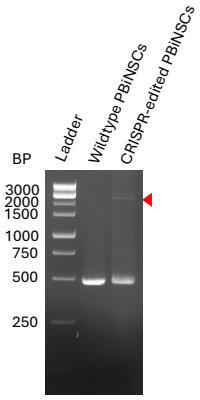

Template 4: PCR at the CLYBL site

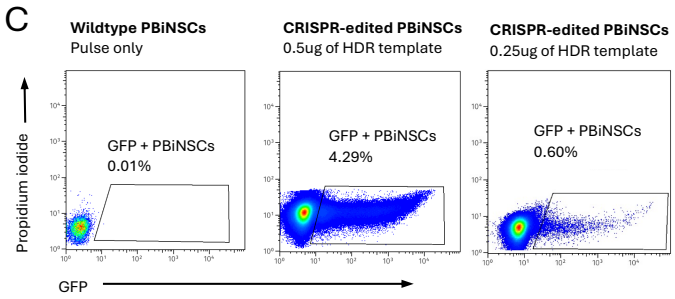

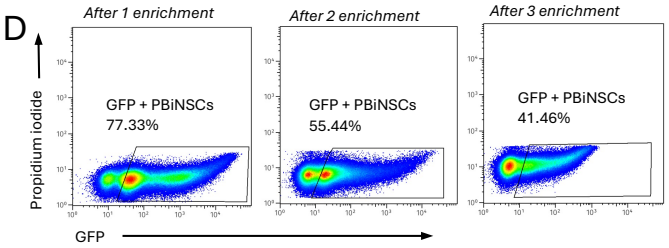

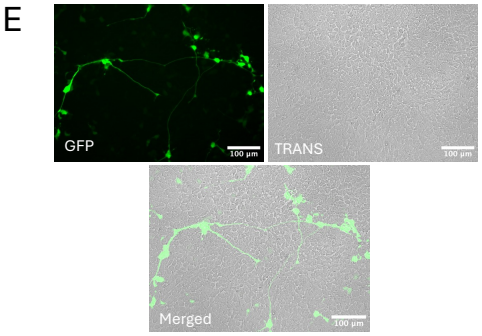

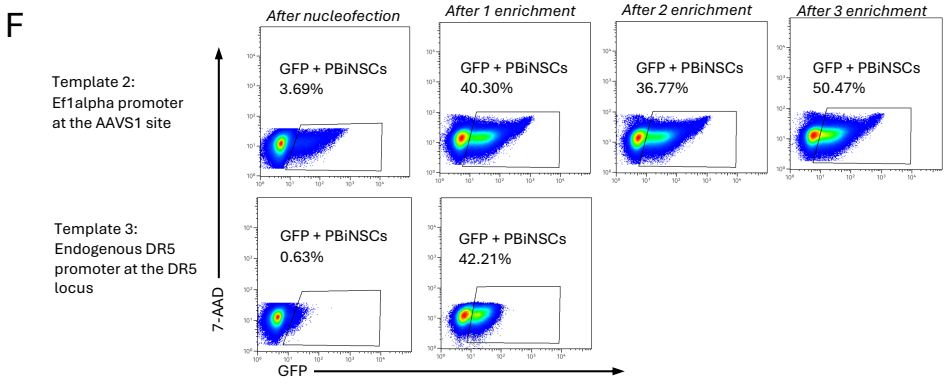

Figure 3.4: **Homology-directed repair (HDR) in PBiNSCs using CRISPR-Cas9 (A)** Schematic of synthetic DNA expression cassettes purchased as double-stranded DNA from IDT. Four templates were tested with varying knock-in loci, promoter sequences, and enhancer elements. **(B)** Gel electrophoresis of PCR product of knock-in sites following HDR editing. Positive GFP cells were isolated through three successive FACS sorts prior to genomic DNA extraction and processing. The larger band (red arrow) corresponds to successful knock-in, while the lower band indicates DNA without template integration. **(C)** Flow cytometric analysis of GFP expression following nucleofection with 0.5 µg and 0.25 µg of template 1. PBiNSCs were sorted two weeks after CRISPR-editing. **(D)** FACS of PBiNSCs following HDR knock-in using template 1 at the AAVS1 site. GFP-positive cells were isolated and cultured for 1 week prior to the next sort. Three enrichment attempts were made. **(E)** Fluorescence and brightfield images of HDR-edited PBiNSCs acquired several weeks post-editing at 10x magnification on the EVOS microscope. PBiNSCs were enriched three times prior to imaging using FACS sorting. **(F)** FACS enrichment of GFP-positive cells using different templates. PBiNSCs were edited using two different templates and enriched as described in image C.

3.1.4 Strategies to enhance homology directed repair are suboptimal, including transduction of p53 dominant-negative (p53dd) plasmid, use of a DNA-PK inhibitor (AZD7648), and transduction of Cas9 nickase plasmids

Emerging research in the CRISPR–Cas9 field has focused on addressing common challenges such as toxicity and low HDR efficiency. This section examines strategies successfully applied in other studies. Toxic responses to CRISPR editing arises at various stages of the process.

DNA-PK inhibitor (AZD7648)

Studies have shown that blocking the activity of DNA-dependent protein kinase (DNA-PK) can enhance HDR efficiency. DNA-PK inhibition suppresses the non-homologous end joining (NHEJ) pathway whereby forcing cells to repair Cas9-induced double-strand breaks through homology-directed repair (HDR). AZD7648 has been reported to increase HDR efficiency across different cell lines and genomic loci (150). In our experiments, we observed a slight increase in HDR efficiency using AZD7648 at a concentration of 5 μM post-nucleofection (Figure 3.5A). However, we also noted mild toxicity, reflected in reduced cell confluence after plating (Figure 3.5B). Additional repeats are required to determine whether this effect is statistically significant.

p53DD plasmid

Transient inhibition of p53 using p53dd, a dominant negative mutant of the p53 protein, has been found in studies to improve toxicity and HDR efficiency simultaneously. In our experiments, co-delivery of a p53DD plasmid during the nucleofection step did not improve cell viability following CRISPR-editing, instead resulted in massive amounts of cell death (Figure 3.5C).

CAS9-nickase plasmids

Different versions of the Cas9 enzyme have been developed to improve editing efficiency and cell viability. Cas9-nickase is a variant that introduces nicks, or single-stranded breaks**,** in the genomic DNA instead of double-stranded breaks. Studies report this process is less toxic and mutagenic. CRISPR-nickase plasmids were borrowed from Wang et al (151).

We found that nucleofection and lipofection of large plasmids encoding Cas9-nickase were toxic to PBiNSCs. Large plasmid DNA amounts (4.8 µg) resulted in extensive cell death within 24 hours post-nucleofection (Figure 3.5D). Delivery of lower amounts of plasmid (0.4 µg) supported cell viability and survival. However, when cells were grown out and subjected to puromycin selection for transgene insertion over several weeks, all cells died within 24 hours of selection. Further optimization might be required to use the Cas-9 nickase system successfully in PBiNSCs.

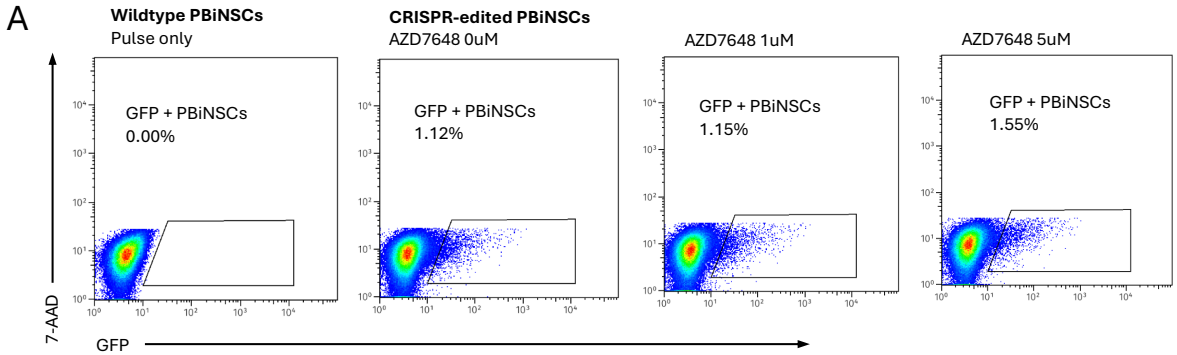
A
Wildtype PBiNSCs
Pulse only
CRISPR-edited PBiNSCs
AZD7648 0uM
AZD7648 1uM
AZD7648 5uM
GFP + PBiNSCs
0.00%
GFP + PBiNSCs
1.12%
GFP + PBiNSCs
1.15%
GFP + PBiNSCs
1.55%
7-AAD
GFP

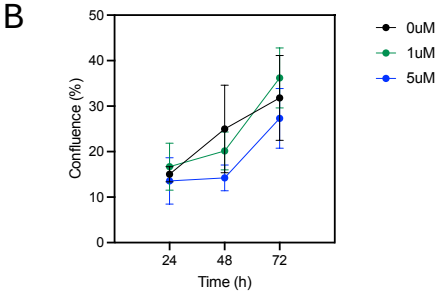
B
Confluence (%)
Time (h)
0uM
1uM
5uM

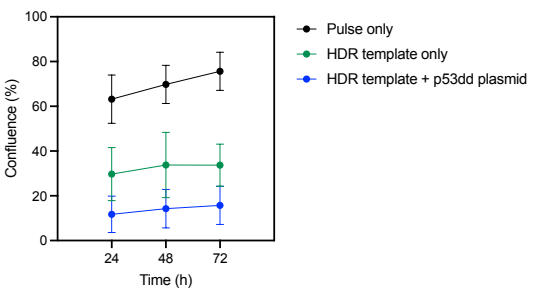
C
Confluence (%)
Time (h)
Pulse only
HDR template only
HDR template + p53dd plasmid

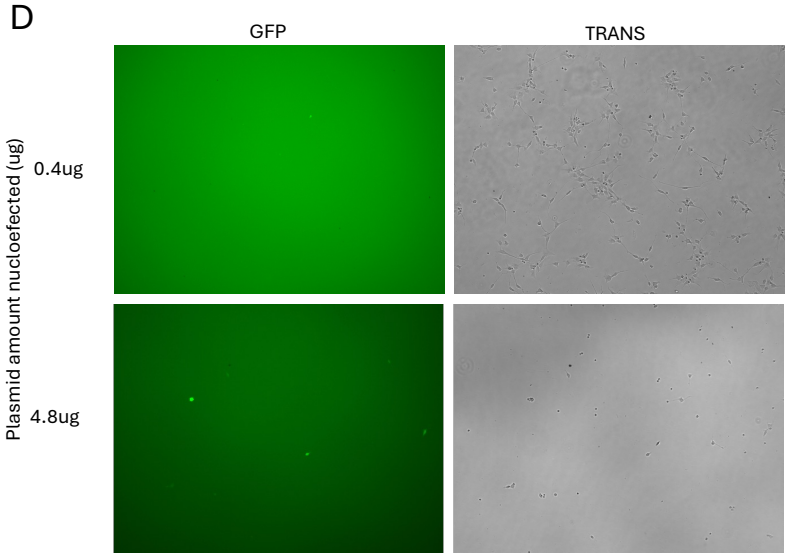
D
GFP
TRANS
Plasmid amount nucloefected (ug)
0.4ug
4.8ug

Figure 3.5: **Strategies to improve HDR efficiency in PBiNSCs (A)** Flow cytometry was used to assess GFP expression following HDR-editing and treatment with various concentrations of AZD7648. Cells were edited using 0.25 µg of template 2. AZD7648 (0, 1 or 5 µM) was added immediately after plating, and drug was removed 24 hours later and replaced with fresh media. **(B)** Cell confluence was assessed after CRISPR HDR-editing with AZD7648 treatment at concentrations of 1 µM or 5 µM. Phase-contrast images were acquired at 24, 48, and 72 hours post-nucleofection. Confluence was quantified using Fiji and averaged across three independent fields of view. Error bars indicate the standard error of the mean (SEM). **(C)** PBiNSCs were HDR-edited alongside delivery of p53dd plasmid. PBiNSCs were nucleofected with 0.5 µg of template 4. In the HDR + p53dd plasmid condition, 1 µg of p53dd was added to the CRISPR cocktail and co-delivered alongside the template DNA. Phase-contrast images were acquired at 24, 48, and 72 hours post-nucleofection. Confluence was quantified using Fiji and averaged across three independent fields of view. Error bars indicate the standard error of the mean. **(D)** PBiNSCs were nucleofected for the CAS9-nickase plasmid alongside other plasmids encoding for the gRNA sequence and DNA template. Using pulse code DR114, different total plasmid concentrations were tested (0.4 and 4.8 µg). Images were taken 24 hours later using the EVOS microscope under both GFP and brightfield channels.

3.2 Exogenous TRAIL Expression in Neural Stem Cells

3.2.1 Exogenous expression of full-length TRAIL from lentiviral vectors in PBiNSCs

To investigate the potential of genetically modifying PBiNSCs for TRAIL delivery, our lab previously engineered PBiNSCs to express the membrane bound variant of the TRAIL protein through lentiviral transduction. The full-length human TRAIL sequence was obtained from Roybal et al. and was PCR-amplified and ligated into a third-generation lentiviral expression vector from Addgene (152). This new construct expresses membrane TRAIL under the CMV promoter alongside a puromycin resistance gene for selection. Lentiviral particles were produced by co-transfecting 293T cells with the TRAIL vector and packaging plasmids. PBiNSCs were transduced with TRAIL lentivirus and selected with puromycin for 3 days to obtain a population of expressing cells (TRAIL-PBiNSCs). Successful expression of exogenous TRAIL in PBiNSCs was confirmed by Western blot by probing total cell lysates. A band corresponding to the expected molecular weight of the membrane monomer protein at approximately 28 kDa was present only in the transduced PBiNSC population (Figure 3.6A). An additional higher molecular weight band at approximately 54 kDa was also observed. This size likely corresponds to multimeric forms of TRAIL that were not fully denatured (153).

Immunocytochemistry was performed to visualize localization of membrane TRAIL in PBiNSCs. In non-permeabilized cells, TRAIL staining was scarce and punctate, appearing in tiny clusters near the nuclei (Figure 3.6C). In contrast, permeabilized cells displayed a markedly stronger TRAIL signal, indicating that most TRAIL expression resides intracellularly. This intracellular pool may represent newly synthesized TRAIL within the secretory pathway (e.g., endoplasmic reticulum and Golgi apparatus) or internalized protein undergoing endocytic recycling.

TRAIL expression in PBiNSCs appeared unstable over multiple passages. Expression declined rapidly and markedly, as indicated by a nearly 23.2-fold decrease in protein levels observed on the Western blot (Figure 3.6B).

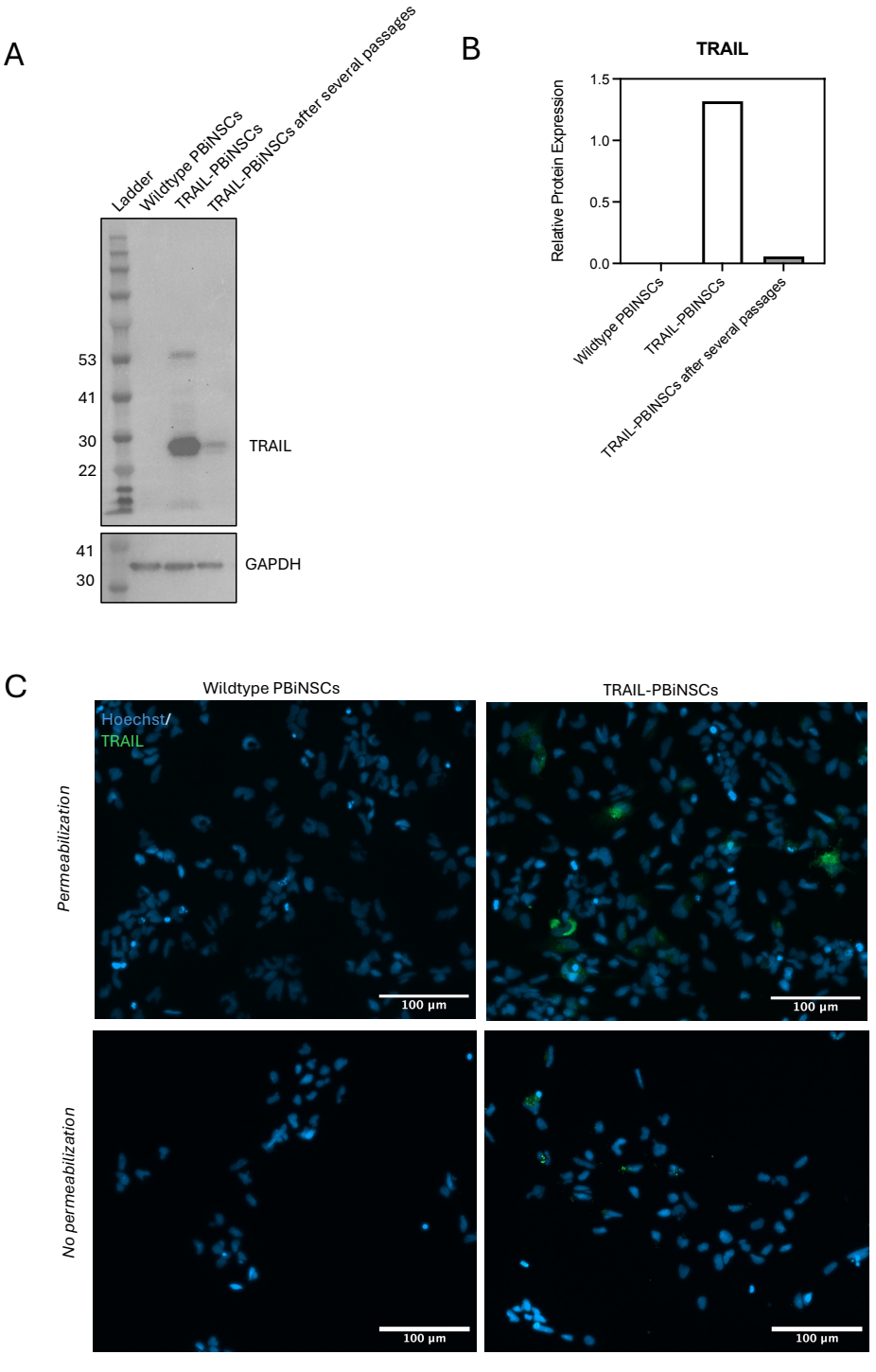
A
Ladder
Wildtype PBiNSCs
TRAIL-PBiNSCs
TRAIL-PBiNSCs after several passages
53
41
30
22
TRAIL
41
30
GAPDH
B
TRAIL
Relative Protein Expression
1.5
1.0
0.5
0.0
Wildtype PBiNSCs
TRAIL-PBiNSCs
TRAIL-PBiNSCs after several passages
C
Wildtype PBiNSCs
TRAIL-PBiNSCs
Hoechst/
TRAIL
Permeabilization
No permeabilization
100 µm
100 µm
100 µm
100 µm

Figure 3.6: **Protein expression in PBiNSCs following lentiviral transduction of full-length TRAIL (A)** Western blot showing TRAIL expression in total cell lysates. Lysates were collected from wildtype PBiNSCs, freshly transduced PBiNSCs, and TRAIL-transduced PBiNSCs after several passages. GAPDH was used as a loading control. **(B)** Quantification of TRAIL protein expression from the Western blot using Fiji. **(C)** TRAIL expression in PBiNSC cultures assessed by immunocytochemistry. Top row: PBiNSCs were processed using the permeabilizing agent Tween-20. Bottom row: PBiNSCs were processed without permeabilization.

3.2.2 Significant autotoxicity observed in NSCs transduced for exogenous TRAIL expression

Previous work from our lab monitoring the growth of TRAIL-transduced PBiNSCs showed that this population proliferated more slowly and reached a growth plateau earlier than non-transduced controls. Others have also reported a similar reduction in proliferative capacity after transduction for exogenous TRAIL expression (154).

To determine whether TRAIL transduction in PBISNCs induced apoptosis in PBiNSCs themselves, we assessed for cleaved caspase-3 signal, a key downstream effector of TRAIL signaling via the extrinsic apoptotic pathway. Staining for cleaved caspase-3 (CC3) revealed a significantly higher proportion of apoptotic cells in the TRAIL-transduced PBiNSC population compared to wildtype PBiNSCs (7.5-fold increase, P = 0.004; Figure 3.7A). Consistent with these findings, Hoechst nuclear staining showed an increased presence of condensed and fragmented nuclei, hallmarks of apoptotic morphology. These results suggest that the attenuated proliferation and growth of TRAIL-PBiNSCs can be attributed to elevated apoptotic activity from ectopic TRAIL expression and signaling within the population. Furthermore, TRAIL-mediated cytotoxicity in PBiNSCs could also explain the unstable TRAIL expression observed as a decrease in TRAIL protein levels in total cell lysates over multiple passages.

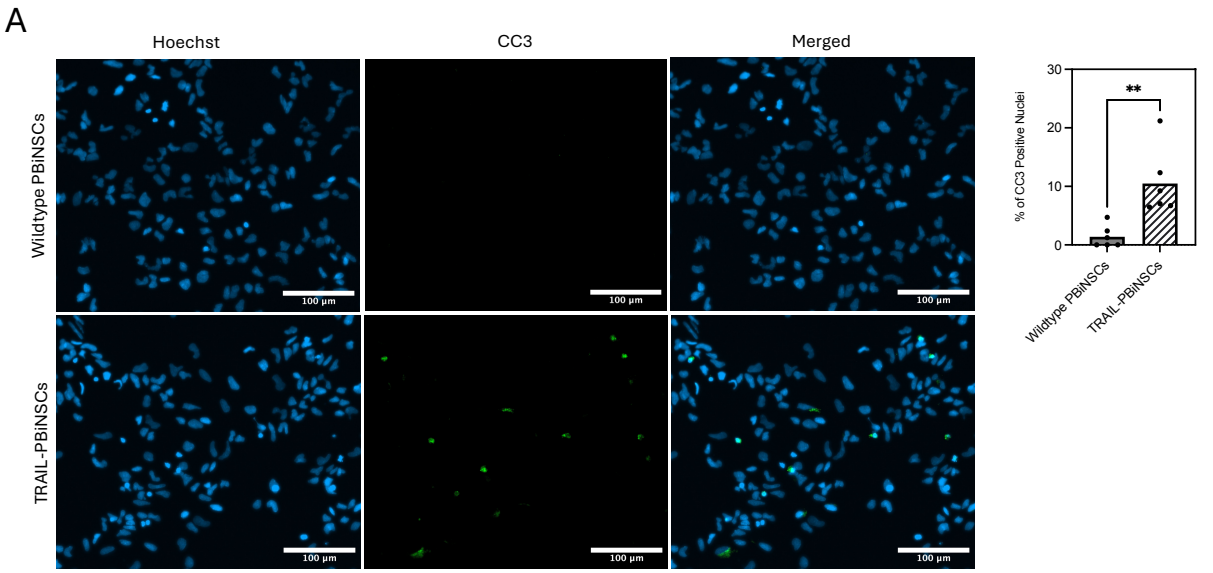
A
Hoechst
CC3
Merged
Wildtype PBiNSCs
TRAIL-PBiNSCs
100 µm
% of CC3 Positive Nuclei
30
20
10
0
**
Wildtype PBiNSCs
TRAIL-PBiNSCs

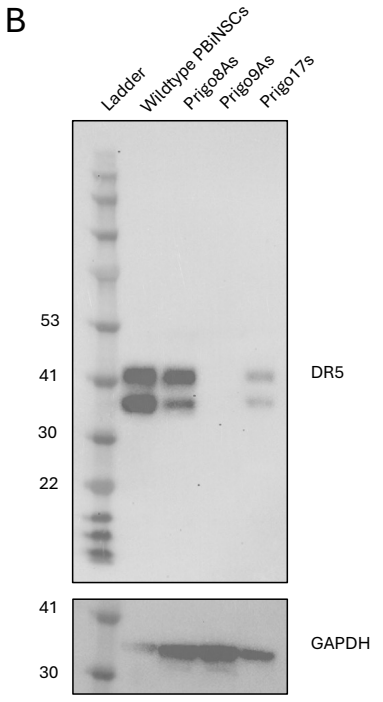
B
Ladder
Wildtype PBiNSCs
Prigo8As
Prigo9As
Prigo17s
53
41
30
22
DR5
41
30
GAPDH

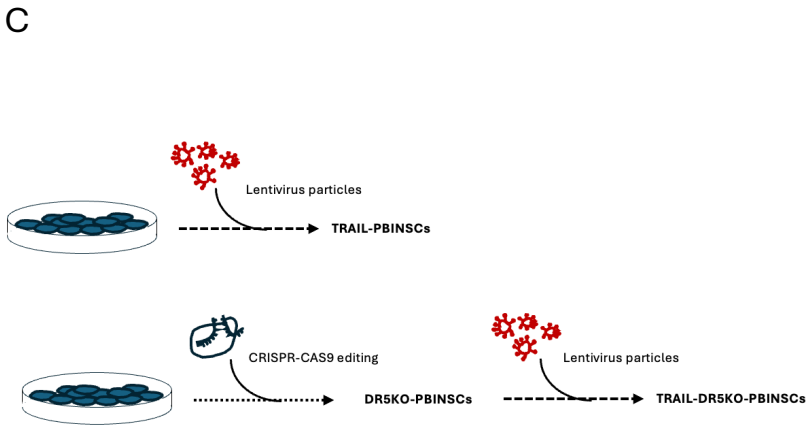
C
Lentivirus particles
TRAIL-PBINSCs
CRISPR-CAS9 editing
DR5KO-PBINSCs
Lentivirus particles
TRAIL-DR5KO-PBINSCs

D

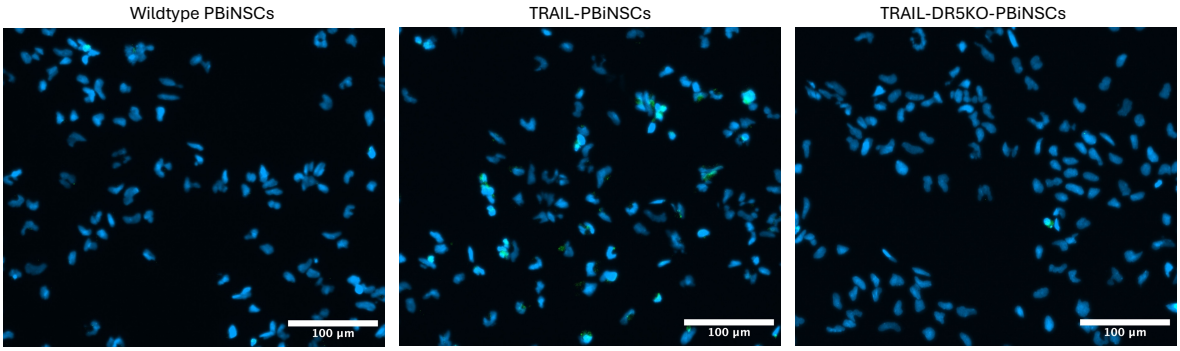

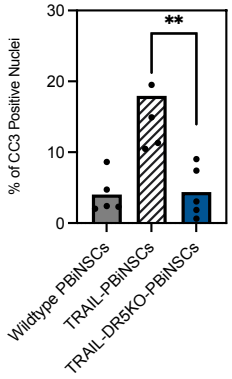

E

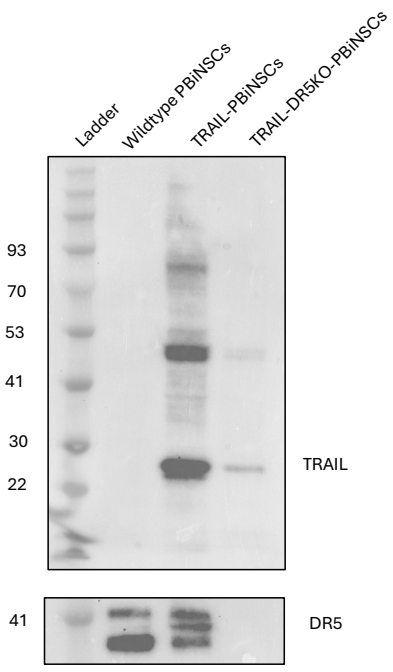

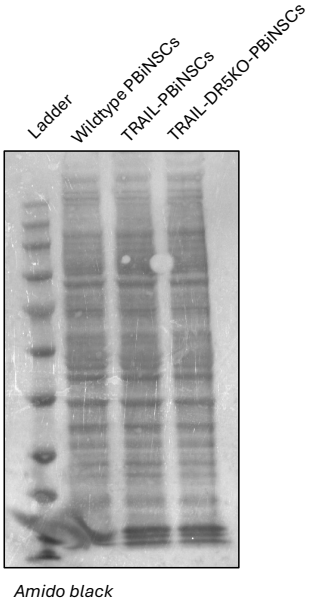

Amido black

Figure 3.7: **DR5 receptor in PBiNSCs mediates apoptosis in the presence of ectopic TRAIL expression (A)** TRAIL-PBiNSCs processed for immunocytochemistry. Nuclear staining is done with Hoechst and imaged under the blue channel. Cleaved caspase-3 was detected using a primary monoclonal antibody, detected with secondary conjugated to AF647. AF564 signal was acquired in the cyan channel and pseudocolored green for visualization. Images were acquired at 20x magnification and analyzed using Fiji. The ratio of cleaved caspase-3 signal associated with nuclei was normalized to the total cell count and expressed as a percent. This percent was calculated across five independent fields of view. Statistical significance was determined using a Mann-Whitney test (P = 0.0022, **P $<$ 0.01). **(B)** Endogenous levels of DR5 protein in wildtype PBiNSCs compared to primary glioblastoma cell lines. GAPDH is used as a loading control. **(C)** Schematic overview of generating TRAIL-DR5KO-PBiNSCs. Wildtype cells are CRISPR-CAS9 edited for knockout of DR5 protein. Cells are FACS sorted for only negative cells and propagated. Then DR5KO-PBiNSCs are transduced for TRAIL expression using lentiviral particles. **(D)** TRAIL-DR5KO-PBiNSCs and TRAIL-PBiNSCs were processed for cleaved caspase-3 activity. Immunocytochemistry is performed the same as above. AF564 signal was acquired in the cyan channel and pseudocolored green for visualization. Statistical significance was determined using a Mann-Whitney test (P = 0.0079, **P $<$ 0.01). **(E)** TRAIL protein expression in transduced PBiNSCs. Following lentiviral transduction, total cell lysates were extracted from TRAIL-PBiNSCs and TRAIL-DR5KO-PBiNSCs to probe for endogenous TRAIL expression. The membrane was stripped and reprobed for endogenous DR5 expression. Amido black staining was used as a loading control.

3.2.3 DR5 knockout in PBiNSCs eliminates TRAIL-mediated toxicity

The DR5 receptor is the primary receptor for TRAIL due to its higher binding affinity and serves as a predictor of TRAIL sensitivity. Interestingly, wildtype PBiNSCs exhibited higher levels of total endogenous DR5 protein compared to three primary glioblastoma cell lines (Figure 3.7B). Flow cytometry data, presented in subsection 2.1.2, demonstrated significant DR5 expression on the cell surface, indicating that the receptor is available for ligand binding. This surface expression can mediate TRAIL-induced cytotoxicity, as has been reported in non-transformed cells such as endothelial cells, hepatocytes, brain cells, and erythropoietic cells (92, 98, 158). Strong surface DR5 expression on PBiNSCs can be problematic, as it can sequester active TRAIL away from target malignant cells and simultaneously render the PBiNSCs themselves susceptible to TRAIL-induced cell death.

We tested the hypothesis that TRAIL signals through DR5 in PBiNSCs, leading to elevated levels of cleaved caspase-3 (CC3) activity. The DR5 receptor was knocked out using CRISPR-Cas9, as described in subsection 2.1.2, with DR5 sgRNA-2. PBiNSCs with complete DR5 knock-out (DR5KO-PBiNSCs) were sorted, cultured, and subsequently transduced to express TRAIL via lentiviral transduction. Following transduction, cells were selected with puromycin. These TRAIL-DR5KO-PBiNSCs lack endogenous DR5 but exogenously express membrane-bound TRAIL (Figure 3.7C). To confirm TRAIL expression in the newly transduced cell line, we performed a Western blot for TRAIL. Interestingly, freshly transduced TRAIL-DR5KO-PBiNSCs showed markedly lower TRAIL expression compared to freshly transduced TRAIL-PBiNSCs (Figure 3.7E).

Apoptotic activity in TRAIL-DR5KO-PBiNSCs was then assessed using immunocytochemistry. Staining for cleaved caspase-3 showed that elevated apoptosis observed in TRAIL-PBiNSCs was eliminated in TRAIL-DR5KO-PBiNSCs (Figure 3.7.D). This suggests that DR5 on PBiNSCs was binding TRAIL and inducing apoptosis within the cell population.

3.2.4 Exogenous TRAIL expression is largely present in the media as exosomes

To determine whether TRAIL is secreted into the media, wildtype PBiNSCs were treated with conditioned media (CM) from TRAIL-transduced PBiNSC cultures (Figure 3.8A). Binding of TRAIL in the CM to the cell surface via DR5 and potential internalization can appear as endogenous protein in Western blots of wildtype lysates. Incubation of wildtype PBiNSCs with CM from TRAIL-transduced cells resulted in detection of a TRAIL band (Figure 3.8B). This confirms that TRAIL is secreted into the culture media, associates with PBiNSCs, and is subsequently detected as endogenous protein. This also explains the lower TRAIL levels observed in TRAIL-DR5KO-PBiNSCs (Figure 3.7E), as the absence of DR5 prevents TRAIL re-binding and subsequent detection in lysates, instead TRAIL accumulates in the media.

Exosomes are secreted by all cell types. To determine whether TRAIL is released into the culture media as exosomal (EV) cargo, we isolated EVs via sequential ultracentrifugation from the supernatant. Successful EV isolation was confirmed by the presence of common EV markers, including syntenin and CD63 (155, 156). Syntenin was enriched in the EV samples, while CD63 displayed a distinct glycosylation pattern compared to whole-cell lysates, a common distinction between parental cells and their associated EVs (157). TRAIL was detected in EVs from TRAIL-transduced cells but was absent in EVs from wildtype cells (Figure 3.8C).

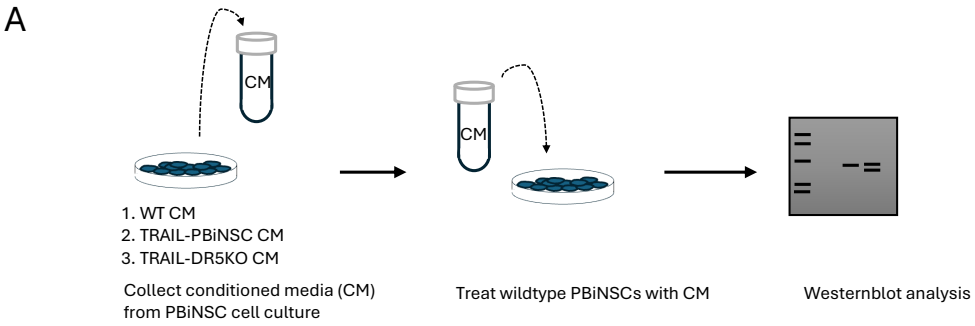
A
CM
CM
1. WT CM
2. TRAIL-PBiNSC CM
3. TRAIL-DR5KO CM
Collect conditioned media (CM) from PBiNSC cell culture
Treat wildtype PBiNSCs with CM
Westernblot analysis

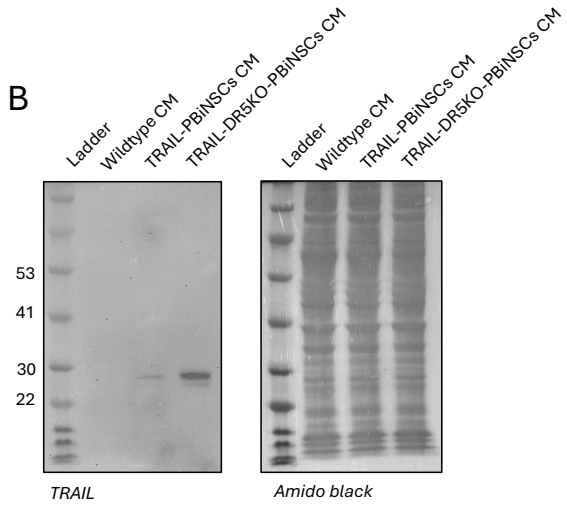
B
Ladder
Wildtype CM
TRAIL-PBiNSCs CM
TRAIL-DR5KO-PBiNSCs CM
Ladder
Wildtype CM
TRAIL-PBiNSCs CM
TRAIL-DR5KO-PBiNSCs CM
53
41
30
22
TRAIL
Amido black

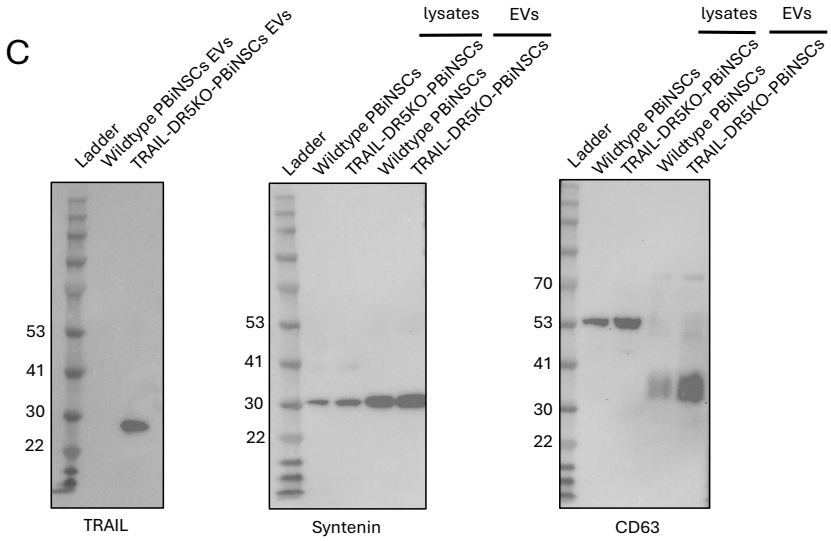
C
lysates
EVs
lysates
EVs
Ladder
Wildtype PBiNSCs EVs
TRAIL-DR5KO-PBiNSCs EVs
Ladder
Wildtype PBiNSCs
TRAIL-DR5KO-PBiNSCs
Wildtype PBiNSCs
TRAIL-DR5KO-PBiNSCs
Ladder
Wildtype PBiNSCs
TRAIL-DR5KO-PBiNSCs
Wildtype PBiNSCs
TRAIL-DR5KO-PBiNSCs
53
41
30
22
53
41
30
22
70
53
41
30
22
TRAIL
Syntenin
CD63

Figure 3.8: **TRAIL is secreted into the media as cargo on exosomes (A)** Schematic overview of the experiment shown in 2.8B. Conditioned media (CM) was collected from wildtype PBiNSC, TRAIL-PBiNSC, and TRAIL-DR5KO-PBiNSC cultures. Wildtype PBiNSCs were treated with CM for 24 hours prior to collection of protein lysates and Western blot analysis. **(B)** Wildtype PBiNSCs were treated with conditioned media (CM) from three different PBiNSC cultures. Supernatant was collected from 3-day cultures, centrifuged to remove debris, and filtered. Wildtype PBiNSCs were then incubated with CM for 24 hours before lysates were collected. Western blotting was performed for TRAIL protein, with Amido black used as a loading control. **(C)** Exosomes were purified from PBiNSC supernatant by sequential ultracentrifugation and probed for two EV protein markers. Purified EV samples (15 µL) were treated with 4 µL of lysis buffer and 6 µL of Laemmli buffer containing beta-mercaptoethanol. Samples were briefly vortexed and then heated at 95°C for 5 minutes before loading. A total of 20 µg of cell lysate was loaded as a negative control. Membranes were probed using classical EV markers such as syntenin and CD63, and TRAIL was also detected in the samples.

3.3 Cytotoxicity in primary glioblastoma cells

3.3.1 evTRAILs secreted by PBiNSCs are bioactive

To evaluate the activity of TRAIL-associated EVs (evTRAIL) secreted by PBiNSCs, three primary glioblastoma cell lines were treated with conditioned media from PBiNSC cultures (Figure 3.9A). Total cell counts were assessed three days after treatment. In PriGO17 cells, a 1.33-fold reduction in cell number was observed with conditioned media from TRAIL-DR5KO PBiNSCs compared to treatment with media from wild-type PBiNSCs (Figure 3.9B). Immunostaining for cleaved caspase-3 demonstrated activation of the apoptotic signaling pathway in PriGO17 cells (Figure 3.9C). This effect was not observed in the two other glioma cell lines tested.

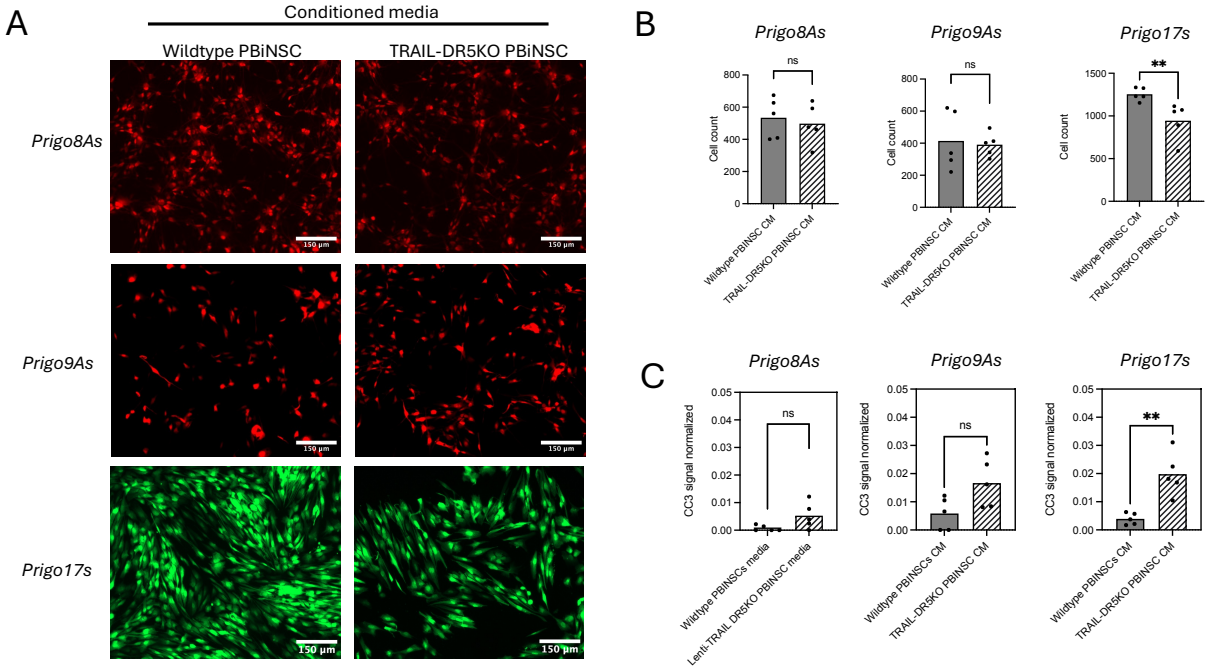
A
Conditioned media
Wildtype PBiNSC
TRAIL-DR5KO PBiNSC
Prigo8As
Prigo9As
Prigo17s
150 µm
B
Prigo8As
Prigo9As
Prigo17s
Cell count
ns
**
Wildtype PBiNSC CM
TRAIL-DR5KO PBiNSC CM
C
Prigo8As
Prigo9As
Prigo17s
CC3 signal normalized
ns
**
Wildtype PBiNSCs media
Lenti-TRAIL DR5KO PBiNSC media
Wildtype PBiNSCs CM
TRAIL-DR5KO PBiNSC CM

Figure 3.9: **Primary glioblastoma cell lines treated with conditioned media (CM) from PBiNSC cultures (A)** PriGO8A, PriGO9A, and PriGO17 cell lines were all previously labeled with fluorescent proteins through viral transduction. PriGO8As and PriGO9As are labeled with mCherry and PriGO17s are labeled with eGFP. PriGOs were plated in 6-well plates on coverslips and treated with conditioned media. Following the three-day incubation period, cells were processed for immunocytochemistry. Images were acquired using a fluorescence microscope at 10× magnification. **(B)** Cells were stained with Hoechst and CC3 primary antibody. Cell counts were quantified using Hoechst signal across five fields of view and averaged for each condition. Statistical significance was determined using a Mann-Whitney test (**P < 0.01, ns = not significant). **(C)** CC3 signal was quantified based on nuclear-associated staining and normalized to total cell count. Statistical significance was determined using a Mann-Whitney test (**P < 0.01, ns = not significant).

3.3.2 TRAIL-DR5KO-PBiNSCs exhibit improved toxicity to a primary glioblastoma cell line in vitro

Co-culture assays confirmed that TRAIL-DR5KO-PBiNSCs are cytotoxic and that knockout of the endogenous DR5 receptor in PBiNSCs is required for effective TRAIL delivery in vitro. Three primary glioblastoma cell lines were co-cultured with PBiNSCs, and mean relative fluorescence units (RFU) were measured after 3 days. Each glioblastoma line had been previously transduced with a lentivirus encoding a fluorescent protein: PriGO8As and PriGO9As expressed mCherry, while PriGO17s expressed eGFP. Mean RFU is proportional to total cell count. After 72 hours of co-culture, only PriGO17 cells appeared sensitive to TRAIL-mediated apoptosis. Increasing the effector-to-target ratio of TRAIL-DR5KO-PBiNSCs to PriGO17s resulted in a proportional decrease in mean RFU (Figure 3.10A). Cytotoxicity was most pronounced at the highest effector-to-target ratio (4:1). Some cytotoxicity was also observed with TRAIL-PBiNSCs. Overall, TRAIL-mediated killing appeared restricted to PriGO17s, consistent with previous work from our lab showing that PriGO8A and PriGO9A cells are largely resistant to TRAIL-induced apoptosis.

A

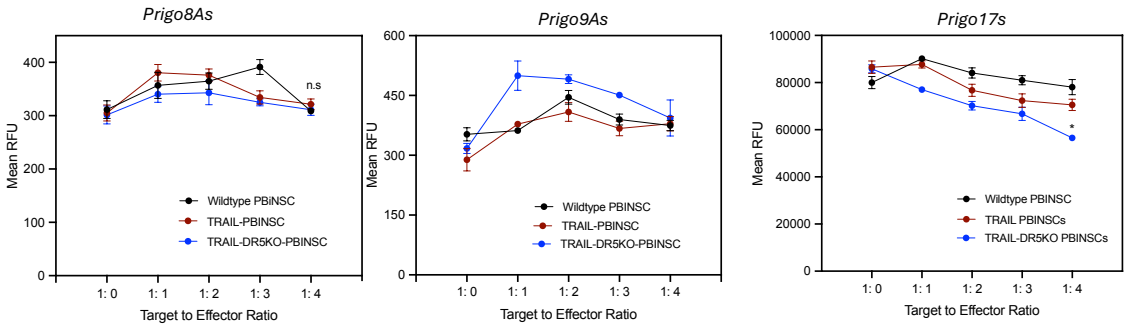
Prigo8As
Mean RFU
400
300
200
100
0
n.s
Wildtype PBiNSC
TRAIL-PBINSC
TRAIL-DR5KO-PBINSC
1: 0
1: 1
1: 2
1: 3
1: 4
Target to Effector Ratio
Prigo9As
Mean RFU
600
450
300
150
0
Wildtype PBINSC
TRAIL-PBINSC
TRAIL-DR5KO-PBINSC
1: 0
1: 1
1: 2
1: 3
1: 4
Target to Effector Ratio
Prigo17s
Mean RFU
100000
80000
60000
40000
20000
0
*
Wildtype PBINSC
TRAIL PBINSCs
TRAIL-DR5KO PBINSCs
1: 0
1: 1
1: 2
1: 3
1: 4
Target to Effector Ratio

Figure 3.10: **Primary glioblastoma cell lines co-cultured with PBiNSCs (A)** Cells were co-cultured in 96-well plates for 3 days, after which mean RFU was measured using a BioTek plate reader. Each effector-to-target ratio was performed in quintuplicate. Error bars represent the standard error of the mean. Statistical significance is determined by a Mann-Whitney test (P=0.0286, *$P < 0.05$, ns = not significant).

3.3.3 Treatment with the Smac mimetic AZD5582 markedly enhanced TRAIL-induced cytotoxicity in one primary glioblastoma cell line while two other primary glioblastoma cell lines were resistant. Additional sensitizing agents including ARV771, IFN-y, SNS-032, and APG115 are being evaluated and molecular basis for sensitivity/resistance is being assessed

TRAIL resistance is widespread and common across cancer cell lines, as evident in PriGO8As and PriGO9As. In this subsection, we investigate multiple sensitizing agents in an effort to enhance TRAIL-mediated killing in vitro. TRAIL-DR5KO-PBiNSCs were co-cultured with glioma cells in the presence of varying concentrations of potential sensitizing drugs. Overall, the three primary glioma cell lines showed distinct responses to each drug, reflecting the heterogeneity observed in the clinic. Of the drugs tested, only AZD5582 markedly reduced PriGO17 cell viability at the tested dose.

AZD5582

AZD5582 enhanced TRAIL-mediated killing in co-culture experiments with PriGO17 cells. AZD5582 alone, even at high doses, had minimal effect on PriGO17 cultures (Figure 3.11A). However, when co-cultured with TRAIL-DR5KO-PBiNSCs, PriGO17 cells were markedly sensitized to killing by the combination of AZD5582 and TRAIL (Figure 3.12A). In contrast, PriGO8As were sensitive to high doses of AZD5582, with complete cell death observed at 2000 nM, regardless of TRAIL presence. PriGO9As remained relatively resistant to both treatments. Although AZD5582 can be toxic to PBiNSCs, the dose range used was tested previously and PBiNSC growth was maintained (Figure 3.11A).

A

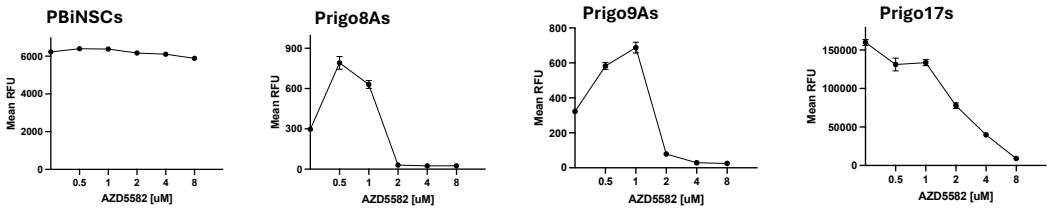
PBiNSCs
Mean RFU
6000
4000
2000
0
0.5
1
2
4
8
AZD5582 [uM]
Prigo8As
Mean RFU
900
600
300
0
0.5
1
2
4
8
AZD5582 [uM]
Prigo9As
Mean RFU
800
600
400
200
0
0.5
1
2
4
8
AZD5582 [uM]
Prigo17s
Mean RFU
150000
100000
50000
0
0.5
1
2
4
8
AZD5582 [uM]

Figure 3.11: **AZD5582 treatment of PriGOs and PBiNSCs. (A)** Cells were seeded in 96-well plates at a density of 5,000 cells per well. Drug treatment was added the following day. Treatment lasted 72 hours after which mean RFU was measured using a BioTek plate reader. Each condition was performed with six biological replicates. Error bars represent the standard error of the mean.

ARV-771

ARV-771 is a small-molecule proteolysis-targeting chimera (PROTAC) that induces protein degradation of bromodomain and extra-terminal (BET) family proteins. No obvious sensitization to TRAIL-mediated apoptosis was observed. However, PriGO8As were completely killed at 500 nM of ARV-771 (Figure 3.12C). The lack of TRAIL sensitization may be due, in part, to PBiNSC toxicity, as high concentrations of ARV-771 also induced cell death in PBiNSCs.

IFN-y

IFN-y has been reported to exert anti-proliferative effects on several glioblastoma cell lines by increasing the production of cyclin-dependent kinase inhibitors, while other studies show sensitization to TRAIL-mediated apoptosis (159, 160). Here, we observed no obvious anti-proliferative effects and no detectable sensitization to TRAIL in any of the cell lines (Figure 3.12D).

APG-115

APG-115 is a clinically tested small-molecule inhibitor of mouse double minute 2 homolog (MDM2). MDM2 is frequently overexpressed in cancers, leading to degradation of p53 and inhibition of apoptosis (161). Stabilized p53 can enhance TRAIL-mediated apoptosis by upregulating the expression of its cognate receptors (162). In our experiments, APG-115 did not sensitize any of the tested cell lines to TRAIL, nor did it induce cytotoxic effects on its own (Figure 3.12E).

SNS-032

Inhibition of cyclin-dependent kinase 9 (CDK9) has been reported to overcome TRAIL resistance by downregulating cFLIP and Mcl-1, two key inhibitors of the extrinsic apoptotic pathway (163). SNS-032 is a selective inhibitor of CDK2, 7, and 9 that has been evaluated in clinical trials. Our experiments showed no drug sensitization to TRAIL. However, the drug alone exhibited some cytotoxic effects, particularly in PriGO17 cells, where an additive effect of TRAIL and SNS-032 toxicity was observed (Figure 3.12F).

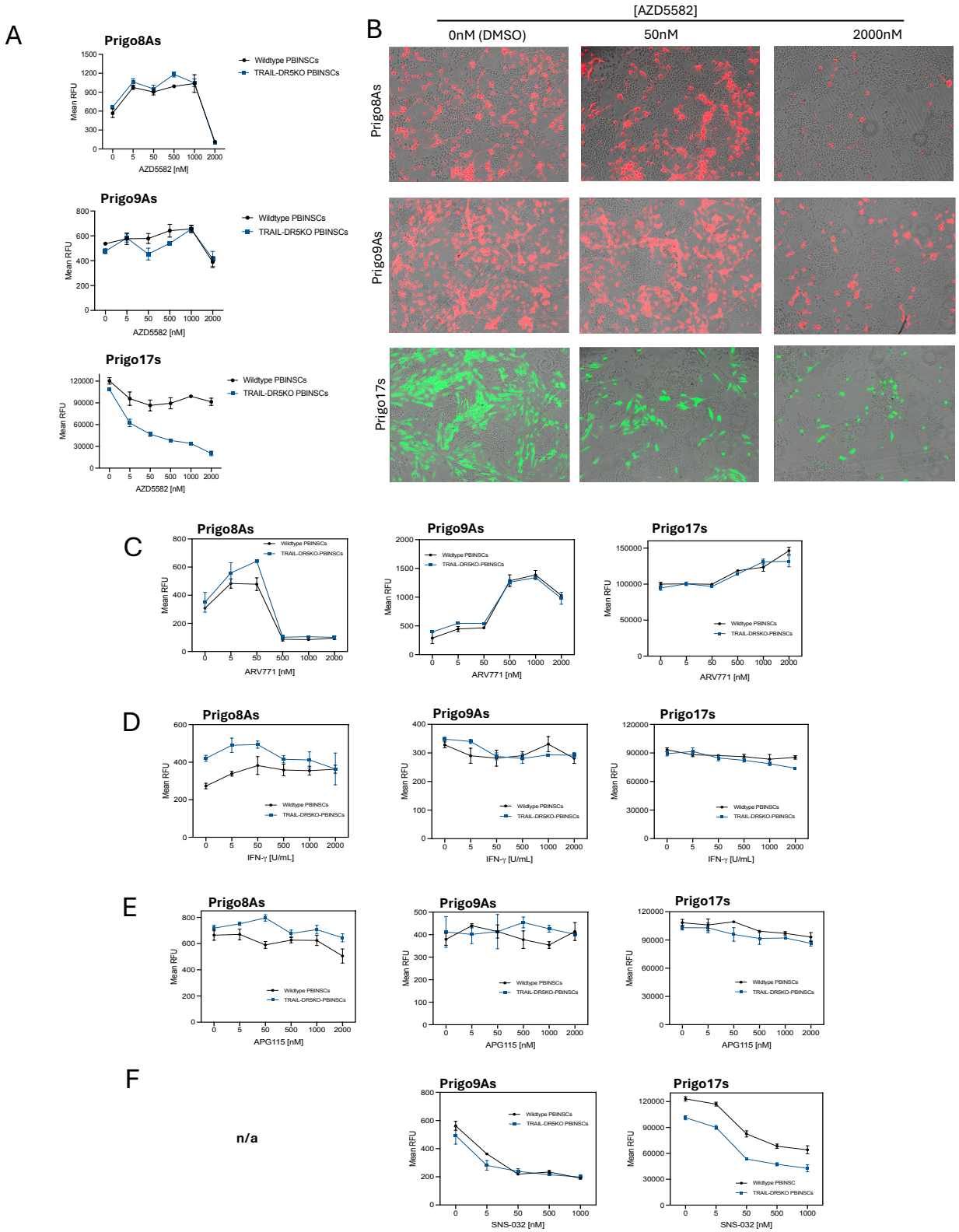
A
Prigo8As
Wildtype PBINSCs
TRAIL-DR5KO PBINSCs
Mean RFU
AZD5582 [nM]
Prigo9As
Wildtype PBINSCs
TRAIL-DR5KO PBINSCs
Mean RFU
AZD5582 [nM]
Prigo17s
Wildtype PBINSCs
TRAIL-DR5KO PBINSCs
Mean RFU
AZD5582 [nM]
B
[AZD5582]
0nM (DMSO)
50nM
2000nM
Prigo8As
Prigo9As
Prigo17s
C
Prigo8As
Prigo9As
Prigo17s
Wildtype PBINSCs
TRAIL-DR5KO-PBINSCs
Mean RFU
ARV771 [nM]
D
Prigo8As
Prigo9As
Prigo17s
Wildtype PBINSCs
TRAIL-DR5KO-PBINSCs
Mean RFU
IFN-γ [U/mL]
E
Prigo8As
Prigo9As
Prigo17s
Wildtype PBINSCs
TRAIL-DR5KO-PBINSCs
Mean RFU
APG115 [nM]
F
n/a
Prigo9As
Prigo17s
Wildtype PBINSCs
TRAIL-DR5KO PBINSCs
Mean RFU
SNS-032 [nM]

Figure 3.12: **Sensitization of glioma cell lines with TRAIL-DR5KO-PBiNSCs in the presence of different drugs.** **(A)** PBiNSCs and glioma cells were co-cultured at a 3:1 effector-to-target ratio, and AZD5582 was added 24 hours later. Each condition was performed in triplicate. After 72 hours of treatment, mean RFU was measured using a BioTek plate reader. **(B)** Representative images were acquired using the EVOS fluorescence microscope after 72 hours of drug treatment. **(C)** Co-culture at a 3:1 ratio with ARV-771 added 24 hours later; mean RFU measured after 72 hours. Each condition was performed in triplicate. **(D)** Co-culture at a 3:1 ratio with IFN-gamma added 24 hours later; mean RFU measured after 72 hours. Each condition was performed in triplicate. **(E)** Co-culture at a 3:1 ratio with APG-115 added 24 hours later; mean RFU measured after 72 hours. Each condition was performed in triplicate. **(F)** Co-culture at a 3:1 ratio with SNS-032 added 24 hours later; mean RFU measured after 72 hours. Each condition was performed in triplicate.

3.3.4 p53 status does not correlate with sensitivity to TRAIL-mediated apoptosis

Previous studies find that lung and colon cancer cells lacking functional p53 are less sensitive to TRAIL-mediated apoptosis compared to isogenic lines expressing wild-type p53 (135). To assess the effect of p53 status in glioma cell lines, RNA was extracted and the TP53 gene was sequenced using four primers spanning the entire gene.

Sequencing of the TP53 gene revealed a single nucleotide polymorphism (SNP) at codon 72 in the tested glioma cell lines (Figure 3.13A). PriGO8As appear heterozygous at this position, carrying both CCC and CGC codons, which encode proline and arginine, respectively. PriGO9As and PriGO17s carried only the CGC allele.

Further sequence alignment with the wildtype TP53 gene reveals a missense mutation in both PriGO9As and PriGO17s, while the PriGO8A sequence remained wildtype. In PriGO9As, a single base change from thymine (T) to guanine (G) in codon 132 results in an amino acid substitution from lysine (Lys) to asparagine (Asn) (Figure 3.13B). In PriGO17s, a base change from cytosine (C) to thymine (T) in codon 248 results in a substitution of arginine (Arg) with tryptophan (Trp) (Figure 3.13B). Both missense mutations are located within the DNA-binding domain of the p53 protein.

R248 is a well-characterized hotspot mutation, representing one of the six most frequently mutated codons in p53 (164). This mutation not only results in the loss of tumor-suppressive functions but also confers oncogenic gain-of-function properties (165). The R248W substitution alters the secondary structure of p53, exposing hydrophobic regions and promoting the formation of amyloid-like aggregates (166). Western blot analysis further supports this in PriGO17s, where a strong band at 53 kDa corresponds to the p53 monomer, alongside characteristic higher-molecular-weight bands indicative of oligomeric self-aggregates (Figure 3.12.C).

K132 is a less frequently occurring and less well studied mutation. The mutation most likely confers a loss-of-function phenotype in PriGO9As.

Interestingly, in PriGO8As, despite expressing wild-type p53, these cells are largely resistant to

TRAIL-mediated apoptosis. This suggests that wild-type p53 is not required for effective apoptotic signaling through TRAIL, as loss of p53 function in PriGO17s does not prevents TRAIL killing.

A

Single Nucleotide Polymorphism: Codon 72

Prigo8As

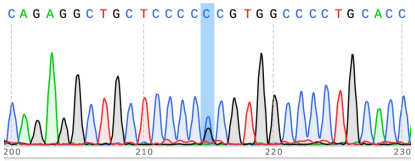

Prigo9As

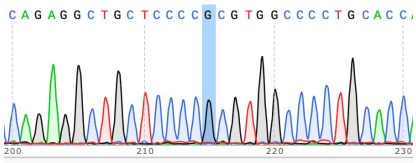

Prigo17s

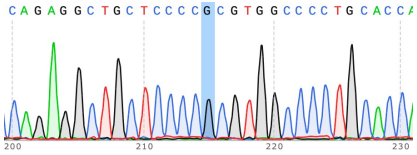

B

Missense mutation in Prigo9As (K132N)

	128	**129**	**130**	**131**	**132**	**133**	**134**	**135**	**136**
Wildtype TP53	CCT pro	GCC ala	CTC leu	AAC asn	AAG lys	ATG met	TTT phe	TGC cys	CAA gln
Prigo9A	CCT pro	GCC ala	CTC leu	AAC asn	AAT asn	ATG met	TTT phe	TGC cys	CAA gln

Missense mutation in Prigo17s (R248W)

	244	**245**	**246**	**247**	**248**	**249**	**250**	**251**	**252**
Wildtype TP53	GGC gly	GGC gly	ATG met	AAC asn	CGG arg	AGG arg	CCC pro	ATC Ile	CTC leu
Prigo17s	GGC gly	GGC gly	ATG met	AAC asn	TGG trp	AGG arg	CCC pro	ATC Ile	CTC leu

C

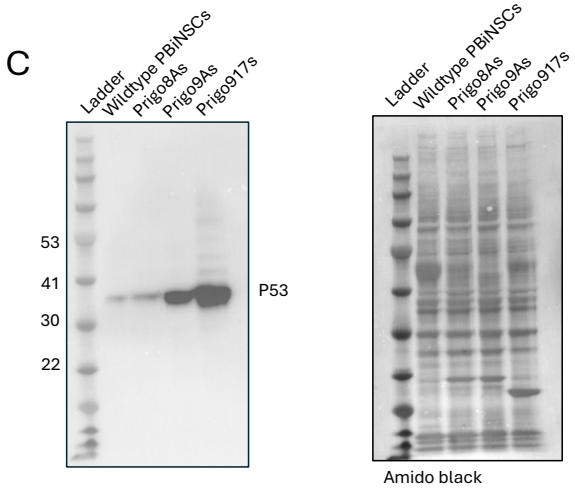

Figure 3.13: **TP53 mutations in glioma cell lines (A)** Identification of a single nucleotide polymorphism at codon 72. PriGO8As are heterozygous, expressing both alleles, whereas PriGO9As and PriGO17s are homozygous. **(B)** Major TP53 mutations in PriGO9As and PriGO17s are missense mutations. PriGO9As carry K132N, while PriGO17s harbor R248W. **(C)** Western blot analysis of total endogenous p53 protein in PBiNSCs compared to glioma cell lines. Equal amounts of protein (15 µg) were loaded across all samples. A band around 53 kDa corresponds to the protein's monomer size. Amido black staining confirms equal protein loading.

3.4 In vivo mice experiments

3.4.1 TRAIL-DR5KO-PBiNSCs stably engraft and persist in mice brain following injection

In vivo experiments were performed to assess the durability of TRAIL-DR5KO-PBiNSCs following transplantation in mice. Immunodeficient mice underwent stereotaxic striatal injection for two PBiNSC cell lines and were collected one month later for immunohistochemistry (Figure 3.14A). All injections and staining were performed by our laboratory technician, Margarita Lui.

Imaging of the striatum revealed stable engraftment of both TRAIL-DR5KO-PBiNSCs and wildtype PBiNSCs at one month, with similar numbers of GFP-positive PBiNSCs persisting in each condition (Figure 3.14B). These findings indicate that DR5 is not required for PBiNSC viability in vivo.

Furthermore, TRAIL expression was maintained in the TRAIL-DR5KO-PBiNSC population at one month. TRAIL staining was observed in close proximity to GFP-positive cell bodies, although signal was also present in the immediate surrounding tissue, consistent with only partial overlap between TRAIL staining and GFP-positive PBiNSCs.

A

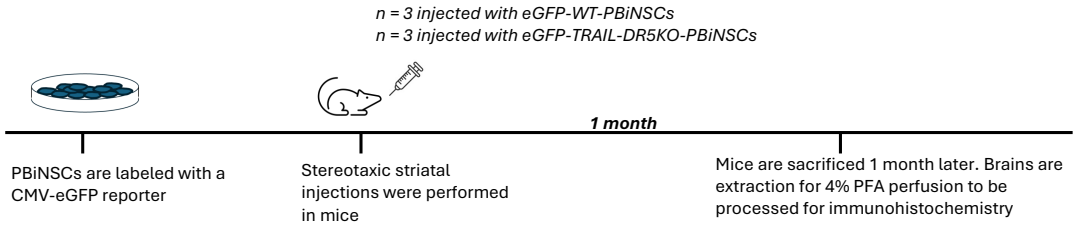

(All injections and immunohistochemistry were performed by Margarita Lui)

B

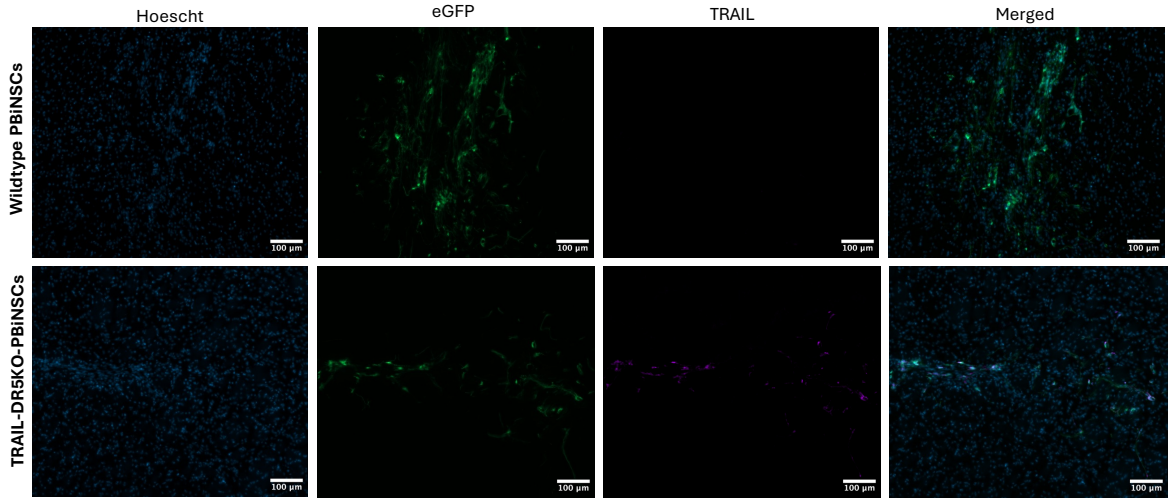

(All injections and immunohistochemistry were performed by Margarita Lui)

Figure 3.14: **In vivo mice injections of PBiNSC cell lines (A)** Schematic overview of the in vivo experiment. PBiNSCs were labeled with an eGFP reporter via lentiviral transduction and confirmed mycoplasma-free prior to injection. Each mouse (n = 6) received 100,000 PBiNSCs into the striatum, with three mice for each cell line. Mice were monitored for one month and then sacrificed for immunohistochemistry. **(B)** Representative brain sections processed for immunohistochemistry and imaged using fluorescence microscopy. Top panels: mice injected with wildtype PBiNSCs. Bottom panels: mice injected with TRAIL-DR5KO-PBiNSCs.

Chapter 4

Discussion

In this study, we investigated the potential of genetic engineering of a novel neural stem cell source to deliver membrane-bound TRAIL as a glioblastoma therapeutic. Our findings show that knocking out the endogenous DR5 receptor via CRISPR-Cas9 enhances TRAIL-mediated cytotoxicity. Furthermore, we report that the combination of TRAIL delivery with IAP inhibition, using AZD5582, markedly increased killing of a primary glioblastoma cell line, highlighting a possible synergistic approach for overcoming apoptotic resistance. These results support the feasibility of using engineered neural stem cells as targeted delivery vehicles in the treatment of glioblastoma and warrant further investigation using in vitro and in vivo models.

4.0.1 Genetic engineering in PBiNSCs

The application of CRISPR-Cas9 technology for genetic engineering presents unique opportunities and challenges, which we explored thoroughly in this study. We found that PBiNSCs are amenable to CRISPR-mediated editing, enabling precise and predictable modifications of the genome. We successfully targeted four genomic sites, including two coding regions and two safe harbor sites, with high efficiency (22-98%). Specifically, by targeting of the endogenous DR5 receptor with our designed crRNA sequence, we demonstrated that knock out of the receptor and subsequent enrichment of this population can generate a stable cell line without obvious compromises to cel-

lular proliferation and stem cell properties. Interestingly, the role of DR5 in stem cells appears cell type dependent, as knockout in intestinal stem cells has been shown to impair proliferative and differentiation capacity (167). While assessing CRISPR-mediated knock-in, we found that attempts at homology directed repair using IDT donor blocks were suboptimal on two fronts: low HDR efficiency and unstable transgene expression.

Low HDR efficiency in part stems from the high toxicity of donor template DNA. When PBiNSCs were nucleofected with RNP complexes alone, cell viability remained high and comparable to the control conditions (with pulse without RNP delivery). In contrast, the addition of template DNA resulted in extensive cell death following nucleofection. This toxicity was proportional to both the amount (ug) and size of the template sequence. Longer donor sequences caused greater cell death following CRISPR editing. These observations suggest that toxicity is not solely driven by the DNA double-stranded break (DSB) mediated by Cas9 enzymatic cleavage, but rather by additional mechanisms as well.

The DSB that underlies CRISPR-mediated editing activates a p53-dependent DNA damage response (168, 169). When genomic instability is detected, p53 coordinates cell cycle arrest and promotes either DNA repair processes or cell death programs. Consistent with this, we observed modest levels of cell death following RNP delivery. Such toxicity has raised concerns that CRISPR editing may impose selection pressures favoring p53-deficient or mutant cells, which are more likely to survive under this stress (168, 169). Studies in retinal epithelial cells and pluripotent stem cells have shown that inhibiting p53 and this pathway can improve survival and HDR efficiency (168, 169). However, our preliminary experiments in PBiNSCs, where a p53 dominant-negative plasmid was co-delivered with CRISPR reagents, did not improve HDR efficiency or survival. Instead, there was increased cell death and reduced viability the next day, suggesting PBiNSCs are highly sensitive to exogenous double stranded donor template, supplied in plasmid form or as donor templates.

Another cellular pathway activated during CRISPR editing that contributes to low cell viability and, consequently, reduced HDR efficiency is the cytosolic DNA-sensing pathway, specifically the

cGAS/STING pathway (170, 171). Naked cytosolic foreign DNA elicits an innate cellular immune response, which functions to mount an antiviral response during infections. cGAS binds cytosolic double-stranded DNA and produces the second messenger cGAMP, which ultimately triggers transcription of inflammatory cytokines or activation of cell death cascades (172). In PBiNSCs, it can be hypothesized that a substantial portion of cell death observed following CRISPR editing is attributable to the activation of this pathway. Future strategies to improve HDR efficiency and cell viability could include transient inhibition of this pathway or the use of single-stranded DNA (ssDNA) templates, which have reduced toxicity and increased HDR efficiency (172, 170). However, a limitation of ssDNA is its restricted template size, making it primarily suitable for supporting smaller edits.

Another problem encountered with CRISPR-mediated gene engineering was the instability and loss of transgene expression in cell culture following HDR editing. After knock-in of GFP at the AAVS1 locus, subsequent enrichment for a fully GFP-positive cell population through FACS proved futile. Despite multiple rounds of sorting, the percentage of GFP-positive cells drastically decreased over successive passages. Several possible explanations can account for transgene instability at the population level. One possibility we explored was epigenetic silencing at the genetic locus. Although safe harbors are theoretically resistant to silencing, there are reports that the AAVS1 locus can undergo silencing in a cell type-dependent manner, during stem cell differentiation, and over time (173, 174). Silencing at the AAVS1 site is also influenced by promoter choice. Thus, it appears that careful selection of a promoter, integration locus, and cell type combination is required to prevent epigenetic silencing. We initially tested GFP expression driven by the CMV promoter because previous work in our lab showed that CMV enables long-term in vivo expression following lentiviral transduction in PBiNSCs. CMV is also one of the most commonly used promoters in field for driving high and robust transgene expression. We tested an alternative promoter at the AAVS1 locus as some studies reported that the EF1alpa promoter is superior to CMV for long term expression in undifferentiated stem cells (175, 176). Using EF1alpha to drive GFP expression at the AAVS1 site yielded the same issue. Following successive sorting, the GFP

positive population slightly increased to 50%; whereas, while using the CMV promoter, GFP positive cells dropped rapidly from 77% to 41%. Due to persistence of this issue, we also tested the use of the endogenous DR5 promoter, which we hypothesized would be more resistant to silencing and enable two genetic modifications in a single step. This strategy was similarly employed in CAR-T cells, where CRISPR insertion of the T-cell receptor at the PD-1 locus simultaneously knocked out the PD-1 protein and inserted the chimeric antigen receptor gene (177). Similarly, by positioning DR5 crRNA-2 to cut right at the ATG start site, we could directly integrate our transgene at the start site to be controlled by the endogenous DR5 promoter, while simultaneously, in theory, knocking out DR5 protein expression. RNA sequencing shows the DR5 transcription site is active in PBiNSCs with robust basal expression. The DR5 gene has two transcriptional start sites at -122 and -137 relative to the ATG start codon, with transcription driven directly by p53 and Sp1 (178). We expected that using an endogenous promoter would be more resistant to silencing compared to viral sequences like CMV and the ways foreign genetic material is recognized by cells. Our donor template consisted of the GFP sequence flanked by homology arms without a promoter; however, the same problem arose where despite sorting for only GFP positive cells, the population expressing GFP was only 40% upon the second sort.

We hypothesize that another plausible explanation for GFP instability at the population level is the outgrowth of wildtype PBiNSCs that lack transgene integration. PCR analysis of genomic DNA after several rounds of enrichment revealed a strong DNA band corresponding to cells lacking transgene integration, indicating that a subpopulation of wild-type cells escaped the sorting process. Bulk sorting by flow cytometry generates a polyclonal cell population, which includes subpopulations with distinct genotypes. One population consists of cells that lack GFP template integration and evade exclusion due to inherent imprecision of the instrument. This is supported by back-sorting experiments, which show that a small fraction of approximately 7% of wild-type or negative PBiNSCs escape into the final GFP positive population. Other populations contain GFP insertions that are either monoallelic or biallelic knock-ins. Previous reports find that bulk sorting for GFP is not appropriate for maintaining high-expressing cells over time, as low- or non-

expressing cells eventually outgrow the high-GFP expressers (179). Consequently, the study concludes isolation of single clones is required to achieve a stable population of uniformly expressing cells (179). Another study finds repeated sorting for the top 0.6% of GFP-positive cells over five rounds was required to obtain a near homogeneous population (180).

The outgrowth of the wildtype GFP-negative population can possibly be explained by several factors. First, expression of the GFP protein may confer a selective disadvantage to edited cells. High intracellular concentration of GFP have been reported to cause oxidative stress and, in some cases, induce apoptosis (181). Furthermore, the production of GFP in successfully edited cells imposes an additional metabolic cost due to extra protein synthesis, which can slow cellular growth (182). A second consideration is the possible off-target effects of CRISPR-edited cells. CRISPR-CAS9 can occasionally induce unintended genomic modifications when gRNA design is poor, which can result in disruption in essential gene coding regions. This explanation appears less likely as GFP-negative PBiNSCs would be equally susceptible to off-target effects. Finally, differentiation of PBiNSCs following HDR-mediated insertions may contribute to the decline of GFP-positive cells. Microscopic observations indicate that following HDR editing many GFP positive cells have an altered appearance suggestive of differentiation. Stress from the HDR process could cause spontaneous differentiation and successfully edited cells could then lose their proliferative capacity.

Further careful investigation is required to determine the exact mechanisms underlying transgene instability in PBiNSCs. Although isolation of single-cell clones is a common strategy to achieve a homogeneous population, PBiNSCs do not expand efficiently from single cells, and the high number of passages required would be impractical for therapeutic applications. Future studies could incorporate a selection marker within the integrated transgene to facilitate more efficient and easier identification of successfully edited cells without flow sorting. Additionally, analysis of differentiation markers in PBiNSCs following CRISPR-mediated HDR could help clarify whether transgene loss is associated with spontaneous differentiation.

CRISPR-editing vs lentivral integration

Lentiviral transduction is a highly efficient method for achieving transgene expression. However, as previously discussed, the semi-random integration of the vector presents significant concerns for clinical applications. In particular, insertional mutagenesis can potentially generate tumors in patients, while the resulting polyclonal cell population may limit therapeutic efficacy. This latter consideration is especially important when delivering a cytotoxic product such as TRAIL, where protein expression must be quantifiable, consistent, and reliable to ensure both safety and therapeutic effectiveness. In this study, we demonstrate that CRISPR-Cas9–mediated genome editing enables precise and predictable integration of the transgene into the target genomic site, resulting in consistent and uniform transgene expression in positively edited PBiNSC.

Currently in the field of CAR-T cell generation, FDA approved CAR-T products are generated from lentivirus and retrovirus. One study finds that selecting for lentivirus transduced T cells with high surface density of CAR performed worse in patients when looking at clinical outcomes, and was found to be associated with increased tonic signaling and exhaustion markers (183). With this in mind, studies have been focused on optimizing non-viral methods of CAR-T cell production to improve therapeutic efficacy. Zhang et al. found that insertion of the CAR into the PD1 locus, essentially inhibiting T cell exhaustion, outperformed CARs made from lentiviral transduction (177).

4.0.2 Membrane bound-TRAIL delivery through PBiNSCs

In our study, we made two key observations surrounding membrane-bound TRAIL delivery in PBiNSCs. First, TRAIL was largely secreted by PBiNSCs into the media as part of extracellular vesicles (EVs). Second, the secreted TRAIL was able to bind back onto PBiNSCs in an autocrine-like manner, thereby engaging the DR5 receptor on the PBiNSCs themselves. These observations emphasize the need for a greater understanding of TRAIL trafficking, secretion, and membrane interactions in order to optimize its therapeutic activity.

Although the initial goal was for TRAIL to be presented on the plasma membrane of PBiN-

SCs, we found that TRAIL was instead predominantly secreted into the media in the form of EVs. The molecular mechanisms that govern the sorting and packaging of membrane proteins into extracellular vesicles are not fully understood, but they involve complex and tightly regulated processes. In many cases, incorporation of proteins into vesicles depends on ubiquitination, which serves as a tag recognized by the endosomal sorting complexes required for transport (ESCRT) machinery (184). Adaptor proteins like ALIX and TSG101 recognize other signal motifs while ESCRT-independent pathways rely on lipid rafts or tetraspanins (184). In most cases, efficient loading of target proteins into exosomes requires specific scaffold proteins, such as Lamp2b, an EV-associated membrane protein (185). Fusion to EV-specific proteins or incorporation of targeting domains promotes integration during biogenesis. The mechanisms by which membrane-bound TRAIL becomes incorporated into EVs are not fully understood, though similar findings have been reported in other systems (120, 186). When endogenous TRAIL is produced by immune cells, the protein is stored on lysosomal-like compartments in the cytoplasm and is secreted upon stimulation in microvesicles (186). Given that the TRAIL construct was designed for plasma membrane localization, a better understanding of protein trafficking in PBiNSCs is needed. It remains unclear whether TRAIL secretion is a constant process or stimulus-dependent. Nonetheless, under normal culture conditions, EV-associated TRAIL is released in exosomes and retains bioactivity. Further work is required to clarify this process and the mechanisms of TRAIL trafficking and EV release in PBiNSCs.

TRAIL bound on the surface of extracellular vesicles has been reported by multiple groups to have superior cytotoxicity than the soluble derivatives. EVs coated with TRAIL produced from mesenchymal cells were efficient at inducing apoptosis in several cancer lines resistant to soluble TRAIL (120). Interestingly, another study found that ectopically expressed soluble TRAIL cound bind to the surface of EVs, despite lacking a transmembrane domain, and exhibited superior cytotoxity activity compared to free TRAIL (187). The reasons for improved killing are likely related to TRAIL oligomerization, as anchoring to lipid membranes allows for higher order clustering, which enables stronger induction of apoptosis on target cells (188).

We demonstrate that knockout of the endogenous DR5 receptor is required to sustain high level TRAIL expression in PBiNSCs. Ectopic expression of TRAIL from PBiNSCs resulted in the secretion of the protein on EVs, which was able to re-engaged these cells through binding to DR5. This binding back to PBiNSCs led to elevated levels of cleaved caspase-3 activity and reduced cell viability. CRISPR–Cas9–mediated knockout of DR5 restored cell viability to baseline levels following TRAIL transduction. Importantly, TRAIL-DR5KO-PBiNSCs exhibited superior cytotoxicity against PriGOs, which can be attributed to **(1)** sustained TRAIL expression in PBiNSCs and **(2)** the elimination of competitive TRAIL binding to DR5 on the PBiNSC surface.

Other studies have reported similar potential toxicities associated with ectopic TRAIL expression in cellular vehicles. For example, Jiang et al. observed that induced neural stem cells engineered to express TRAIL formed smaller neurospheres and took longer to form them compared to untransduced cells, although no mechanistic explanation was provided (154). In another study, the expression of soluble TRAIL in mesenchymal stem cells was unstable and declined rapidly after several passages (189). Other studies have reported that although the cellular vehicles themselves express TRAIL receptors, they were largely resistant to TRAIL-mediated apoptosis. We demonstrate that the knockout of these receptors in the cellular vehicles can enhance cytotoxic killing in vitro by freeing up available ligands and removing auto toxic problems.

TRAIL-DR5KO-PBiNSCs represent a stable cell line, as demonstrated in vivo experiments. Following striatal injection in mice, TRAIL-DR5KO-PBiNSCs exhibited persistent engraftment at one-month follow-up. TRAIL expression was maintained, and loss of DR5 did not negatively impact cell viability in vivo. These in vivo experiments suggests that TRAIL-DR5KO-PBiNSCs are suitable platform for longterm therapeutic delivery.

4.0.3 TRAIL-mediated apoptosis in glioblastoma

Resistance to TRAIL-mediated apoptosis is widespread in cancer cell lines, with more than half of tested lines in vitro exhibiting various degrees of resistance (129). Studies using common glioblastoma cell lines, such as U87MG and T98G, show resistance to TRAIL cytotoxicity, while although

other glioma lines exhibit partial sensitivity. We observed similar outcomes in both co-culture assays and conditioned media experiments. Among the glioblastoma lines we tested, PriGO17s showed partial sensitivity to TRAIL treatment, whereas PriGO8As and PriGO9As were highly resistant, appearing to modulate resistance via distinct mechanisms.

Heterogeneity

Targeting specific cellular pathways in cancer is often limited by inter- and intratumoral heterogeneity. Pronounced genetic and molecular differences among glioma cells allow certain clonal populations to escape treatment and acquire drug resistance. In this study, we investigated three primary glioblastoma cell lines derived from patient samples. These patient-derived lines were enriched for stem cell–like properties, including the ability to generate diffuse glioblastomas in vivo and to differentiate along neuronal lineages (190). All three cell lines exhibited distinct responses to TRAIL treatment. PriGO8As and PriGO9As were highly resistant, with PriGO9As showing slight stimulation at low doses of TRAIL-DR5KO-PBiNSCs. PriGO17s had partial sensitivity to TRAIL-induced killing as a significant fraction of cells remained unrepsonsive, reflecting intratumoral heterogeneity.

evTRAIL delivery

EvTRAILs have been reported to induce apoptosis more effectively than soluble TRAIL in cancer cell lines, likely due to their higher-order clustering on lipid membranes (120, 187, 188). However, in our glioma cell lines, TRAIL presentation on EVs was insufficient to overcome resistance in PriGO8As and PriGO9As, indicating that there are likely downstream inhibitions of the extrinsic apoptotic pathway. Interestingly, in PriGO17s, previous work in our lab found that treatment with high concentrations of soluble recombinant TRAIL reached a plateau in cytotoxic action. In contrast, when increasing the effector-to-target ratio for evTRAIL treatment, no plateau was observed, suggesting that sustained delivery and presentation of evTRAIL can enhance apoptotic activity.

Delivery of extracellular vesicles as a stand-alone therapeutic has received considerable attention for cancer treatment. EVs have been explored for the delivery of anti-tumor cargo, including nucleic acids, microRNAs, siRNAs, proteins, and chemotherapeutic drugs. Interest in the delivery of EVs is primarily due to their biocompatibility, as naturally produced entities from the body, which minimizes immune rejection, their stability in body fluids, and their potential for tumor-specific targeting (191). To date, no EV-based clinical trials for glioblastoma have been conducted, despite ongoing trials and promising results in other tumor types. We propose a separate therapeutic approach whereby using TRAIL-coated EVs purified from PBiNSC culture as a stand-alone treatment. EVs have been shown to be stable in systemic circulation, capable of crossing the blood–brain barrier, and can also be delivered intranasally for direct targeting of brain regions (192).

Resistance mechanisms

Mapping TRAIL resistance to underlying genetic and molecular differences between glioma cell lines can help better inform strategies for combination treatment. We investigated protein expression, genetic alterations, and responses to various sensitizing agents in order to better understand the mechanisms of TRAIL sensitivity and resistance.

Surface level of DR5 is often associated with TRAIL sensitivity; however, this relationship is confounded by alterations in downstream signaling pathways that cannot be predicted by receptor expression alone (193). Similarly, we found that total DR5 protein levels do not correlate with TRAIL-mediated killing. Despite PriGO8As expressing significant levels of DR5, this cell line remained resistant to both soluble TRAIL and evTRAIL. PriGO9As, which lack DR5 expression entirely, showed similar resistance. In contrast, PriGO17s, which express lower DR5 levels than PriGO8As, exhibited a partial response to TRAIL treatment. We conclude that while DR5 is required for TRAIL-mediated cytotoxic activity, its presence alone is not sufficient to determine sensitivity. Further work is needed to determine expression of DR5 at the cell surface level, as it is possible that DR5 is not properly presented on the surface of PriGO8As.

We also investigated the relationship between the tumor suppressor protein p53 and TRAIL-mediated apoptosis. The role of p53 is largely indirect: it can transcriptionally upregulate death receptors, potentiate the intrinsic apoptotic pathway, and regulate expression of other pro-apoptotic genes (135, 194). In certain contexts, however, p53 can also exert anti-apoptotic effects through transcriptional targets such as decoy receptors, EGFR2, Akt, and NF-kB (194). In many in vitro cancer cell lines, partial TRAIL sensitivity can be restored through p53 activation (194). However, we find in the three glioma cell lines we tested, wild-type p53 function was not necessary for TRAIL-induced apoptosis. Despite expressing wild-type p53 and high levels of DR5, PriGO8As showed no apoptotic response or decreased cell viability following TRAIL treatment. In contrast, the only TRAIL sensitive line PriGO17s harbor a missense R248W mutation in p53, a gain-of-function variant in which DNA binding to canonical consensus sequences is impaired. In addition to losing tumor-suppressor activity, p53 R248W acquires oncogenic properties, such as enhanced proliferation and invasion (195). Furthermore, the substitution of arginine with tryptophan destabilizes its secondary structure, exposing hydrophobic cores responsible for protein aggregation (166). Aggregation of p53 in PriGO17s was consistent with our Western blot data. Based on sequencing and functional assays, we conclude that wild-type p53 is not required for TRAIL-mediated apoptosis in these glioma cells. This is further supported by treatment with APG115, which inhibits MDM2 to increase intracellular p53 levels. High doses of APG115 had no effect on TRAIL sensitivity, indicating that levels of wildtype p53 are not significant for the extrinsic apoptotic pathway.

Future work should investigate the potential cleavage of TRAIL from the lipid membrane by glioblastoma-derived proteases. Membrane-bound TRAIL contains a sequence proximal to the transmembrane domain that allows for proteolytic processing into soluble TRAIL. Secretion by metalloproteases, such as ADAMTS3, could be a possible mechanism by which PriGO8As and PriGO9As escape apoptotic signaling (188).

TRAIL sensitization

We tested several agents to sensitize cells to TRAIL-mediated apoptosis and found that only AZD5582 exhibited a synergistic effect in PriGO17s. AZD5582 is a SMAC mimetic that inhibits anti-apoptotic proteins XIAP, cIAP1, and cIAP2 with IC50s in the 15-20 nM range. IAPs suppress apoptosis by binding to and inhibiting active caspases, thereby blocking execution of the apoptotic program. In the presence of evTRAIL, AZD5582 had an IC50 of approximately 50 nM, consistent with this effect being on-target. In contrast, AZD5582 alone induced cytotoxicity only at ¿1000 nM, with strong effects at 2000 nM in PriGO8As and PriGO9As and at 8000 nM in PriGO17s. These effects are probably off-target. Effective killing in these glioblastoma cells requires both a potent pro-apoptotic signal and inhibition of anti-apoptotic signals. However, this is only effective in a subset of glioblastoma cells, and further work on strategies to enhance TRAIL cytotoxicity are needed.

Chapter 5

Conclusion

In this work, we advance the field of cell-based cancer therapies by establishing PBiNSCs as a novel delivery platform. PBiNSCs can be efficiently engineered through CRISPR-Cas9 editing and lentiviral transduction to achieve stable expression of therapeutic proteins. Knockout of the endogenous DR5 receptor enables sustained, high-level TRAIL expression without impairing cell viability, thereby enhancing the cytotoxity of product. Furthermore, we show that PBiNSCs secrete TRAIL into the extracellular environment via incorporation into EV cargo, providing a natural mechanism to multimerize TRAIL for greater potency.

From these findings, we identify two complementary therapeutic strategies. (1) Direct transplantation of TRAIL-DR5KO-PBiNSCs into the brain, which demonstrated stable engraftment and TRAIL expression at one month in vivo, and (2) the use of evTRAILs as a standalone therapeutic. The latter offer the potential for non-invasive delivery, such as intranasal administration.

Future studies should work towards optimizing TRAIL-mediated cytotoxicity across diverse glioblastoma subtypes. Our findings reveal strong resistance to TRAIL-mediated killing in patient-derived glioma cell lines. TRAIL sensitization was only achieved following IAP inhibition in PriGO17s.

Author Contributions

The content of this manuscript was written by Shu Song with editorial suggestions from Dr. Ian Lorimer. All of the experiments presented in this manuscript are the work of Shu Song with the exception of in vivo mice experiments and immunohistochemistry done by Margarita Lui. As noted above, all operations involving the Beckman Coulter MoFlo XDP cell sorter and Sanger sequencing experiments were conducted through the OHRI Core Facilities.

References

[1] Louis DN, Perry A, Wesseling P, Brat DJ, Cree IA, Figarella-Branger D, et al. The 2021 WHO Classification of Tumors of the Central Nervous System: a summary. Neuro Oncol. 2021;23(8):1231-51. doi.org/10.1093/neuonc/noab106

[2] Stupp R, Mason WP, van den Bent MJ, Weller M, Fisher B, Taphoorn MJB, et al. Radiotherapy plus concomitant and adjuvant temozolomide for glioblastoma. N Engl J Med. 2005;352(10):987-96. doi.org/10.1056/NEJMoa043330

[3] Tamimi AF, Juweid M. Epidemiology and outcome of glioblastoma. In: De Vleeschouwer S, editor. Glioblastoma [Internet]. Brisbane (AU): Codon Publications; 2017 Sep 27. Chapter 8. doi.org/10.15586/codon.glioblastoma.2017.ch8

[4] Ostrom QT, Gittleman H, Farah P, Ondracek A, Chen Y, Wolinsky Y, et al. CBTRUS statistical report: primary brain and central nervous system tumors diagnosed in the United States in 2006-2010. Neuro Oncol. 2013;15 Suppl 2:ii1-56. doi.org/10.1093/neuonc/not151

[5] Vaz-Salgado M, Villamayor M, Albarrán V, Alía V, Sotoca P, Chamorro J, et al. Recurrent glioblastoma: a review of the treatment options. Cancers (Basel). 2023;15(17):4279. doi.org/10.3390/cancers15174279

[6] Rapp M, Baernreuther J, Turowski B, Steiger HJ, Sabel M, Kamp MA. Recurrence pattern analysis of primary glioblastoma. World Neurosurg. 2017;103:733-40. doi.org/10.1016/j.wneu.2017.04.053

[7] McKinnon C, Nandhabalan M, Murray SA, Plaha P. Glioblastoma: clinical presentation, diagnosis, and management. BMJ. 2021;374:n1560. doi.org/10.1136/bmj.n1560

[8] Fernandes C, Costa A, Osório L, Lago RC, Linhares P, Carvalho B, et al. Current standards of care in glioblastoma therapy. In: De Vleeschouwer S, editor. Glioblastoma [Internet]. Brisbane (AU): Codon Publications; 2017 Sep 27. Chapter 11. doi.org/10.15586/codon.glioblastoma.2017.ch11

[9] Larjavaara S, Mäntylä R, Salminen T, Haapasalo H, Raitanen J, Jääskeläinen J, et al. Incidence of gliomas by anatomic location. Neuro Oncol. 2007;9:319-25. doi.org/10.1215/15228517-2007-016

[10] Davis ME. Glioblastoma: overview of disease and treatment. Clin J Oncol Nurs. 2016;20(5 Suppl):S2-8. doi.org/10.1188/16.CJON.S1.2-8

[11] Nelson SJ, Cha S. Imaging glioblastoma multiforme. Cancer J. 2003;9(2):134-45. doi.org/10.1097/00130404-200303000-00009

[12] Hanif F, Muzaffar K, Perveen K, Malhi SM, Simjee SU. Glioblastoma multiforme: a review of its epidemiology and pathogenesis through clinical presentation and treatment. Asian Pac J Cancer Prev. 2017;18(1):3-9. doi.org/10.22034/APJCP.2017.18.1.3

[13] Brat DJ, Castellano-Sanchez AA, Hunter SB, Pecot M, Cohen C, Hammond EH, et al. Pseudopalisades in glioblastoma are hypoxic, express extracellular matrix proteases, and are formed by an actively migrating cell population. Cancer Res. 2004;64(3):920-7. doi.org/10.1158/0008-5472.CAN-03-2073

[14] Rojiani AM, Dorovini-Zis K. Glomeruloid vascular structures in glioblastoma multiforme: an immunohistochemical and ultrastructural study. J Neurosurg. 1996;85(6):1078-84. doi.org/10.3171/jns.1996.85.6.1078

[15] Ballato M, Germanà E, Ricciardi G, Giordano WG, Tralongo P, Buccarelli M, et al. Understanding neovascularization in glioblastoma: insights from the current literature. Int J Mol Sci. 2025;26(6):2763. doi.org/10.3390/ijms26062763

[16] Muscatello LV, Avallone G, Serra F, Seuberlich T, Mandara MT, Siso S, et al. Glomeruloid microvascular proliferation, desmoplasia, and high proliferative index as potential indicators of high grade canine choroid plexus tumors. Vet Pathol. 2018;55(1):49-58. doi.org/10.1177/0300985817754124

[17] Park JH, Lee HK. Current understanding of hypoxia in glioblastoma multiforme and its response to immunotherapy. Cancers. 2022;14(5):1176. doi.org/10.3390/cancers14051176

[18] Comba A, Faisal SM, Varela ML, Hollon T, Al-Holou WN, Umemura Y, et al. Uncovering spatiotemporal heterogeneity of high-grade gliomas: from disease biology to therapeutic implications. Front Oncol. 2021;11:703764. doi.org/10.3389/fonc.2021.703764

[19] Torp SH, Granli US. Proliferative activity in human glioblastomas assessed by various methods. Apmis. 2001;109(11):865-9. doi.org/10.1034/j.1600-0463.2001.091209

[20] Zong H, Verhaak RGW, Canoll P. The cellular origin for malignant glioma and prospects for clinical advancements. Expert Rev Mol Diagn. 2012;12(4):383-94. doi.org/10.1586/erm.12.30

[21] Yao M, Li S, Wu X, Diao S, Zhang G, He H, et al. Cellular origin of glioblastoma and its implication in precision therapy. Cell Mol Immunol. 2018;15(8):737-9. doi.org/10.1038/cmi.2017.159

[22] Batlle E, Clevers H. Cancer stem cells revisited. Nat Med. 2017;23(10):1124-34. doi.org/10.1038/nm.4409

[23] Singh SK, Hawkins C, Clarke ID, Squire JA, Bayani J, Hide T, et al. Identification of human brain tumour initiating cells. Nature. 2004;432(7015):396-401. doi.org/10.1038/nature03128

[24] Liu G, Yuan X, Zeng Z, Tunici P, Ng H, Abdulkadir IR, et al. Analysis of gene expression and chemoresistance of CD133+ cancer stem cells in glioblastoma. Mol Cancer. 2006;5:67. doi.org/10.1186/1476-4598-5-67

[25] Mesrati MH, Behrooz AB, Abuhamad AY, Syahir A. Understanding glioblastoma biomarkers: knocking a mountain with a hammer. Cells. 2020;9(5):1236. doi.org/10.3390/cells9051236

[26] Melhem JM, Detsky J, Lim-Fat MJ, Perry JR. Updates in IDH-wildtype glioblastoma. Neurotherapeutics. 2022;19(6):1705-23. doi.org/10.1007/s13311-022-01251-6

[27] Lan Z, Li X, Zhang X. Glioblastoma: an update in pathology, molecular mechanisms and biomarkers. Int J Mol Sci. 2024;25(5):3040. doi.org/10.3390/ijms25053040

[28] Verhaak RGW, Hoadley KA, Purdom E, Wang V, Qi Y, Wilkerson MD, et al. Integrated genomic analysis identifies clinically relevant subtypes of glioblastoma characterized by abnormalities in PDGFRA, IDH1, EGFR, and NF1. Cancer Cell. 2010;17(1):98-110. doi.org/10.1016/j.ccr.2009.12.020

[29] Mandel JJ, Yust-Katz S, Patel AJ, Cachia D, Liu D, Park M, et al. Inability of positive phase II clinical trials of investigational treatments to subsequently predict positive phase III clinical trials in glioblastoma. Neuro Oncol. 2018;20(1):113-22. doi.org/10.1093/neuonc/nox144

[30] Patel AP, Tirosh I, Trombetta JJ, Shalek AK, Gillespie SM, Wakimoto H, et al. Single-cell RNA-seq highlights intratumoral heterogeneity in primary glioblastoma. Science. 2014;344(6190):1396-401. doi.org/10.1126/science.1254257

[31] Sottoriva A, Spiteri I, Piccirillo SGM, Touloumis A, Collins VP, Marioni JC, et al. Intratumor heterogeneity in human glioblastoma reflects cancer evolutionary dynamics. Proc Natl Acad Sci U S A. 2013;110(10):4009-14. doi.org/10.1073/pnas.1219747110

[32] García-Montaño LA, Licón-Muñoz Y, Martinez FJ, Keddari YR, Ziemke MK, Chohan MO, et al. Dissecting intra-tumor heterogeneity in the glioblastoma microenvironment using fluorescence-guided multiple sampling. Mol Cancer Res. 2023;21(8):755-67. doi.org/10.1158/1541-7786.MCR-23-0048

[33] Meyer M, Reimand J, Lan X, Head R, Zhu X, Kushida M, et al. Single cell-derived clonal analysis of human glioblastoma links functional and genomic heterogeneity. Proc Natl Acad Sci U S A. 2015;112(3):851-6. doi.org/10.1073/pnas.1320611111

[34] Pant A, Lim M. CAR-T therapy in GBM: current challenges and avenues for improvement. Cancers (Basel). 2023;15(4):1249. doi.org/10.3390/cancers15041249

[35] Chan JTN, Henley-Waters J, Kayhanian S. Chimeric antigen receptor (CAR)-T-cell therapy for glioblastoma: what can we learn from the early clinical trials? A systematic review. Neuro-Oncol Adv. 2025;7(1):vdaf115. doi.org/10.1093/noajnl/vdaf115

[36] Park S, Maus MV, Choi BD. CAR-T cell therapy for the treatment of adult high-grade gliomas. npj Precis Oncol. 2024;8:279. doi.org/10.1038/s41698-024-00753-0

[37] O'Rourke DM, Nasrallah MP, Desai A, Melenhorst JJ, Mansfield K, Morrissette JJD, et al. A single dose of peripherally infused EGFRvIII-directed CAR T cells mediates antigen loss and induces adaptive resistance in patients with recurrent glioblastoma. Sci Transl Med. 2017;9(399):eaaa0984. doi.org/10.1126/scitranslmed.aaa0984

[38] Bagley SJ, Desai AS, Fraietta JA, Silverbush D, Chafamo D, Freeburg NF, et al. Intracerebroventricular bivalent CAR T cells targeting EGFR and IL-13R2 in recurrent glioblastoma: a phase 1 trial. Nat Med. 2025;31(8):2778-87. doi.org/10.1038/s41591-025-03745-0

[39] Pandit R, Chen L, Götz J. The blood-brain barrier: physiology and strategies for drug delivery. Ageing Res Rev. 2020;64:101174. doi.org/10.1016/j.addr.2019.11.009

[40] Ahmed MH, Canney M, Carpentier A, Idbaih A. Overcoming the blood-brain barrier in glioblastoma: status and future perspective. Rev Neurol (Paris). 2023;179(12):931-42. doi.org/10.1016/j.neurol.2023.03.013

[41] Syková E, Nicholson C. Diffusion in brain extracellular space. Physiol Rev. 2008;88(4):1277-340. doi.org/10.1152/physrev.00027.2007

[42] Gaietto A, Panetta JC, Pauley JL, Relling MV, Ribeiro RC, Ehrhardt MJ, et al. Ommaya reservoir use in pediatric ALL and NHL: a review at St. Jude Children's Research Hospital. Cancer Chemother Pharmacol. 2024;93(6):617-25. doi.org/10.1007/s00280-024-04653-9

[43] Carvey PM, Maag TJ, Lin D. Injection of biologically active substances into the brain. In: Flanagan TRJ, Emerich DF, Winn SR, editors. Providing pharmacological access to the brain: alternate approaches. Methods Neurosci. Vol. 21. San Diego: Academic Press; 1994. p. 214-36. doi.org/10.1016/B978-0-12-185291-7.50019-9

[44] Pardridge WM. A historical review of brain drug delivery. Pharmaceutics. 2022;14(6):1283. doi.org/10.3390/pharmaceutics14061283

[45] Gabrusiewicz K, Ellert-Miklaszewska A, Lipko M, Sielska M, Frankowska M, Kaminska B. Characteristics of the alternative phenotype of microglia/macrophages and its modulation in experimental gliomas. PLoS One. 2011;6(8):e23902. doi.org/10.1371/journal.pone.0023902

[46] Wesolowska A, Kwiatkowska A, Slomnicki L, Dembinski M, Master A, Sliwa M, et al. Microglia-derived TGF- as an important regulator of glioblastoma invasion—an inhibition of TGF--dependent effects by shRNA against human TGF- type II receptor. Oncogene. 2008;27(7):918-30. doi.org/10.1038/sj.onc.1210683

[47] Sørensen MD, Dahlrot RH, Boldt HB, Hansen S, Kristensen BW. Tumour-associated microglia/macrophages predict poor prognosis in high-grade gliomas and correlate with an aggressive tumour subtype. Neuropathol Appl Neurobiol. 2018;44(2):185-206. doi.org/10.1111/nan.12428

[48] Martinez-Lage M, Lynch TM, Bi Y, Cocito C, Way GP, Pal S, et al. Immune landscapes associated with different glioblastoma molecular subtypes. Acta Neuropathol Commun. 2019;7(1):203. doi.org/10.1186/s40478-019-0803-6

[49] Woroniecka KI, Chongsathidkiet P, Rhodin KE, Kemeny H, Dechant C, Farber SH, et al. T-cell exhaustion signatures vary with tumor type and are severe in glioblastoma. Clin Cancer Res. 2018;24(17):4175-86. doi.org/10.1158/1078-0432.CCR-17-1846

[50] Martinez-Lage M, Lynch TM, Bi Y, Cocito C, Way GP, Pal S, et al. Immune landscapes associated with different glioblastoma molecular subtypes. Acta Neuropathol Commun. 2019;7(1):203. doi.org/10.1186/s40478-019-0803-6

[51] Liu Y, Zhou F, Ali H, Lathia JD, Chen P. Immunotherapy for glioblastoma: current state, challenges, and future perspectives. Cell Mol Immunol. 2024;21(12):1354-75. doi.org/10.1038/s41423-024-01226-x

[52] Weller M, Cloughesy T, Perry JR, Wick W. Standards of care for treatment of recurrent glioblastoma—are we there yet? Neuro Oncol. 2013;15(1):4-27. doi.org/10.1093/neuonc/nos273

[53] Vollmann-Zwerenz A, Leidgens V, Feliciello G, Klein CA, Hau P. Tumor cell invasion in glioblastoma. Int J Mol Sci. 2020;21(6):1932. doi.org/10.3390/ijms21061932

[54] Leahy AB, Elgarten CW, Grupp SA, Maude SL, Teachey DT. Tisagenlecleucel for the treatment of B-cell acute lymphoblastic leukemia. Expert Rev Hematol. doi.org/10.1080/14737140.2018.1512411

[55] Jacobson CA, Locke FL, Ma L, Asubonteng J, Hu ZH, Siddiqi T, et al. Real-world evidence of axicabtagene ciloleucel for the treatment of large B-cell lymphoma in the United States. Transplant Cell Ther. 2022;28(9):581.e1-581.e8. doi.org/10.1016/j.jtct.2022.05.026

[56] U.S. Food and Drug Administration. FDA approves tisagenlecleucel for B-cell ALL and tocilizumab for cytokine release syndrome. Published September 7, 2017.

[57] U.S. Food and Drug Administration. FDA approves axicabtagene ciloleucel for large B-cell lymphoma. Published October 18, 2017.

[58] Li L, Harms KM, Ventura PB, Lagace DC, Eisch AJ, Cunningham LA. Focal cerebral ischemia induces a multilineage cytogenic response from adult subventricular zone that is predominantly gliogenic. Glia. 2010;58(13):1610-9. doi.org/10.1002/glia.21033

[59] Williamson MR, Jones TA, Drew MR. Functions of subventricular zone neural precursor cells in stroke recovery. Behav Brain Res. 2019;376:112209. doi.org/10.1016/j.bbr.2019.112209

[60] Kavari SL, Shah K. Engineered stem cells targeting multiple cell surface receptors in tumors. Stem Cells. 2020;38(1):34-44. doi.org/10.1002/stem.3069

[61] Park SA, Ryu CH, Kim SM, Lim JY, Park SI, Jeong CH, et al. CXCR4-transfected human umbilical cord blood-derived mesenchymal stem cells exhibit enhanced migratory capacity toward gliomas. Int J Oncol. 2011;38(1):97-103.

[62] Koizumi S, Gu C, Amano S, Yamamoto S, Ihara H, Tokuyama T, et al. Migration of mouse-induced pluripotent stem cells to glioma-conditioned medium is mediated by tumor-associated specific growth factors. Int J Oncol. 2012;41(4):1247-54. doi.org/10.3892/ol.2011.234

[63] Glass R, Synowitz M, Kronenberg G, Walzlein JH, Markovic DS, Wang LP, et al. Glioblastoma-induced attraction of endogenous neural precursor cells is associated with improved survival. J Neurosci. 2005;25(10):2637-46. doi.org/10.1523/JNEUROSCI.5118-04.2005

[64] Aboody KS, Brown A, Rainov NG, Bower KA, Liu S, Yang W, et al. Neural stem cells display extensive tropism for pathology in adult brain: evidence from intracranial gliomas. Proc Natl Acad Sci USA. 2000;97(23):12846-51. doi.org/10.1073/pnas.97.23.12846

[65] Jeon JY, An JH, Kim SU, Park HG, Lee MA. Migration of human neural stem cells toward an intracranial glioma. Exp Mol Med. 2008;40(1):84-91. doi.org/10.3858/emm.2008.40.1.84

[66] Bagó JR, Alfonso-Pecchio A, Okolie O, Dumitru R, Rinkenbaugh A, Baldwin AS, et al. Therapeutically engineered induced neural stem cells are tumour-homing and inhibit progression of glioblastoma. Nat Commun. 2016;7:10593. doi.org/10.1038/ncomms10593

[67] Heese O, Disko A, Zirkel D, Westphal M, Lamszus K. Neural stem cell migration toward gliomas in vitro. Neuro Oncol. 2005;7(4):476-84. doi.org/10.1215/S1152851704000754

[68] An J, Yan H, Li X, Tan R, Chen X, Zhang Z, et al. The inhibiting effect of neural stem cells on proliferation and invasion of glioma cells. Oncotarget. 2017;8(44):76949-60. doi.org/10.18632/oncotarget.20270

[69] Yin X, Liu X, Xiao X, Yi K, Chen W, Han C, et al. Human neural stem cells repress glioma cell progression in a paracrine manner by downregulating the Wnt/-catenin signalling pathway. FEBS Open Bio. 2023;13(9):1127-37. doi.org/10.1002/2211-5463.13671

[70] Lee HJ, Doo SW, Kim DH, Cha YJ, Kim JH, Song YS, et al. Cytosine deaminase-expressing human neural stem cells inhibit tumor growth in prostate cancer-bearing mice. Cancer Lett. 2013;335(1):58-65. doi.org/10.1016/j.canlet.2013.01.048

[71] Kucerova L, Matuskova M, Pastorakova A, Tyciakova S, Jakubikova J, Bohovic R, et al. Cytosine deaminase expressing human mesenchymal stem cells mediated tumour regression in melanoma bearing mice. J Gene Med. 2008;10(10):1071-82. doi.org/10.1002/jgm.1239

[72] Chang DY, Yoo SW, Hong Y, Kim S, Kim SJ, Yoon SH, et al. The growth of brain tumors can be suppressed by multiple transplantation of mesenchymal stem cells expressing cytosine deaminase. Int J Cancer. 2010;127:1975-83. doi.org/10.1002/ijc.25383

[73] Gutova M, Goldstein L, Metz M, Hovsepyan A, Tsurkan LG, Tirughana R, et al. Optimization of a neural stem-cell-mediated carboxylesterase/irinotecan gene therapy for metastatic neuroblastoma. Mol Ther Oncolytics. 2016;4:67-76. doi.org/10.1016/j.omto.2016.11.004

[74] Kauer TM, Figueiredo JL, Hingtgen S, Shah K. Encapsulated therapeutic stem cells implanted in the tumor resection cavity induce cell death in gliomas. Nat Neurosci. 2012;15(2):197-204. doi.org/10.1038/nn.3019

[75] Spano C, Grisendi G, Golinelli G, Rossignoli F, Prapa M, Bestagno M, et al. Soluble TRAIL armed human MSC as gene therapy for pancreatic cancer. Sci Rep. 2019;9(1):1788. doi.org/10.1038/s41598-018-37433-6

[76] Studeny M, Marini FC, Champlin RE, Zompetta C, Fidler IJ, Andreeff M. Bone marrow-derived mesenchymal stem cells as vehicles for interferon-beta delivery into tumors. Cancer Res. 2002;62(13):3603-8.

[77] Portnow J, Synold TW, Badie B, Tirughana R, Lacey SF, D'Apuzzo M, et al. Neural stem cell-based anticancer gene therapy: a first-in-human study in recurrent high-grade glioma patients. Sci Transl Med. 2017;9(399):eaaa0984. doi.org/10.1158/1078-0432.CCR-16-1518

[78] Benmelouka AY, Munir M, Sayed A, Attia MS, Ali MM, Negida A, et al. Neural stem cell-based therapies and glioblastoma management: Current evidence and clinical challenges. Int J Mol Sci. 2021;22(5):2258. doi.org/10.3390/ijms22052258

[79] Ehtesham M, Kabos P, Kabosova A, Neuman T, Black KL, Yu JS. The use of interleukin 12-secreting neural stem cells for the treatment of intracranial glioma. Cancer Res. 2002;62(20):5657-63.

[80] Benedetti S, Pirola B, Pollo B, Magrassi L, Bruzzone MG, Rigamonti D, et al. Gene therapy of experimental brain tumors using neural progenitor cells. Nat Med. 2000;6(4):447-50. doi.org/10.1038/74710

[81] Portnow J, Badie B, Blanchard MS, Kilpatrick J, Tirughana R, Metz M, et al. Feasibility of intracerebrally administering multiple doses of genetically modified neural stem cells to locally produce chemotherapy in glioma patients. Cancer Gene Ther. 2021;28(3-4):294-306. doi.org/10.1038/s41417-020-00219-y

[82] Satterlee AB, Dunn DE, Valdivia A, Malawsky D, Buckley A, Gershon T, et al. Spatiotemporal analysis of induced neural stem cell therapy to overcome advanced glioblastoma recurrence. Mol Ther Oncolytics. 2022;26:49-62. doi.org/10.1016/j.omto.2022.06.004

[83] Bagó JR, Okolie O, Dumitru R, Ewend MG, Parker JS, Vander Werff R, et al. Tumor-homing cytotoxic human induced neural stem cells for cancer therapy. Sci Transl Med. 2017;9(375):eaah6510. doi.org/10.1126/scitranslmed.aah6510

[84] Calinescu AA, Kauss MC, Sultan Z, Al-Holou WN, O'Shea SK. Stem cells for the treatment of glioblastoma: a 20-year perspective. CNS Oncol. 2021;10(1):CNS73. doi.org/10.2217/cns-2020-0026

[85] Hemmer K, Zhang M, van Wüllen T, Sakalem M, Tapia N, Baumuratov A, et al. Induced neural stem cells achieve long-term survival and functional integration in the adult mouse brain. Stem Cell Reports. 2014;3(3):423-31. doi.org/10.1016/j.stemcr.2014.06.017

[86] Hong JY, Lee SH, Lee SC, Kim JW, Kim KP, Kim SM, et al. Therapeutic potential of induced neural stem cells for spinal cord injury. J Biol Chem. 2014;289(47):32512-25. doi.org/10.1074/jbc.M114.588871

[87] Yao H, Gao M, Ma J, Maoying Z, Li S, Wu B, et al. Transdifferentiation-induced neural stem cells promote recovery of middle cerebral artery stroke rats. PLoS One. 2015;10(8):e0137211. doi.org/10.1371/journal.pone.0137211

[88] Takahashi K, Yamanaka S. Induction of pluripotent stem cells from mouse embryonic and adult fibroblast cultures by defined factors. Cell. 2006;126(4):663-76. doi.org/10.1016/j.cell.2006.07.024

[89] Sheng C, Jungverdorben J, Wiethoff H, Lin Q, Flitsch LJ, Stadler V, et al. A stably self-renewing adult blood-derived induced neural stem cell exhibiting patternability and epigenetic rejuvenation. Nat Commun. 2018;9(1):4047. doi.org/10.1038/s41467-018-06398-5

[90] Berg LJ, Lee CK, Matsumura H, Leinhaas A, Konang R, Shaib AH, et al. Human neural stem cells directly programmed from peripheral blood show functional integration into the adult mouse brain. Stem Cell Res Ther. 2024;15(1):488. doi.org/10.1186/s13287-024-04110-7

[91] Wiley SR, Schooley K, Smolak PJ, Din WS, Huang CP, Nicholl JK, et al. Identification and characterization of a new member of the TNF family that induces apoptosis. Immunity. 1995;3(6):673-82. doi.org/10.1016/1074-7613(95)90057-8

[92] Daniels RA, Turley H, Kimberley FC, Lui XS, Mongkolsapaya J, Ch'en P, et al. Expression of TRAIL and TRAIL receptors in normal and malignant tissues. Cell Res. 2005;15(6):430-8. doi.org/10.1038/sj.cr.7290311

[93] Fanger NA, Maliszewski CR, Schooley K, Griffith TS. Human dendritic cells mediate cellular apoptosis via tumor necrosis factor-related apoptosis-inducing ligand (TRAIL). J Exp Med. 1999;190(8):1155-64. doi.org/10.1084/jem.190.8.1155

[94] Griffith TS, Wiley SR, Kubin MZ, Sedger LM, Maliszewski CR, Fanger NA. Monocyte-mediated tumoricidal activity via the tumor necrosis factor-related cytokine, TRAIL. J Exp Med. 1999;189(7):1343-54. doi.org/10.1084/jem.189.8.1343

[95] Kemp TJ, Moore JM, Griffith TS. Human B cells express functional TRAIL/Apo-2 ligand after CpG-containing oligodeoxynucleotide stimulation. J Immunol. 2004;173(2):892-9. doi.org/10.4049/jimmunol.173.2.892

[96] Zamai L, Ahmad M, Bennett IM, Azzoni L, Alnemri ES, Perussia B. Natural killer (NK) cell-mediated cytotoxicity: differential use of TRAIL and Fas ligand by immature and mature primary human NK cells. J Exp Med. 1998;188(12):2375-80. doi.org/10.1084/jem.188.12.2375

[97] Cassatella MA, Huber V, Calzetti F, Margotto D, Tamassia N, Peri G, et al. Interferon-activated neutrophils store a TNF-related apoptosis-inducing ligand (TRAIL/Apo-2 ligand) intracellular pool that is readily mobilizable following exposure to proinflammatory mediators. J Leukoc Biol. 2006;79(1):123-32. doi.org/10.1189/jlb.0805431

[98] Wang S, El-Deiry WS. TRAIL and apoptosis induction by TNF-family death receptors. Oncogene. 2003;22(56):8628-33. doi.org/10.1038/sj.onc.1207232

[99] Naval J, de Miguel D, Gallego-Lleyda A, Anel A, Martínez-Lostao L. Importance of TRAIL molecular anatomy in receptor oligomerization and signaling: implications for cancer therapy. Cancers (Basel). 2019;11(4):444. doi.org/10.3390/cancers11040444

[100] Pan G, O'Rourke K, Chinnaiyan AM, Gentz R, Ebner R, Ni J, et al. The receptor for the cytotoxic ligand TRAIL. Science. 1997;276(5309):111-3. doi.org/10.1126/science.276.5309.111

[101] Walczak H, Degli-Esposti MA, Johnson RS, Smolak PJ, Waugh JY, Boiani N, et al. TRAIL-R2: a novel apoptosis-mediating receptor for TRAIL. EMBO J. 1997;16(17):5386-97. doi.org/10.1093/emboj/16.17.5386

[102] Kischkel FC, Lawrence DA, Cauntharapai A, Schow P, Kim KJ, Ashkenazi A. Apo2L/TRAIL-dependent recruitment of endogenous FADD and caspase-8 to Death Receptors 4 and 5. Immunity. 2000;12(6):611-20. doi.org/10.1016/S1074-7613(00)80212-5

[103] Johnstone RW, Frew AJ, Smyth MJ. The TRAIL apoptotic pathway in cancer onset, progression and therapy. Nat Rev Cancer. 2008;8(10):782-98. doi.org/10.1038/nrc2465

[104] Ashkenazi A, Pai RC, Fong S, Leung S, Lawrence DA, Marsters SA, et al. Safety and antitumor activity of recombinant soluble Apo2 ligand. J Clin Invest. 1999;104(2):155-62. doi.org/10.1172/JCI6926

[105] Griffith TS, Chin WA, Jackson GC, Lynch DH, Kubin MZ. Intracellular regulation of TRAIL-induced apoptosis in human melanoma cells. J Immunol. 1998;161(6):2833-40.

[106] Pitti RM, Marsters SA, Ruppert S, Donahue CJ, Moore A, Ashkenazi A. Induction of apoptosis by Apo-2 ligand, a new member of the tumor necrosis factor cytokine family. J Biol Chem. 1996;271(22):12687-90. doi.org/10.1074/jbc.271.22.12687

[107] Ganten TM, Koschny R, Sykora J, Schulze-Bergkamen H, Büchler P, Haas TL, et al. Preclinical differentiation between apparently safe and potentially hepatotoxic applications of TRAIL either alone or in combination with chemotherapeutic drugs. Clin Cancer Res. 2006;12(8):2640-6. doi.org/10.1158/1078-0432.CCR-05-2635

[108] Jo M, Kim TH, Seol DW, Esplen JE, Dorko K, Billiar TR, et al. Apoptosis induced in normal human hepatocytes by tumor necrosis factor-related apoptosis-inducing ligand. Nat Med. 2000;6(5):564-7. doi.org/10.1038/75045

[109] Lawrence D, Shahrokh Z, Marsters S, Achilles K, Shih D, Mounho B, et al. Differential hepatocyte toxicity of recombinant Apo2L/TRAIL versions. Nat Med. 2001;7(4):383-5. doi.org/10.1038/86397

[110] Kim SH, Kim KH, Kwagh JG, Dicker DT, Herlyn M, Rustgi AK, et al. Death induction by recombinant native TRAIL and its prevention by a caspase-9 inhibitor in primary human esophageal epithelial cells. J Biol Chem. 2004;279(38):40044-52. doi.org/10.1074/jbc.M404541200

[111] Nesterov A, Ivashchenko Y, Kraft AS. Tumor necrosis factor-related apoptosis-inducing ligand (TRAIL) triggers apoptosis in normal prostate epithelial cells. Oncogene. 2002;21(11):1135-40. doi.org/10.1038/sj.onc.1205151

[112] Leverkus M, Neumann M, Mengling T, Rauch CT, Bröcker EB, Krammer PH, et al. Regulation of tumor necrosis factor-related apoptosis-inducing ligand sensitivity in primary and transformed human keratinocytes. Cancer Res. 2000;60(3):553-9.

[113] Herbst RS, Eckhardt SG, Kurzrock R, Ebbinghaus S, O'Dwyer PJ, Gordon MS, et al. Phase I dose-escalation study of recombinant human Apo2L/TRAIL, a dual proapoptotic receptor agonist, in patients with advanced cancer. J Clin Oncol. 2009;27(28):4531-6. doi.org/10.1200/JCO.2009.25.1991

[114] Ouyang X, Shi M, Jie F, Bai Y, Shen P, Yu Z, et al. Phase III study of dulanermin (recombinant human tumor necrosis factor-related apoptosis-inducing ligand/Apo2 ligand) combined with vinorelbine and cisplatin in patients with advanced non-small-cell lung cancer. Invest New Drugs. 2018;36(2):315-22. doi.org/10.1007/s10637-017-0536-y

[115] Di Cristofano F, George A, Tajiknia V, Ghandali M, Wu L, Zhang Y, et al. Therapeutic targeting of TRAIL death receptors. Biochem Soc Trans. 2023;51(1):57-70. doi.org/10.1042/BST20220098

[116] Naval J, de Miguel D, Gallego-Lleyda A, Anel A, Martinez-Lostao L. Importance of TRAIL molecular anatomy in receptor oligomerization and signaling. Implications for cancer therapy. Cancers (Basel). 2019;11(4):444. doi.org/10.3390/cancers11040444

[117] De Miguel D, Gallego-Lleyda A, Ayuso JM, Pejenaute-Ochoa D, Jarauta V, Marzo I, et al. High-order TRAIL oligomer formation in TRAIL-coated lipid nanoparticles enhances DR5 cross-linking and increases antitumour effect against colon cancer. J Nanobiotechnology. 2016;14:71. doi.org/10.1016/j.canlet.2016.10.005

[118] Wang H, Davis JS, Wu X. Immunoglobulin Fc domain fusion to TRAIL significantly prolongs its plasma half-life and enhances its antitumor activity. Mol Cancer Ther. 2014;13(3):643-50. doi.org/10.1158/1535-7163.MCT-13-0645

[119] Han JH, Moon AR, Chang JH, Chang JH, Bae J, Choi JM, et al. Potentiation of TRAIL killing activity by multimerization through isoleucine zipper hexamerization motif. BMB Rep. 2016;49(5):282-7. doi.org/10.5483/bmbrep.2016.49.5.245

[120] Yuan ZQ, Kolluri KK, Gowers KHC, Janes SM. TRAIL delivery by MSC-derived extracellular vesicles is an effective anticancer therapy. J Extracell Vesicles. 2017;6(1):1265291. doi.org/10.1080/20013078.2017.1265291

[121] Sheridan JP, Marsters SA, Pitti RM, Gurney A, Skubatch M, Baldwin D, et al. Control of TRAIL-induced apoptosis by a family of signaling and decoy receptors. Science. 1997;277:818-21. doi.org/10.1126/science.277.5327.818

[122] Riccioni R, Pasquini L, Mariani G, Saulle E, Rossini A, Diverio D, et al. TRAIL decoy receptors mediate resistance of acute myeloid leukemia cells to TRAIL. Haematologica. 2005;90(5):612-24.

[123] Degli-Esposti MA, Dougall WC, Smolak PJ, Waugh JY, Smith CA, Goodwin RG. The novel receptor TRAIL-R4 induces NF-kappaB and protects against TRAIL-mediated apoptosis, yet retains an incomplete death domain. Immunity. 1997;7(6):813-20. doi.org/10.1016/s1074-7613(00)80399-4

[124] Pan G, Ni J, Wei YF, Yu G, Gentz R, Dixit VM. An antagonist decoy receptor and a death domain-containing receptor for TRAIL. Science. 1997;277(5327):815-8. doi.org/10.1126/science.277.5327.815

[125] Van Dijk M, Halpin-McCormick A, Sessler T, Samali A, Szegezdi E. Resistance to TRAIL in non-transformed cells is due to multiple redundant pathways. Cell Death Dis. 2013;4(7):e702. doi.org/10.1038/cddis.2013.214

[126] Oikonomou E, Kosmidou V, Katseli A, Kothonidis K, Mourtzoukou D, Kontogeorgos G, et al. TRAIL receptor upregulation and the implication of KRAS/BRAF mutations in human colon cancer tumors. Int J Cancer. 2009;125(9):2127-35. doi.org/10.1002/ijc.24613

[127] Wu GS, Burns TF, McDonald ER, Jiang W, Meng R, Krantz ID, et al. KILLER/DR5 is a DNA damage-inducible p53-regulated death receptor gene. Nat Genet. 1997;17(2):141-3. doi.org/10.1038/ng1097-141

[128] Qiao X, Guo S, Meng Z, Gan H, Wu Z, Sun Y, et al. Advances in the study of death receptor 5. Front Pharmacol. 2025;16:1549808. doi.org/10.3389/fphar.2025.1549808

[129] Thorburn A, Behbakht K, Ford H. TRAIL receptor-targeted therapeutics: resistance mechanisms and strategies to avoid them. Drug Resist Updat. 2008;11(1-2):17-24. doi.org/10.1016/j.drup.2008.02.001

[130] Nieminen AI, Partanen JI, Hau A, Klefström J. c-Myc primed mitochondria determine cellular sensitivity to TRAIL-induced apoptosis. EMBO J. 2007;26(4):1055-67. doi.org/10.1038/sj.emboj.7601551

[131] Ricci MS, Jin Z, Dews M, Yu D, Thomas-Tikhonenko A, Dicker DT, et al. Direct repression of FLIP expression by c-myc is a major determinant of TRAIL sensitivity. Mol Cell Biol. 2004;24(19):8541-55. doi.org/10.1128/MCB.24.19.8541-8555.2004

[132] Harrington CT, Sotillo E, Robert A, Hayer KE, Bogusz AM, Psathas J, et al. Transient stabilization, rather than inhibition, of MYC amplifies extrinsic apoptosis and therapeutic responses in refractory B-cell lymphoma. Leukemia. 2019;33(10):2429-41. doi.org/10.1038/s41375-019-0454-4

[133] Safa AR. c-FLIP, a master anti-apoptotic regulator. Exp Oncol. 2012;34(3):176-84.

[134] Siegmund D, Hadwiger P, Pfizenmaier K, Vornlocher HP, Wajant H. Selective inhibition of FLICE-like inhibitory protein (FLIP) expression with small interfering RNA oligonucleotides (siRNAs) is sufficient to sensitize tumor cells for TRAIL-induced apoptosis. Mol Med. 2002;8(11):725-32. doi.org/10.1007/BF03402036

[135] Willms A, Schittek H, Rahn S, Sosna J, Mert U, Adam D, et al. Impact of p53 status on TRAIL-mediated apoptotic and non-apoptotic signaling in cancer cells. PLoS One. 2019;14(4):e0214847. doi.org/10.1371/journal.pone.0214847

[136] Whang YE, Yuan XJ, Liu Y, Majumder S, Lewis TD. Regulation of sensitivity to TRAIL by the PTEN tumor suppressor. Vitam Horm. 2004;67:409-26. doi.org/10.1016/S0083-6729(04)67021-X

[137] Milone MC, O'Doherty U. Clinical use of lentiviral vectors. Leukemia. 2018;32(7):1529-41. doi.org/10.1038/s41375-018-0106-0

[138] Gaj T, Gersbach CA, Barbas CF. ZFN, TALEN, and CRISPR/Cas-based methods for genome engineering. Trends Biotechnol. 2013;31(7):397-405. doi.org/10.1016/j.tibtech.2013.04.004

[139] Gupta RM, Musunuru K. Expanding the genetic editing toolkit: ZFNs, TALENs, and CRISPR-Cas9. J Clin Invest. 2014;124(10):4154-61. doi.org/10.1172/JCI72992

[140] Jinek M, Chylinski K, Fonfara I, Hauer M, Doudna JA, Charpentier E. A programmable dual-RNA–guided DNA endonuclease in adaptive bacterial immunity. Science. 2012;337(6096):816-21. doi.org/10.1126/science.1225829

[141] Scully R, Panday A, Elango R, Willis NA. DNA double-strand break repair-pathway choice in somatic mammalian cells. Nat Rev Mol Cell Biol. 2019;20(10):698-714. doi.org/10.1038/s41580-019-0152-0

[142] Tisato V, Gonelli A, Voltan R, Secchiero P, Zauli G. Clinical perspectives of TRAIL: insights into central nervous system disorders. Cell Mol Life Sci. 2016;73(10):2017-27. doi.org/10.1007/s00018-016-2164-7

[143] Cannella B, Gaupp S, Omari KM, Raine CS. Multiple sclerosis: death receptor expression and oligodendrocyte apoptosis in established lesions. J Neuroimmunol. 2007;188(1-2):128-37. doi.org/10.1016/j.jneuroim.2007.05.018

[144] Gont A, Hanson JE, Lavictoire SJ, Parolin DA, Daneshmand M, Restall IJ, et al. PTEN loss represses glioblastoma tumor initiating cell differentiation via inactivation of Lgl1. Oncotarget. 2013;4(8):1266-79. doi.org/10.18632/oncotarget.1164

[145] Brinkman EK, van Steensel B. Rapid quantitative evaluation of CRISPR genome editing by TIDE and TIDER. Methods Mol Biol. 2019;1961:29-44. doi.org/10.1007/978-1-4939-9170-9-3

[146] Wedge ME, Jennings VA, Crupi MJF, Poutou J, Jamieson T, Pelin A, et al. Virally programmed extracellular vesicles sensitize cancer cells to oncolytic virus and small molecule therapy. Nat Commun. 2022;13:1898. doi.org/10.1038/s41467-022-29526-8

[147] Integrated DNA Technologies. Homology-directed repair using the Alt-R CRISPR-Cas9 system and Alt-R HDR donor oligos in induced pluripotent stem cells (iPSCs) [Internet]. Version 1. July 2023.

[148] Schubert M, Rettig GR, Kurgan G, McNeill MS, Wang J, Fiedler S, et al. Evaluate CRISPR-Cas9 edits quickly and accurately with rhAmpSeq targeted sequencing. Integrated DNA Technologies.

[149] Cerbini T, Funahashi R, Luo Y, Liu C, Park K, Rao M, et al. Transcription activator-like effector nuclease (TALEN)-mediated CLYBL targeting enables enhanced transgene expression and one-step generation of dual reporter human iPSC and NSC lines. PLoS One. 2015;10(1):e0116032. doi.org/10.1371/journal.pone.0116032

[150] Wimberger S, Akrap N, Firth M, Brengdahl J, Engberg S, Schwinn MK, et al. Simultaneous inhibition of DNA-PK and Pol improves integration efficiency and precision of genome editing. Nat Commun. 2023;14:4761. doi.org/10.1038/s41467-023-40344-4

[151] Wang Q, Liu J, Janssen JM, Goncalves MAFV. Precise homology-directed installation of large genomic edits in human cells with cleaving and nicking high-specificity Cas9 variants. Nucleic Acids Res. 2023;51(7):3465-84. doi.org/10.1093/nar/gkad165

[152] Roybal KT, Williams JZ, Morsut L, Rupp LJ, Kolinko I, Choe JH, et al. Engineering T cells with customized therapeutic response programs using synthetic Notch receptors. Cell. 2016;167(2):419-432.e16. doi.org/10.1016/j.cell.2016.09.011

[153] Di Pietro R, Secchiero P, Rana R, Gibellini D, Visani G, Bemis K, et al. Ionizing radiation sensitizes erythroleukemic cells but not normal erythroblasts to tumor necrosis factor-related apoptosis-inducing ligand (TRAIL)-mediated cytotoxicity by selective up-regulation of TRAIL-R1. Blood. 2001;97(9):2596-603. doi.org/10.1182/blood.v97.9.2596

[154] Jiang W, Yang Y, Mercer-Smith AR, Valdivia A, Bago JR, Woodell AS, et al. Development of next-generation tumor-homing induced neural stem cells to enhance treatment of metastatic cancers. Sci Adv. 2021;7(24):eabf1526. doi.org/10.1126/sciadv.abf1526

[155] Kugeratski FG, Hodge K, Lilla S, McAndrews KM, Zhou X, Hwang RF, et al. Quantitative proteomics identifies the core proteome of exosomes with syntenin-1 as the highest abundant protein and a putative universal biomarker. Nat Cell Biol. 2021;23(2):209-20. doi.org/10.1038/s41556-021-00693-y

[156] Welsh JA, Goberdhan DCI, O'Driscoll L, Buzas EI, Blenkiron C, Bussolati B, et al; MISEV Consortium. Minimal information for studies of extracellular vesicles (MISEV2023): From basic to advanced approaches. J Extracell Vesicles. 2024;13(1):e12482. doi.org/10.1002/jev2.12482

[157] Wu L, Gao C. Comprehensive overview of the role of glycosylation of extracellular vesicles in cancers. ACS Omega. 2023;8(50):47380-92. doi.org/10.1021/acsomega.3c07441

[158] Mori E, Thomas M, Motoki K, Nakazawa K, Tahara T, Tomizuka K, et al. Human normal hepatocytes are susceptible to apoptosis signal mediated by both TRAIL-R1 and TRAIL-R2. Cell Death Differ. 2004;11(2):203-7. doi.org/10.1038/sj.cdd.4401331

[159] Kominsky SL, Johnson HM, Bryan G, Tanabe T, Hobeika AC, Subramaniam PS, et al. IFN inhibition of cell growth in glioblastomas correlates with increased levels of the cyclin dependent kinase inhibitor p21 WAF1/CIP1. Oncogene. 1998;17(23):2973-9. doi.org/10.1038/sj.onc.1202217

[160] Park SY, Seol JW, Lee YJ, Cho JH, Kang HS, Kim IS, et al. IFN- enhances TRAIL-induced apoptosis through IRF-1. European Journal of Biochemistry. 2004;271(18):4222-8. doi.org/10.1111/j.1432-1033.2004.04362.x

[161] Kung CP, Weber JD. It's getting complicated—a fresh look at p53-MDM2-ARF triangle in tumorigenesis and cancer therapy. Front Cell Dev Biol. 2022;10:818744. doi.org/10.3389/fcell.2022.818744

[162] Singh AK, Chauhan SS, Singh SK, Verma VV, Singh A, Arya RK, et al. Dual targeting of MDM2 with a novel small-molecule inhibitor overcomes TRAIL resistance in cancer. Carcinogenesis. 2016;37(11):1027-40. doi.org/10.1093/carcin/bgw088

[163] Lemke J, von Karstedt S, Abd El Hay M, Conti A, Arce F, Montinaro A, et al. Selective CDK9 inhibition overcomes TRAIL resistance by concomitant suppression of cFLIP and Mcl-1. Cell Death Differ. 2014;21(3):491-502. doi.org/10.1038/cdd.2013.179

[164] Olivier M, Hollstein M, Hainaut P. TP53 mutations in human cancers: origins, consequences, and clinical use. Cold Spring Harb Perspect Biol. 2010;2(1):a001008. doi.org/10.1101/cshperspect.a001008

[165] Chen X, Zhang T, Su W, Dou Z, Zhao D, Jin X, et al. Mutant p53 in cancer: from molecular mechanism to therapeutic modulation. Cell Death Dis. 2022;13(11):974. doi.org/10.1038/s41419-022-05408-1

[166] Liu Q, Yu Y, Wei G. Oncogenic R248W mutation induced conformational perturbation of the p53 core domain and the structural protection by proteomimetic amyloid inhibitor ADH-6. Phys Chem Chem Phys. 2024;26(29):20068-86. doi.org/10.1039/d4cp02046d

[167] Liu J, Liu K, Wang Y, Shi Z, Xu R, Zhang Y, et al. Death receptor 5 is required for intestinal stem cell activity during intestinal epithelial renewal at homoeostasis. Cell Death Dis. 2024;15(1):27. doi.org/10.1038/s41419-023-06409-4

[168] Ihry RJ, Worringer KA, Salick MR, Frias E, Ho D, Theriault K, et al. p53 inhibits CRISPR–Cas9 engineering in human pluripotent stem cells. Nat Med. 2018;24:939-46. doi.org/10.1038/s41591-018-0050-6

[169] Haapaniemi E, Botla S, Persson J, Schmierer B, Taipale J. CRISPR-Cas9 genome editing induces a p53-mediated DNA damage response. Nat Med. 2018;24:927-30. doi.org/10.1038/s41591-018-0049-z

[170] Sarkar MK, Uppala R, Zeng C, Billi AC, Tsoi LC, Kidder A, et al. Keratinocytes sense and eliminate CRISPR DNA through STING/IFN- activation and APOBEC3G induction. J Clin Invest. 2023;133(9):e159393. doi.org/10.1172/JCI159393

[171] Langereis MA, Rabouw HH, Holwerda M, Visser LJ, van Kuppeveld FJM. Knockout of cGAS and STING rescues virus infection of plasmid DNA-transfected cells. J Virol. 2015;89(21):11169-73. doi.org/10.1128/JVI.01781-15

[172] Banerjee D, Langberg K, Abbas S, Odermatt E, Yerramothu P, Volaric M, et al. A non-canonical, interferon-independent signaling activity of cGAMP triggers DNA damage response signaling. Nat Commun. 2021;12(1):6207. doi.org/10.1038/s41467-021-26240-9

[173] Ordovás L, Boon R, Pistoni M, Chen Y, Wolfs E, Guo W, et al. Efficient recombinase-mediated cassette exchange in hPSCs to study the hepatocyte lineage reveals AAVS1 locus-mediated transgene inhibition. Stem Cell Reports. 2015;5(5):918-31. doi.org/10.1016/j.stemcr.2015.09.004

[174] Bhagwan JR, Collins E, Mosqueira D, Bakar M, Johnson B, Thompson A, et al. Variable expression and silencing of CRISPR-Cas9 targeted transgenes identifies the AAVS1 locus as not an entirely safe harbour. F1000Research. 2020;8:1911. doi.org/10.12688/f1000research.19894.2

[175] Hong S, Hwang DY, Yoon S, Isacson O, Ramezani A, Hawley E, et al. Functional analysis of various promoters in lentiviral vectors at different stages of in vitro differentiation of mouse embryonic stem cells. Mol Ther. 2007;15(9):1630-9. doi:10.1038/sj.mt.6300251.

[176] Wang R, Liang J, Jiang H, Qin LJ, Yang HT. Promoter-dependent EGFP expression during embryonic stem cell propagation and differentation. Stem Cells Dev. 2008;17(2):345–51. doi:10.1089/scd.2007.0084.

[177] Zhang J, Hu Y, Yang J, Li W, Zhang M, Wang X, et al. Non-viral, specifically targeted CAR-T cells achieve high safety and efficacy in B-NHL. Nature. 2022;609(7928):369–74. doi:10.1038/s41586-022-05140-y.

[178] Yoshida T, Maeda A, Tani N, Sakai T. Promoter structure and transcription initiation sites of the human death receptor 5/TRAIL-R2 gene. FEBS Lett. 2001;507(3):381–385. doi:10.1016/S0014-5793(01)02947-7.

[179] Zeyda M, Borth N, Kunert R, Katinger H. Optimization of sorting conditions for the selection of stable, high-producing mammalian cell lines. Biotechnol Prog. 1999;15(5):953–7. doi:10.1021/bp990089g.

[180] Hunter M, Yuan P, Vavilala D, Fox M. Optimization of Protein Expression in Mammalian Cells. Curr Protoc Protein Sci. 2019;95(1):e77. doi:10.1002/cpps.77.

[181] Ganini D, Leinisch F, Kumar A, Jiang J, Tokar EJ, Malone CC, et al. Fluorescent proteins such as eGFP lead to catalytic oxidative stress in cells. Redox Biol. 2017;12:462-8. doi:10.1016/j.redox.2017.03.002.

[182] Kafri M, Metzl-Raz E, Jona G, Barkai N. The cost of protein production. Cell Rep. 2016 Jan 5;14(1):22–31. doi:10.1016/j.celrep.2015.12.015.

[183] Rodriguez-Marquez P, Calleja-Cervantes ME, Serrano G, Oliver-Caldes A, Palacios-Berraquero ML, Martin-Mallo A, et al. CAR density influences antitumoral efficacy of BCMA CAR T cells and correlates with clinical outcome. Sci Adv. 2022 Sep 30;8(39):eabo0514. doi:10.1126/sciadv.abo0514.

[184] Henne WM, Buchkovich NJ, Emr SD. The ESCRT pathway. Dev Cell. 2011 Jul 19;21(1):77–91. doi:10.1016/j.devcel.2011.05.015.

[185] Wiklander OPB, Brennan MÁ, Lötvall J, Breakefield XO, Andaloussi SE. Advances in therapeutic applications of extracellular vesicles. Sci Transl Med. 2019;11(492):eaav8521. doi:10.1126/scitranslmed.aav8521.

[186] Monleón I, Martínez-Lorenzo MJ, Monteagudo L, Lasierra P, Taulés M, Iturralde M, et al. Differential secretion of Fas ligand- or APO2 ligand/TNF-related apoptosis-inducing ligand-carrying microvesicles during activation-induced death of human T cells. J Immunol. 2001;167(12):6736-44. doi:10.4049/jimmunol.167.12.6736.

[187] Zhang X, Taylor H, Valdivia A, Dasari R, Buckley A, Bonacquisti E, et al. Auto-loaded TRAIL-exosomes derived from induced neural stem cells for brain cancer therapy. J Control Release. 2024 Aug;372:433–45. doi:10.1016/j.jconrel.2024.06.048.

[188] Wajant H, Moosmayer D, Wüest T, Bartke T, Gerlach E, Schönherr U, et al. Differential activation of TRAIL-R1 and -2 by soluble and membrane TRAIL allows selective surface antigen-directed activation of TRAIL-R2 by a soluble TRAIL derivative. Oncogene. 2001 Jul;20(20):4101–6. doi:10.1038/sj.onc.1204558.

[189] Yuan Z, Kolluri KK, Sage EK, Gowers KH, Janes SM. Mesenchymal stromal cell delivery of full-length tumor necrosis factor-related apoptosis-inducing ligand is superior to soluble type for cancer therapy. Cytotherapy. 2015;17(7):885-96. doi:10.1016/j.jcyt.2015.03.603.

[190] Pollard SM, Yoshikawa K, Clarke ID, Danovi D, Stricker S, Russell R, et al. Glioma stem cell lines expanded in adherent culture have tumor-specific phenotypes and are suitable for chemical and genetic screens. Cell Stem Cell. 2009 Jun;4(6):568–80. doi:10.1016/j.stem.2009.03.014.

[191] Kumar MA, Baba SK, Sadida HQ, Al Marzooqi S, Jerobin J, Altemani FH, et al. Extracellular vesicles as tools and targets in therapy for diseases. Signal Transduct Target Ther. 2024;9(1):27. doi:10.1038/s41392-024-01735-1

[192] Zhuang X, Xiang X, Grizzle W, Sun D, Zhang S, Axtell RC, et al. Treatment of brain inflammatory diseases by delivering exosome encapsulated anti-inflammatory drugs from the nasal region to the brain. Mol Ther. 2011 Oct;19(10):1769–79. doi:10.1038/mt.2011.164.

[193] Deng L, Zhai X, Liang P, Cui H. Overcoming TRAIL resistance for glioblastoma treatment. Biomolecules. 2021 Apr 14;11(4):572. doi:10.3390/biom11040572.

[194] Zhao J, Lu Y, Shen HM. Targeting p53 as a therapeutic strategy in sensitizing cancer cells to TRAIL induced apoptosis in cancer cells. Cancer Lett. 2012;314(2):126–34. doi:10.1016/j.canlet.2011.09.040.

[195] Klemke L, Fehlau CF, Winkler N, Toboll F, Singh SK, Moll UM, et al. The gain-of-function p53 R248W mutant promotes migration by STAT3 deregulation in human pancreatic cancer cells. Front Oncol. 2021;11:642603. doi:10.3389/fonc.2021.642603.

Appendix

A

crRNA	Description	Sequence (5′-3′)
AAVS1crRNA	Targeting of the AAVS1 locus; sequence borrowed from Schuber et al (148).	CCTCTAAGGTTTGCTTACGA
CLYBLcrRNA	Targeting of the CLYBL locus; sequence borrowed from Cerbini et al (149).	TCCTACATACCGTTATCCTG
DR5crRNA-1	Targeting of the DR5 locus developed by IDT's predesigned guide library.	GACAACGAGCACAAGGGTCT
DR5crRNA-2	Targeting of the DR5 locus developed by USCS genome browser.	CTGTCCCCGTTGTTCCATGG
LLGL1-crRNA	Targeting of the LLGL1 locus developed by IDT's predesigned guide library.	GGACCACTGTGACTCGGGTA

B

Target Locus	Description	Forward (5′-3′)	Reverse (5′-3′)
AAVS1 locus	Primer set for sequencing around the AAVS1crRNA cut site	CTATGTCCACTTCAGGACAG	CTACTGGCCTTATCTCACAG
CLYBL locus	Primer set for sequencing around the CLYBLcrRNA cut site	CTGGACAGTGGAATTTGTGG	GGACAGAGTCTTCTCAGTGG
DR5 locus	Primer set for sequencing around the DR5crRNA-1 cut site	TCTGCGCCCACAAAATACAC	AACTGAGCGAGGAAGGAAGG
DR5 5 locus	Primer set for sequencing around the DR5crRNA-2 cut site	ACCCAGAAACAAACCACAGC	CGCAGCTTACTCGGGAATTC
LLGL1 locus	Primer set for sequencing around the LLGL1crRNA cut site	TCCATCTCCCTGCTGACATC	CCTACATACCTGGTTCCCC

C

Sequencing TP53 mRNA	
Primer Description:	Sequence:
Primer set was used to perform RT-PCR on TP53 mRNA to generate cDNA. The same primers were then used for Sanger sequencing.	Forward (5′-3′) GTGCTTTCCACGACGGTGACACG Reverse (5′-3′) CGCACACCTATTGCAAGCAAGG
Internal primer used for Sanger sequencing.	5' -3' CAGCCAAGTCTGTGACTTGCACG
Internal primer used for Sanger sequencing.	5' – 3' GACTTGGCTGTCCCAGAATGC

Supplemental Figure S1: Primer and crRNA sequences

(A) All crRNA sequences used in this study for CRISPR-CAS9 editing. **(B)** All primer sets used to sequence genomic DNA following CRISPR-mediated cutting. **(C)** Primer sequences used to sequence the TP53 mRNA in PriGOs.

A.

CGCCCCGCCCCGAATGACGCCTGCCCGGAGGCAGTGAAAGTACAGCCGCGCCGCCCCAAGTCAGCCTGGACACA
TAAATCAGCACGCGGCCGGAGAACCCCGCAATCTCTGCGCCCACAAAATACACCGACGATGCCCGATCTACTTT
AAGGGCTGAAACCCACGGGCCTGAGAGACTATAAGAGCGTTCCCTACCGCCATGGTATCCAAAGGCGAGGAACT
CTTTACAGGAGTGGTCCCCATTTTGGTAGAGCTCGATGGAGATGTCAATGGGCACAAGTTCTCTGTATCTGGGG
AAGGCGAAGGGGATGCGACCTATGGCAAATTGACGCTGAAGTTCATTTGTACTACAGGTAAATTGCCAGTACCT
TGGCCTACGCTTGTAACGACTTTGACTTACGGAGTGCAATGCTTCTCCCGCTATCCTGACCATATGAAGCAACA
TGACTTTTTCAAAAGCGCGATGCCCGAGGGCTATGTGCAAGAGCGAACGATCTTTTTTAAAGACGACGGGAACT
ATAAAACGAGAGCAGAAGTTAAATTCGAGGGGGATACACTGGTTAATCGAATCGAACTTAAGGGCATTGATTTC
AAGGAAGACGGTAACATTCTGGGACATAAGCTGGAATACAACTATAACTCACACAATGTCTACATAATGGCGGA
CAAACAGAAGAATGGTATCAAGGTCAATTTCAAAATTCGACATAACATAGAAGACGGTTCCGTTCAACTTGCCG
ACCATTACCAACAGAACACTCCAATCGGGGACGGGCCGGTACTTCTTCCGGATAATCATTATCTTAGTACCCAG
AGTGCTCTCAGCAAAGACCCTAACGAGAAGAGGGACCATATGGTGCTTCTCGAGTTCGTAACGGCGGCGGGAAT
CACACTGGGTATGGATGAACTTTACAAGTAAAGCGGCCGCGTCGACGAATTAACTTGTTTATTGCAGCTTATAA
TGGTTACAAATAAAGCAATAGCATCACAAATTTCACAAATAAAGCATTTTTTTCACTGCATTCTAGTTGTGGTT
TGTCCAAACTCATCAATGTATCTTATGGAACAACGGGGACAGAACGCCCCGGCCGCTTCGGGGGCCCGGAAAAG
GCACGGCCCAGGACCCAGGGAGGCGCGGGGAGCCAGGCCTGGGCCCCGGGTCCCCAAGACCCTTGTGCTCGTTG
TCGCCGCGGTCCTGCTGTTGGTGAGTCCCCGCCGCGGTCCCTGGCTGGGGAAGAGCGTGCCTGGCGCCTGGAGA
GGG

Homology arm	EGFP	SV40 polyadenylation	Homology arm

200bp homology arms

Total: 1261 bp

Supplemental Figure S2: DNA template sequence for homologous directed repair at the DR5 locus.

(A) Referenced as Template 3 in Section 3.1.3. Grey-highlighted text indicates homology arms. Yellow text represents the codon-optimized enhanced GFP coding sequence, and magenta text corresponds to the SV40 polyadenylation signal.

A.

CTGCTTCTCCTCTTGGGAAGTGTAAGGAAGCTGCAGCACCAGGATCAGTGAAACGCACCAGACGGCCGCGTCAG
AGCAGCTCAGGTTCTGGGAGAGGGTAGCGCAGGGTGGCCACTGAGAACCGGGCAGGTCACGCATCCCCCCCTTC
CCTCCCACCCCCTGCCAAGCTCTCCCTCCCAGGATCCTCTCTGGCTCCATCGGGGCAGAGCGCACATCGCCCAC
AGTCCCCGAGAAGTTGGGGGGAGGGGTCGGCAATTGATCCGGTGCCTAGAGAAGGTGGCGCGGGGTAAACTGGG
AAAGTGATGTCGTGTACTGGCTCCGCCTTTTTCCCGAGGGTGGGGGAGAACCGTATATAAGTGCAGTAGTCGCC
GTGAACGTTCTTTTTCGCAACGGGTTTGCCGCCAGAACACAGCGTTTAGTGAACCGTCAGATCGCCTGGAGACG
CCATCCACGCTGTTTTGACCTCCATAGAAGACACCGACTCTAGAGGATCCACCGGTCGCCACCATGGTGAGCAA
GGGCGAGGAGCTGTTCACCGGGGTGGTGCCCATCCTGGTCGAGCTGGACGGCGACGTAAACGGCCACAAGTTCA
GCGTGTCCGGCGAGGGCGAGGGCGATGCCACCTACGGCAAGCTGACCCTGAAGTTCATCTGCACCACCGGCAAG
CTGCCCGTGCCCTGGCCCACCCTCGTGACCACCCTGACCTACGGCGTGCAGTGCTTCAGCCGCTACCCCGACCA
CATGAAGCAGCACGACTTCTTCAAGTCCGCCATGCCCGAAGGCTACGTCCAGGAGCGCACCATCTTCTTCAAGG
ACGACGGCAACTACAAGACCCGCGCCGAGGTGAAGTTCGAGGGCGACACCCTGGTGAACCGCATCGAGCTGAAG
GGCATCGACTTCAAGGAGGACGGCAACATCCTGGGGCACAAGCTGGAGTACAACTACAACAGCCACAACGTCTA
TATCATGGCCGACAAGCAGAAGAACGGCATCAAGGTGAACTTCAAGATCCGCCACAACATCGAGGACGGCAGCG
TGCAGCTCGCCGACCACTACCAGCAGAACACCCCCATCGGCGACGGCCCCGTGCTGCTGCCCGACAACCACTAC
CTGAGCACCCAGTCCGCCCTGAGCAAAGACCCCAACGAGAAGCGCGATCACATGGTCCTGCTGGAGTTCGTGAC
CGCCGCCGGGATCACTCTCGGCATGGACGAGCTGTACAAGTAAAGCGGCCGCGTCGACGAATTAACTTGTTTAT
TGCAGCTTATAATGGTTACAAATAAAGCAATAGCATCACAAATTTCACAAATAAAGCATTTTTTTCACTGCATT
CTAGTTGTGGTTTGTCCAAACTCATCAATGTATCTTATAAGCAAACCTTAGAGGTTCTGGCAAGGAGAGAGATG
GCTCCAGGAAATGGGGGTGTGTCACCAGATAAGGAATCTGCCTAACAGGAGGTGGGGGTTAGACCCAATATCAG
GAGACTAGGAAGGAGGAGGCCTAAGGATGGGGCTTTTCTGTCACCAATCCTGTCCCTAGTGGCCCCACTGTGGG
GTGGAGGGGACAGAT

Homology arm	EF1A core promoter	EGFP	SV40 polyadenylation	Homology arm

200 bp homology arms

Total: 1569 bp

Supplemental Figure S3: DNA template sequence for homologous directed repair at the AAVS1 locus.

(A) Referenced as Template 2 in Section 3.1.3. Grey-highlighted text indicates homology arms. Yellow text represents the enhanced GFP coding sequence, and magenta text corresponds to the SV40 polyadenylation signal. Teal text corresponds to WPRE regulatory sequence.

A.

CTGCTTCTCCTCTTGGGAAGTGTAAGGAAGCTGCAGCACCAGGATCAGTGAAACGCACCAGACGGCCGCGTCAG
AGCAGCTCAGGTTCTGGGAGAGGGTAGCGCAGGGTGGCCACTGAGAACCGGGCAGGTCACGCATCCCCCCCTTC
CCTCCCACCCCCTGCCAAGCTCTCCCTCCCAGGATCCTCTCTGGCTCCATCGCGTTACATAACTTACGGTAAAT
GGCCCGCCTGGCTGACCGCCCAACGACCCCCGCCCATTGACGTCAATAATGACGTATGTTCCCATAGTAACGCC
AATAGGGACTTTCCATTGACGTCAATGGGTGGAGTATTTACGGTAAACTGCCCACTTGGCAGTACATCAAGTGT
ATCATATGCCAAGTACGCCCCCTATTGACGTCAATGACGGTAAATGGCCCGCCTGGCATTATGCCCAGTACATG
ACCTTATGGGACTTTCCTACTTGGCAGTACATCTACGTATTAGTCATCGCTATTACCATGGTGATGCGGTTTTG
GCAGTACATCAATGGGCGTGGATAGCGGTTTGACTCACGGGGATTTCCAAGTCTCCACCCCATTGACGTCAATG
GGAGTTTGTTTTGGCACCAAAATCAACGGGACTTTCCAAAATGTCGTAACAACTCCGCCCCATTGACGCAAATG
GGCGGTAGGCGTGTACGGTGGGAGGTCTATATAAGCAGAGCTCGTTTAGTGAACCGTCAGATCGCCTGGAGACG
CCATCCACGCTGTTTTGACCTCCATAGAAGACACCGACTCTAGAGGATCCACCGGTCGCCACCATGGTGAGCAA
GGGCGAGGAGCTGTTCACCGGGGTGGTGCCCATCCTGGTCGAGCTGGACGGCGACGTAAACGGCCACAAGTTCA
GCGTGTCCGGCGAGGGCGAGGGCGATGCCACCTACGGCAAGCTGACCCTGAAGTTCATCTGCACCACCGGCAAG
CTGCCCGTGCCCTGGCCCACCCTCGTGACCACCCTGACCTACGGCGTGCAGTGCTTCAGCCGCTACCCCGACCA
CATGAAGCAGCACGACTTCTTCAAGTCCGCCATGCCCGAAGGCTACGTCCAGGAGCGCACCATCTTCTTCAAGG
ACGACGGCAACTACAAGACCCGCGCCGAGGTGAAGTTCGAGGGCGACACCCTGGTGAACCGCATCGAGCTGAAG
GGCATCGACTTCAAGGAGGACGGCAACATCCTGGGGCACAAGCTGGAGTACAACTACAACAGCCACAACGTCTA
TATCATGGCCGACAAGCAGAAGAACGGCATCAAGGTGAACTTCAAGATCCGCCACAACATCGAGGACGGCAGCG
TGCAGCTCGCCGACCACTACCAGCAGAACACCCCCATCGGCGACGGCCCCGTGCTGCTGCCCGACAACCACTAC
CTGAGCACCCAGTCCGCCCTGAGCAAAGACCCCAACGAGAAGCGCGATCACATGGTCCTGCTGGAGTTCGTGAC
CGCCGCCGGGATCACTCTCGGCATGGACGAGCTGTACAAGTAAAGCGGCCGCGTCGACAATCAACCTCTGGATT
ACAAAATTTGTGAAAGATTGACTGGTATTCTTAACTATGTTGCTCCTTTTACGCTATGTGGATACGCTGCTTTA
ATGCCTTTGTATCATGCTATTGCTTCCCGTATGGCTTTCATTTTCTCCTCCTTGTATAAATCCTGGTTGCTGTC
TCTTTATGAGGAGTTGTGGCCCGTTGTCAGGCAACGTGGCGTGGTGTGCACTGTGTTTGCTGACGCAACCCCCA
CTGGTTGGGGCATTGCCACCACCTGTCAGCTCCTTTCCGGGACTTTCGCTTTCCCCCTCCCTATTGCCACGGCG
GAACTCATCGCCGCCTGCCTTGCCCGCTGCTGGACAGGGGCTCGGCTGTTGGGCACTGACAATTCCGTGGTGTT
GTCGGGGAAGCTGACGTCCTTTCCATGGCTGCTCGCCTGTGTTGCCACCTGGATTCTGCGCGGGACGTCCTTCT
GCTACGTCCCTTCGGCCCTCAATCCAGCGGACCTTCCTTCCCGCGGCCTGCTGCCGGCTCTGCGGCCTCTTCCG
CGTCTTCGCCTTCGCCCTCAGACGAGTCGGATCTCCCTTTGGGCCGCCTCCCCGCCTGGAATTAACTTGTTTAT
TGCAGCTTATAATGGTTACAAATAAAGCAATAGCATCACAAATTTCACAAATAAAGCATTTTTTTCACTGCATT
CTAGTTGTGGTTTGTCCAAACTCATCAATGTATCTTATAAGCAAACCTTAGAGGTTCTGGCAAGGAGAGAGATG
GCTCCAGGAAATGGGGGTGTGTCACCAGATAAGGAATCTGCCTAACAGGAGGTGGGGGTTAGACCCAATATCAG
GAGACTAGGAAGGAGGAGGCCTAAGGATGGGGCTTTTCTGTCACCAATCCTGTCCCTAGTGGCCCCACTGTGGG
GTGGAGGGGACAGAT

Homology arm	CMV enhancer/promoter	EGFP	WPRE	SV40 polyadenylation	Homology arm

200 bp homology arms

Total: 2457 bp

Supplemental Figure S4: DNA template sequence for homologous directed repair at AAVS1 locus.

(A) Referenced as Template 1 in Section 3.1.3. Grey-highlighted text indicates homology arms. Yellow text represents the enhanced GFP coding sequence, and magenta text corresponds to the SV40 polyadenylation signal. Teal text corresponds to WPRE regulatory sequence.

A.

TCTAGAACCGAGAGAGAGTATTCAGAATGCTTTAATGGAGTAAGAAGGGCCACTGCTTAGAGTGGGGCTGAAGA
GAAAAGAAAGAAGGAGACCCTGCGGAAGCGGCAATACCAGGAAGGCAGTTGTATGCACATCATGCAGACCAGGA
GTAGCCTAGGGGTAGGGGACATGCCTGGGCTGGACAGTGGAATTTGTGGGAAATCAGATTTCCCTGAGCAAAAA
CCAGTGGGCAGCAGCCAAACTGGTGAGCAAGAACTGGCTGTGGTGGCTGGGCCCGAATTGGGAGCTACACCTGC
CCGGGCAGGTGTAGCTGCGAGGGAGGTCTCTGCCAACAACTCAGCTGTGCCGTGCCTGCTGAACGGCCTCACCT
TGGCCTCTGGCTCTGTTGCAGCTGTGTGGGGCTCGTGCTCCTACATACCGTTATCCGTTACATAACTTACGGTA
AATGGCCCGCCTGGCTGACCGCCCAACGACCCCCGCCCATTGACGTCAATAATGACGTATGTTCCCATAGTAAC
GCCAATAGGGACTTTCCATTGACGTCAATGGGTGGAGTATTTACGGTAAACTGCCCACTTGGCAGTACATCAAG
TGTATCATATGCCAAGTACGCCCCCTATTGACGTCAATGACGGTAAATGGCCCGCCTGGCATTATGCCCAGTAC
ATGACCTTATGGGACTTTCCTACTTGGCAGTACATCTACGTATTAGTCATCGCTATTACCATGGTGATGCGGTT
TTGGCAGTACATCAATGGGCGTGGATAGCGGTTTGACTCACGGGGATTTCCAAGTCTCCACCCCATTGACGTCA
ATGGGAGTTTGTTTTGGCACCAAAATCAACGGGACTTTCCAAAATGTCGTAACAACTCCGCCCCATTGACGCAA
ATGGGCGGTAGGCGTGTACGGTGGGAGGTCTATATAAGCAGAGCTCGTTTAGTGAACCGTCAGATCGCCTGGAG
ACGCCATCCACGCTGTTTTGACCTCCATAGAAGACACCGACTCTAGAGGATCCACCGGTCGCCACCATGGCTAT
GATGGAGGTCCAGGGGGGACCCAGCCTGGGACAGACCTGCGTGCTGATCGTGATCTTCACAGTGCTCCTGCAGT
CTCTCTGTGTGGCTGTAACTTACGTGTACTTTACCAACGAGCTGAAGCAGATGCAGGACAAGTACTCCAAAAGT
GGCATTGCTTGTTTCTTAAAAGAAGATGACAGTTATTGGGACCCCAATGACGAAGAGAGTATGAACAGCCCCTG
CTGGCAAGTCAAGTGGCAACTCCGTCAGCTCGTTAGAAAGATGATTTTGAGAACCTCTGAGGAAACCATTTCTA
CAGTTCAAGAAAAGCAACAAAATATTTCTCCCCTAGTGAGAGAAAGAGGTCCTCAGAGAGTAGCAGCTCACATA
ACTGGGACCAGAGGAAGAAGCAACACATTGTCTTCTCCAAACTCCAAGAATGAAAAGGCTCTGGGCCGCAAAAT
AAACTCCTGGGAATCATCAAGGAGTGGGCATTCATTCCTGAGCAACTTGCACTTGAGGAATGGTGAACTGGTCA
TCCATGAAAAAGGGTTTTACTACATCTATTCCCAAACATACTTTCGATTTCAGGAGGAAATAAAAGAAAACACA
AAGAACGACAAACAAATGGTCCAATATATTTACAAATACACAAGTTATCCTGACCCTATATTGTTGATGAAAAG
TGCTAGAAATAGTTGTTGGTCTAAAGATGCAGAATATGGACTCTATTCCATCTATCAAGGGGGAATATTTGAGC
TTAAGGAAAATGACAGAATTTTTGTTTCTGTAACAAATGAGCACTTGATAGACATGGACCATGAAGCCAGTTTT
TTTGGGGCCTTTTTAGTTGGCTAAAGCGGCCGCGTCGACAATCAACCTCTGGATTACAAAATTTGTGAAAGATT
GACTGGTATTCTTAACTATGTTGCTCCTTTTACGCTATGTGGATACGCTGCTTTAATGCCTTTGTATCATGCTA
TTGCTTCCCGTATGGCTTTCATTTTCTCCTCCTTGTATAAATCCTGGTTAGTTCTTGCCACGGCGGAACTCATC
GCCGCCTGCCTTGCCCGCTGCTGGACAGGGGCTCGGCTGTTGGGCACTGACAATTCCGTGGTGTTGAATTAACT
TGTTTATTGCAGCTTATAATGGTTACAAATAAAGCAATAGCATCACAAATTTCACAAATAAAGCATTTTTTTCA
CTGCATTCTAGTTGTGGTTTGTCCAAACTCATCAATGTATCTTACTGTGGTAGAGTTTTACCGTGGACCAGAGC
CATCTAGAGGACATTGAGTTACCCACATACTTTCTGTGGGAGAGGCCAAGGAGTCAGGGGGGGAGGCCGGGACC
TGAAGATCAACTCTTTACTGCAGAGATCCCTCCCTCCCTCTCTCTGTCCCATGGATCCAGAGGGAAGTTGAGGA
CAGTTTCATGCCACATGCTTGACCCGACTCAACTGAGTAACTGTGGCCACTGAGAAGACTCTGTCCTTGCAAAT
AACTCTCCTTAGTGCCCATATTCTGCAGAATGTTTGAGTGGCACGAGTACTTCATTCGTCTAGAAATATTTCAT
GGTAGTCAGTTGCTAATAACAGGATATCTGCAGGTAGTGTGTTCTCAGGAGGCACACCTGAAGCCTCAAAGGTG
AGGACATAGACATGGCTGTGGGTGA

425 bp homology arms

Total: 2689 bp

Supplemental Figure S5: DNA template sequence for homologous directed repair at CLYBL locus

(A) Referenced as Template 4 in Section 3.1.3. Grey-highlighted text indicates homology arms. Yellow text represents the membrane TRAIL coding sequence, and magenta text corresponds to the SV40 polyadenylation signal. Teal text corresponds to WPRE regulatory sequence.